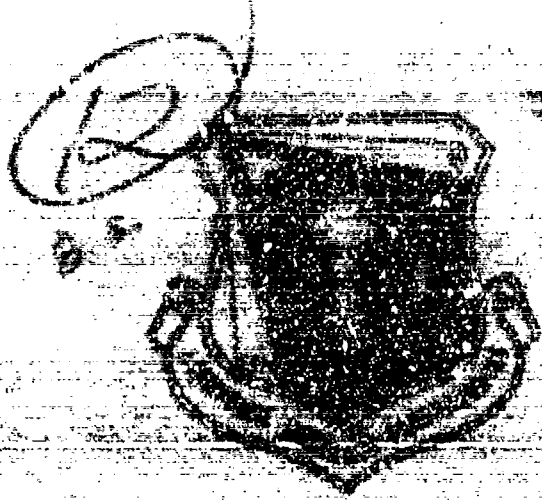


AD A 024104



**OXIDE SCALE ADHERENCE MECHANISMS
AND THE EFFECTS OF VITRUM, OXIDE
PARTICLES AND EXTERNALLY APPLIED LOADS
ON THE OX OXIDATION OF NICKEL AND
COBALT ALLOYS**

RESEARCH & DEVELOPMENT DIVISION
UNITED TECHNOLOGIES CORPORATION
EAST HARTFORD, CONNECTICUT 06103

JUNE 1974

FINAL REPORT - 1 APRIL 1972 - 31 MAY 1974

D. D. C.
APPROVED FOR
MAY 18 1974
AERONAUTICAL
LABORATORY

Approved for public release; distribution unlimited

METALLURGY & CERAMICS RESEARCH LABORATORY
MONROE RESEARCH LABORATORIES
Bldg 207, Area B
Wright-Patterson Air Force Base, Ohio 45433

AD A 024104
UNCLASSIFIED

NOTICE

When Government drawings, specifications, or other data are used for any purpose other than in connection with a specifically related Government procurement transaction, the United States Government thereby incurs no responsibility for any copyright infringement, and the fact that the Government may have furnished such data in any way does not constitute a specification or other data, or not to be regarded by anyone as a contract or agreement, or as implying any rights or privileges to make a copy, use, or sell any patented invention that may in any way be related thereto.

Organizations or individuals receiving reports via Aerospace Research Laboratories standard mailing lists should refer to the ARL number of the report received when contemplating a change of address or cancellation. Such changes should be directed to the specific laboratory originating the report. Do not return this copy; retain or destroy.

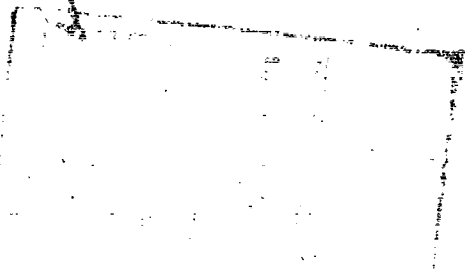
Reports are not stocked by the Aerospace Research Laboratories. Copies may be obtained from:

National Technical Information Service
Cameron Station
Springfield, VA 22161

This technical report has been reviewed and is approved for publication.

FOR THE COMMANDER:


Technical Director
and SIBOL Office



UNCLASSIFIED

SECURITY CLASSIFICATION OF THIS PAGE (When Data Entered)

REPORT DOCUMENTATION PAGE		READ INSTRUCTIONS BEFORE COMPLETING FORM
1. REPORT NUMBER (18) ARL 75-0234 (19) TR-75-02341	2. REPORT ACCESSION NO.	3. RECIPIENT'S CATALOG NUMBER
4. TITLE (and Subtitle) (6) OXIDE SCALE ADHERENCE MECHANISMS and the Effects of Yttrium, Oxide Particles and Externally Applied Loads on the Oxidation of NiCrAl and CoCrAl Alloys	5. TYPE OF REPORT & PERIOD COVERED (9) Final Technical Report 1 Jun 72 - 31 May 75	6. PERFORMING ORG. REPORT NUMBER (14) PWA-5364
7. AUTHOR(s) (10) C/S/Giggins and F.S. Pettit	8. CONTRACT OR GRANT NUMBER(s) (15) F33615-72-C-1702	
9. PERFORMING ORGANIZATION NAME AND ADDRESS Pratt & Whitney Aircraft Division of United Technologies Corporation East Hartford, Connecticut 06108	10. PROGRAM ELEMENT, PROJECT, TASK AREA & WORK UNIT NUMBERS 70210326	
11. CONTROLLING OFFICE NAME AND ADDRESS Aerospace Research Laboratories Air Force Systems Command United States Air Force Wright-Patterson AFB Ohio 45433	12. REPORT DATE (11) Jun 75 (12) B4	13. NUMBER OF PAGES 130
14. MONITORING AGENCY NAME & ADDRESS (if different from Controlling Office) (16) AF-7021 (17) 702103	15. SECURITY CLASS. (of this report) Unclassified	15a. DECLASSIFICATION/DOWNGRADING SCHEDULE
16. DISTRIBUTION STATEMENT (of this Report) Approved for public release; distribution unlimited.		
17. DISTRIBUTION STATEMENT (of the abstract entered in Block 20, if different from Report)		
18. SUPPLEMENTARY NOTES		
19. KEY WORDS (Continue on reverse side if necessary and identify by block number) Oxidation Oxide Adherence Oxide Scale Morphologies Yttrium Enhanced Oxide Adherence Nickel-Chromium-Aluminum Alloys Cobalt-Chromium-Aluminum Alloys		
20. ABSTRACT (Continue on reverse side if necessary and identify by block number) Studies have been performed to examine the effects of yttrium, oxide dispersions, fabrication conditions and externally applied loads on the oxidation of Ni-15Cr-6Al (wt. %) and Co-25Cr-6Al (wt. %) alloys at 1000 - 1200 degrees Celsius in air. External layers of alumina were developed on all of the alloys during oxidation and growth of these scales was controlled by diffusion of oxygen along their grain boundaries. The growth rates and mechanism for the alumina scales were not dependent upon alloy fabrication condition, yttrium, or oxide dispersions. Alumina scales spalled, during cooling, from alloys which did not contain yttrium or oxide dispersions. Voids were developed at the alumina-alloy interfaces		

D D C
MAY 10 1976

UNCLASSIFIED

SECURITY CLASSIFICATION OF THIS PAGE(When Data Entered)

during oxidation but they did not substantially influence spallation since the stresses generated during cooling exceeded the interfacial bond strengths. Yttrium and oxide dispersions improved the adhesion of alumina by providing vacancy sinks and by causing the development of macro- and micropegs at the alumina-alloy interfaces which mechanically keyed the scales to the alloys. Fabrication conditions which produced the most homogeneous distribution of yttrium or oxide dispersions within the alloys were the most effective procedures for improving the alumina scale adherence. Externally applied loads did not affect the growth rates of the alumina scales.

UNCLASSIFIED

SECURITY CLASSIFICATION OF THIS PAGE(When Data Entered)

PREFACE

This final report covers the work performed under Contract F33615-72-C-1702 during the period 1 June 1972 through 31 May 1975.

The research program discussed in this report was conducted by the Materials Engineering and Research Laboratory of the Pratt & Whitney Aircraft Division of United Technologies Corporation, East Hartford, Connecticut 06108. Its purpose is to determine the factors which affect the adherence of Al_2O_3 on NiCrAl and CoCrAl alloys.

The contract was accomplished under the technical direction of Dr. H.C. Graham of the Aerospace Research Laboratory, Air Force Systems Command, United States Air Force, Wright-Patterson Air Force Base, Ohio 45433. Dr. Graham is now with the Air Force Materials Laboratory (AFML/LLM).

Dr. F.S. Pettit, Program Manager, Materials Engineering and Research Laboratory, Pratt & Whitney Aircraft Division of United Technologies Corporation, directed this project. Mr. C.S. Giggins, of the P&WA Materials Engineering and Research Laboratory was the principal investigator. The authors wish to acknowledge helpful discussions concerning the results provided by G.W. Goward, B.H. Kear, E.J. Felten, and J.A. Goebel as well as technical assistance from V. Nevins, A.R. Geary, C.E. Londin, J.D. Hostetler, K.P. Gumz and O.G. Mollica.

NOTE: The Aerospace Research Laboratories was permanently closed
30 June 1975.

TABLE OF CONTENTS

SECTION	PAGE
I INTRODUCTION	1
1. SELECTIVE OXIDATION	1
2. OXIDE SCALE ADHESION	1
3. PROBLEMS TO BE STUDIED	2
II EXPERIMENTAL	4
1. MATERIALS	4
2. ALLOY FABRICATION AND CHARACTERIZATION	4
a. As-Cast Alloys	4
b. Hot-Worked and Annealed Alloys	5
c. Vapor-Deposited Alloys	6
d. Alloys Containing Oxide Dispersions	8
3. DESCRIPTION OF EXPERIMENTS	9
a. Isothermal Oxidation	9
b. Cyclic Oxidation	10
c. Oxidation Under Externally Applied Compressive Stress	11
d. Oxidation Under Externally Applied Tensile Stress	11
e. Specimen Geometry and Preparation	12
f. Examination of Oxidized Specimens	12
III RESULTS AND DISCUSSION	13
1. INTRODUCTION	13
2. THE RATES AND MECHANISMS OF OXIDE GROWTH ON NiCrAl AND CoCrAl ALLOYS	13
a. Oxide Formation	13
b. Morphologies of Al ₂ O ₃ Scales and Substrate Surfaces	14
c. Mechanism of Al ₂ O ₃ Growth	16
d. Rate of Al ₂ O ₃ Growth	17
3. THE ADHESION OF Al ₂ O ₃ ON NiCrAl AND CoCrAl ALLOYS	20
a. Experimental Results	20
b. Morphological Features of Al ₂ O ₃ Scales	20

TABLE OF CONTENTS (Cont'd)

SECTION	PAGE
c. Mechanism For Spalling From NiCrAl And CoCrAl Alloys	22
4. THE EFFECT OF YTTRIUM ON THE RATE OF GROWTH AND THE GROWTH MECHANISM OF Al ₂ O ₃	23
a. Oxide Formation	23
b. Morphologies of Al ₂ O ₃ Scales	23
c. The Effect of Yttrium on the Growth Rate of Al ₂ O ₃	26
d. The Effect of Yttrium on the Growth Mechanism of Al ₂ O ₃	27
5. THE EFFECT OF YTTRIUM ON THE ADHERENCE OF Al ₂ O ₃	29
a. Cyclic Oxidation Test Results	29
b. Mechanism By Which Yttrium Affects Adherence of Al ₂ O ₃	30
(1) Enhanced Oxide Plasticity	30
(2) Graded Seal Mechanism	30
(3) Chemical Bonding	31
(4) Vacancy Sink Mechanism	31
(5) Mechanical Keying or Pegging Mechanism	31
(6) Summary	33
6. THE EFFECT OF OXIDE DISPERSIONS IN ALLOYS ON THE ADHERENCE OF Al ₂ O ₃	33
a. Introduction	33
b. Experimental Results	33
c. Comparison of Mechanisms By Which Oxide Particles and Yttrium Improve Adherence of Al ₂ O ₃	35
7. OXIDATION OF NiCrAl (Y) AND CoCrAl (Y) ALLOYS WITH EXTERNALLY APPLIED LOADS	35
a. Introduction	35
b. Oxidation In The Presence Of Externally Applied Compressive Loads	36

TABLE OF CONTENTS (Cont'd)

SECTION	PAGE
c. Oxidation In The Presence of Externally Applied Tensile Loads	38
d. Effect of Externally Applied Stress On The Oxidation of NiCrAl (Y) And CoCrAl (Y) Alloys At 1100°C	38
IV SUMMARY AND CONCLUDING REMARKS	40
1. CONCERNING THE RATES AND MECHANISMS OF Al_2O_3 GROWTH ON NiCrAl AND CoCrAl ALLOYS	40
2. CONCERNING THE ADHESION OF Al_2O_3 TO NiCrAl AND CoCrAl ALLOYS	40
3. CONCERNING THE EFFECT OF YTTRIUM ON THE RATE OF GROWTH AND GROWTH MECHANISM OF Al_2O_3	41
4. CONCERNING THE EFFECT OF YTTRIUM ON THE ADHESION OF Al_2O_3	41
5. CONCERNING THE EFFECT OF OXIDE PARTICLES ON THE ADHERENCE OF Al_2O_3 TO NiCrAl AND CoCrAl ALLOYS	41
6. CONCERNING THE EFFECT OF ALLOY MICRO-STRUCTURE ON THE ADHESION OF Al_2O_3	41
7. CONCERNING THE EFFECT OF APPLIED STRESS ON THE OXIDATION OF THESE ALLOYS	42
REFERENCES	118

LIST OF ILLUSTRATIONS

FIGURE		PAGE
1	Typical Mold and the Resulting Investment Casting Used to Produce Specimens for the Oxidation Experiments.	43
2	Photographs Showing the Microstructures of the As-Cast Alloys.	44
3	Photographs Showing the Details of the Microstructures of As-Cast NiCrAl and NiCrAlY Alloys in the Etched Condition.	45
4	Photographs Showing the Details of the Microstructures of As-Cast CoCrAl and CoCrAlY Alloys in the Etched Condition.	46
5	Microstructures of Hot-Worked and Annealed NiCrAl and NiCrAlY Alloys in the Etched Condition.	47
6	Microstructures of Hot-Worked and Annealed CoCrAl and CoCrAlY Alloys in the Etched Condition.	48
7	Schematic Diagram of the Electron Beam Evaporation Apparatus Used to Produce Vapor-Deposited Alloys.	49
8	Microstructure of Vapor-Deposited NiCrAl, NiCrAlY, CoCrAl and CoCrAlY Alloys in the Etched Condition.	50
9	Microstructures of NiCrAl - ThO ₂ , CoCrAl - Al ₂ O ₃ and CoCrAl - Y ₂ O ₃ in the As-Polished and Etched Conditions.	51
10	Specimen Configurations for Oxidation During Applied Tensile and Compressive Loading.	52
11	Schematic Diagram Illustrating the Processes by Which Continuous Al ₂ O ₃ Layers Are Developed on NiCrAl Alloys.	53
12	Typical Transient Oxidation Features Developed During Oxidation of the NiCrAl Alloy.	54
13	Typical Morphological Features Developed at the Al ₂ O ₃ - Gas Interface of Al ₂ O ₃ Scales on NiCrAl and CoCrAl Alloys.	55
14	Photographs Showing Development of Wrinkles in Oxide Formed on CoCrAl (AC) During Oxidation at 1100°C in 1 atm of Dry Air.	56

LIST OF ILLUSTRATIONS (Cont'd)

FIGURE		PAGE
15	Morphological Features Typical of NiCrAl and CoCrAl Alloys from Which the Al ₂ O ₃ Scales Had Spalled.	57
16	Photographs Showing Details of NiCrAl and CoCrAl Alloys from Which the Al ₂ O ₃ Had Spalled.	58
17	Photographs Showing Al ₂ O ₃ Crystals In Situ on Alloy Surface and Position of Continuous Al ₂ O ₃ Layer.	59
18	Photographs Showing Details of Wrinkles in Al ₂ O ₃ Scales on NiCrAl and CoCrAl Alloys.	60
19	Morphological Features Observed on Surfaces of Oxide Flakes Which Spalled from CoCrAl (HWA) After 1000 hrs of Oxidation at 1200°C in Air.	61
20	Photographs Showing Details of Al ₂ O ₃ Scales Which Spalled from NiCrAl and CoCrAl Alloys.	62
21	Depressions in Al ₂ O ₃ Scales at the Al ₂ O ₃ - Substrate Interface.	63
22	Scanning Micrographs Showing Microstructural Features of Polished and Etched (10 minutes in Hot Phosphoric Acid), Transverse Sections Through Al ₂ O ₃ Scales Formed on NiCrAl and CoCrAl Alloys After Oxidation at 1200°C in Air.	64
23	Schematic Diagram Illustrating the Formation of Voids at the Al ₂ O ₃ - Substrate Interfaces of Al ₂ O ₃ Scales Formed on NiCrAl and CoCrAl Alloys.	65
24	Typical Kinetic Data Obtained for the Oxidation of NiCrAl (Y) or CoCrAl (Y) Alloys.	66
25	Arrhenius Plots of Parabolic Rate Constants Obtained from the Oxidation of Hot-Worked and Annealed NiCrAl, CoCrAl, NiCrAlY and CoCrAlY Alloys in 1 atm of Dry Air.	67
26	Weight-Change Versus Time Data for the Discontinuous Cyclic Oxidation (2-hr Cycles) of Hot-Worked and Annealed Alloys in Air.	68
27	Photographs Showing the Effects of Specimen Surface Preparation on the Oxide and Substrate Morphological Features of NiCrAl (AC) After 24 hrs at 1200°C in 1 atm of Dry Air.	69

LIST OF ILLUSTRATIONS (Cont'd)

FIGURE		PAGE
28	Oxide Scale and Alloy Surface Morphologies of Electropolished Fe-25Cr-4Al After Isothermal Oxidation at 1200°C for 24 hrs in 1 atm of Air.	70
29	Comparison of Oxide and Substrate Morphologies After Oxidation of NiCrAl (HWA) at 1200°C in a CO ₂ - CO Mixture (CO ₂ /CO = 3) and in Air.	71
30	Oxide and Substrate Morphologies on NiCrAl (HWA) After Oxidation for 2 hrs in a CO ₂ - CO Mixture (CO ₂ /CO = 3) and Then 20 hrs in Air at 1200°C.	72
31	Morphological Features of Oxides Developed on NiCrAlY and CoCrAlY Alloys.	73
32	Morphological Features of Oxides and Substrates After Oxidation of NiCrAlY and CoCrAlY Alloys.	74
33	Photographs Showing the Network of Oxide Protrusions Which Were Formed on NiCrAlY and CoCrAlY Alloys.	75
34	Photographs Showing Features of Yttrium Oxide After Oxidation of NiCrAlY and CoCrAlY Alloys.	76
35	Photographs of Extracted Al ₂ O ₃ Flakes From CoCrAlY (HWA) Showing Al ₂ O ₃ - Substrate Interfaces.	77
36	Intensity Profiles Showing the Distribution of Aluminum and Yttrium Across NiCrAlY (HWA) and CoCrAlY (HWA) Alloy Specimens After 100 hrs of Oxidation at 1200°C in 1 atm of Dry Air.	78
37	Intensity Profiles Showing the Distribution of Aluminum and Yttrium Parallel to the Al ₂ O ₃ - Alloy Interface at Distances of 3 and 20 Microns into the NiCrAlY Alloy Described in Figure 36.	78
38	Features Developed on a Ni-15Cr-6Al-3Y Alloy (Plane-Front Solidified) After Oxidation at 1200°C in 1 atm of Air.	79
39	Electron Back Scatter Photomicrograph and X-ray Image Photographs Showing Features of Preferential Yttride Oxidation.	80

LIST OF ILLUSTRATIONS (Cont'd)

FIGURE		PAGE
40	Photographs Showing Features of Transverse Sections through Al_2O_3 Formed on CoCrAlY (HWA) After Oxidation at $1200^\circ C$ in Air.	81
41	Data Obtained From Thickness Measurements of the Al_2O_3 Scales Formed on CoCrAl, CoCrAlY and NiCrAlY Alloys After Isothermal Oxidation at $1200^\circ C$ in Air.	82
42	Schematic Diagrams Illustrating the Oxidation Mechanism of NiCrAlY and CoCrAlY Alloys.	83
43	Continuous Weight-Change Versus Time Data Obtained for the Oxidation of NiCrAl (HWA) and CoCrAl (HWA) Specimens at $1100^\circ C$ in 1 atm of Dry Air.	84
44	Continuous Weight-Change Versus Time Data Obtained for the Cyclic Oxidation of NiCrAlY (HWA) and CoCrAlY (HWA) Specimens at $1100^\circ C$ in 1 atm of Dry Air.	85
45	Photographs Showing Microstructures of Transverse Sections Through CoCrAlY Specimens After Cyclic Oxidation Testing at $1100^\circ C$ in Air.	86
46	Weight-Change Versus Time Data Obtained for the Cyclic Oxidation of As-Cast NiCrAl and NiCrAlY Alloys in Air at $1150^\circ C$.	87
47	Photographs Showing the Networks of Yttrium Oxide Developed at the Al_2O_3 - Substrate Interfaces of As-Cast, Hot-Worked and Annealed and Vapor-Deposited Alloys.	88
48	Photograph Showing Large Flakes (Arrows) of Al_2O_3 Which Spalled from CoCrAl (VD) Specimen upon Cooling to Room Temperature After 2 hrs of Oxidation at $1100^\circ C$ in Air.	89
49	Photographs Showing Morphological Features of Spalling of Al_2O_3 as a Result of Bending an Oxidized CoCrAlY (VD) Specimen.	90
50	Photographs Showing the Surfaces of CoCrAl - Al_2O_3 and CoCrAl (VD) After 20 hrs of Oxidation at $1100^\circ C$ in a CO_2 - CO Gas Mixture With $CO_2/CO = 3$.	91
51	Transverse Section Through CoCrAlY (HWA) After Oxidation at $1200^\circ C$ for 1000 hrs in 1 atm of Air.	92

LIST OF ILLUSTRATIONS (Cont'd)

FIGURE		PAGE
52	Oxidation Features Developed on NiCrAlY (VD) Specimen Which Had Been Oxidized 1000 hrs at 1200°C, Repolished and Then Oxidized 24 hrs at 1200°C in Air.	93
53	Weight-Change Versus Time Data Obtained for the Cyclic Oxidation (1 hr Cycles) of NiCrAl and CoCrAl Alloys and These Alloys Containing Oxide Particles or Yttrium.	94
54	Photomicrographs Showing Microstructures of Specimens After 1000 hrs of Cyclic Oxidation (1 hr Cycles) at 1100°C in Air.	95
55	Scanning Micrographs and An X-ray Energy Spectroscopy Profile Which Show the Surface of NiCrAl-ThO ₂ After 100 hrs of Oxidation at 1100°C in Air.	96
56	Scanning Micrographs Showing Features of the Al ₂ O ₃ Scale at the Substrate Interface from NiCrAl-ThO ₂ and the Matching Substrate Surface After 100 hrs of Oxidation at 1100°C in Air.	97
57	Scanning Micrographs Which Show the Surface of Oxidized CoCrAl-Y ₂ O ₃ After 100 hrs of Oxidation at 1100°C in Air.	98
58	Additional Scanning Micrographs of Specimen Described in Figure 57.	99
59	Scanning Micrographs Showing Morphological Features of CoCrAl-Al ₂ O ₃ After 20 hrs of Oxidation at 1100°C in a CO ₂ - CO Gas Mixture With CO ₂ /CO = 3.	100
60	Comparison of Oxide (Al ₂ O ₃) Thicknesses Formed on Unstressed and Stressed (Compression and Tension) CoCrAl and CoCrAlY Alloys.	101
61	Comparison of Oxide (Al ₂ O ₃) Thicknesses Formed on Unstressed and Stressed (Compression and Tension) NiCrAl and NiCrAlY Alloys.	102
62	Optical Photographs Showing Surface Features of CoCrAl (HV 1) After 24 hrs of Oxidation at 1100°C in Air with an Applied Compressive Stress Producing 1% Strain (0.042%/hr).	103

LIST OF ILLUSTRATIONS (Cont'd)

FIGURE		PAGE
63	Scanning Micrographs Showing Some of the Typical, Morphological Structures of Oxide Scales and Substrates Formed on Alloys That Did Not Contain Yttrium After 16 hrs of Oxidation at 1100°C in Air with a Constant Strain Rate (Compressive) of 0.04%/hr.	104
64	Scanning Micrographs to Compare Surface Features of Unstressed and Stressed CoCrAl (HWA) After Oxidation at 1100°C in Air.	105
65	Scanning Micrographs Showing Typical, Morphological Structures of Oxide Scale and Substrate of NiCrAl (HWA) After 16 hrs of Oxidation at 1100°C in Air at a Constant Strain Rate (Compressive) of 0.42%/hr.	106
66	Scanning Micrographs Showing Morphological Structures of Oxide Scales Formed on NiCrAlY (HWA) Specimens After Oxidation at 1100°C in Air.	107
67	Scanning Micrographs Showing Typical, Morphological Structures of Oxide Scale and Substrate of CoCrAlY (HWA) After Oxidation at 1100°C for 16 hrs in Air at a Constant Strain Rate (Compressive) of 0.42%/hr.	108
68	Scanning Micrographs Showing Typical, Morphological Structures of NiCrAlY (HWA) After 16 hrs of Oxidation at 1100°C in Air at a Constant Strain Rate (Compressive) of 0.42%/hr.	109
69	Scanning Micrographs Showing Typical, Morphological Structures of Oxide Scale and Substrate of CoCrAlY (HWA) After Oxidation at 1100°C in Air for 16 hrs at a Constant Strain Rate (Compressive) of 0.63%/hr.	110
70	Scanning Micrographs Showing the Morphological Structures of the Alloy-Oxide Surface for an Oxide Flake Spalled from the Specimen Shown in Figure 69.	111
71	Scanning Micrographs of a Metallographically Polished Section of the Transverse Ridges on the Specimen Shown in Figure 69.	112
72	Scanning Micrographs of Another Deformed Area of the Specimen Shown in Figure 71.	113
73	Scanning Micrographs Showing Morphological Structures of Oxide Scales Formed on a CoCrAl (HWA) Specimen After Oxidation at 1100°C in Air With an Applied Tensile Stress.	114

LIST OF ILLUSTRATIONS (Cont'd)

FIGURE		PAGE
74	Replica Micrographs of Alloy Surfaces from Which the Oxide Scales Shown in Figure 73 Were Removed.	115
75	Scanning Micrographs Showing Morphological Structures of Oxide Scales Formed on CoCrAlY (HWA) Specimens After Oxidation at 1100°C in Air.	116
76	Photographs Showing Surface Features of NiCrAl (HWA) Specimen After Oxidation for 21 hrs at 1100°C in Air with an Applied Tensile Stress Producing 17.4% Strain.	117

SECTION I

INTRODUCTION

In developing oxidation resistant materials for service at elevated temperatures, two requirements must be satisfied. Diffusion through the oxide scales which are formed on the surfaces of such materials must occur at the slowest possible rates and these oxide scales must be as resistant as possible to spalling when subjected to growth and thermal stresses. As a result of the need to have adherent layers of particular oxides formed on alloys and coatings during exposure to elevated temperatures, two types of studies have evolved. One type has been concerned with the factors which affect the selective oxidation of elements in alloys and transport through oxides and the other has been concerned with the adhesion of oxides to metals and alloys.

1. SELECTIVE OXIDATION

Studies of selective oxidation of elements in alloys are important because of the need to have developed on the surfaces of alloys those oxide phases through which transport occurs at the slowest possible rate. The basic principles required for an examination of the selective oxidation of elements in alloys were developed in papers by Wagner (ref. 1 to 4) and by Rapp (ref. 5 and 6). Generally speaking, it has been found that the oxidation of most oxidation resistant alloys can be conveniently divided chronologically into two stages, in particular, transient oxidation and oxidation under steady-state conditions (ref. 7, 8, and 9). Transient oxidation is temporary and is usually confined to the initial period of oxidation when numerous, different oxide-phases are formed on the alloy surface. Oxidation under steady-state conditions follows transient oxidation and is established through the action of displacement reactions which develop the stable oxide phase on the alloy surface.

While there is still much to be learned about the factors affecting the selective oxidation of elements in alloys, the desired oxide-phase can usually be developed on the surface of an alloy by having the alloy contain a sufficient amount of the metallic component of the desired oxide.

2. OXIDE SCALE ADHESION

The formation of an external, protective scale on an alloy or coating during oxidation, however, is not the sole criterion for optimum oxidation performance. For example, the nickel base superalloy B-1900 (Ni-8Cr-10Co-1.0Ti-6Al-6Mo-0.11C-4.3Ta-0.07Zr-0.015B*) which forms a continuous Al_2O_3 scale after a period of transient oxidation under isothermal conditions, cannot be used uncoated in the hotter sections of gas turbine engines. In addition, the lifetime of aluminide coatings in gas turbine engines, under conditions where hot corrosion (sulfidation) is not a significant factor, is only a small fraction of that expected from calculations using the parabolic rate constant for the growth of Al_2O_3 . In view of these results, as well as examination of tested hardware which shows that Al_2O_3

*All compositions are presented in weight percent unless noted otherwise.

and other types of oxide scales spall from most alloys and coatings in the presence of thermally induced stresses, it has become apparent that the performance of the alloys and coatings currently in service can be improved by developing adherence of their oxide scales.

There are numerous factors which affect the adhesion of oxides to metallic substrates. The general subject of oxide adhesion has been analyzed by Tylecote (ref. 10) and by Stringer (ref. 11). From a practical viewpoint, the observation (ref. 12) that small amounts (e.g., ~0.1 - 1.0%) of alkali earths or rare earths in alloys can significantly improve the adherence of oxides to alloys is of substantial importance. A considerable effort has been made to use such elements in developing improved, oxidation resistant alloys and coatings as well as determining the reasons for the improved adhesion of the oxides.

The utilization of such oxygen active elements to improve oxide scale adhesion is now commonplace. For example, yttrium is used to improve the adherence of Al_2O_3 scales on FeCrAl (ref. 13) and CoCrAl (ref. 14) alloys. Several mechanisms have been tentatively proposed to account for the influence of the alloy additions, such as yttrium, on enhancing oxide adherence. These mechanisms include: 1) the mechanical keying of the oxide scale through the protrusions of oxide pegs into the alloy substrate (ref. 13, 15, and 16), 2) the formation of an interlayer to act as a graded-seal between the oxide and the substrate (ref. 17), 3) accommodation of growth and thermal stresses through enhanced oxide plasticity due to the incorporation of the alloying elements in the oxide (ref. 18), and 4) the precipitation of fine particles of alloying-element oxides in the substrate or the solution of such elements in the alloy which act as preferred condensation sites for excess vacancies and, thereby, improve adherence by preventing void formation at the oxide-substrate interface (ref. 11 and 19).

At present, none of the proposed mechanisms can be considered to be generally valid, and much remains to be learned about the nature of the oxide-substrate interface and the quantities and distribution of active elements or their oxides which produce the optimum improvement in the adhesion of oxide scales. In addition, the growth of an oxide on a metal or alloy is almost always accompanied by the development of stresses in the oxide as well as in the alloy immediately adjacent to the oxide. These stresses arise because of growth of the oxide scale, thermal fluctuations and externally applied loads. The development of stresses in oxide scales during isothermal oxidation has been reviewed by Stringer (ref. 20). Hancock and Hurst (ref. 21) have also considered this topic as well as the effect of thermally induced stresses and externally applied loads on surface oxide scales. Progress is beginning to be made in describing the sources of stress and the effects of such stress on the oxidation of alloys but more work is still required to further observe and describe the development of stresses in oxide scales. It is especially important to attempt to interrelate stress development in oxide scales and oxide scale adhesion.

3. PROBLEMS TO BE STUDIED

One of the requirements for satisfactory performance of an oxidation resistant alloy or coating is that reaction between the alloy or coating and the gas produces a product which retards further reaction. Because of this requirement and in response to the demand

for systems which retain adequate surface integrity for longer times at higher temperatures, the alloys and coatings which have evolved are those upon which protective scales such as Al_2O_3 , Cr_2O_3 , or SiO_2 are formed. While transport through Cr_2O_3 and SiO_2 scales is slow compared to that of NiO and CoO , it has become apparent from experience that the best performance of nickel-and cobalt-base alloys and coatings in the hot sections of aircraft gas turbine engines is obtained when Al_2O_3 scales are formed. The purpose of this program was to study the adhesion of Al_2O_3 scales on nickel-and cobalt-base alloys and to consider the effects of yttrium, oxide dispersions and externally applied stresses on the adherence of the Al_2O_3 scales to these alloys.

Alloys of NiCrAl and CoCrAl, with and without yttrium or an oxide dispersion, and having compositions such that external α - Al_2O_3 scales were developed during oxidation, were employed in this investigation. These particular alloy systems have been selected because they constitute the major elements used in alloys and coatings for gas turbine engines. The objectives of this program were as follows:

- Compare the adherence of Al_2O_3 on NiCrAl and CoCrAl alloys.
- Determine the effect of yttrium on the growth mechanism and rate of growth of Al_2O_3 on NiCrAl and CoCrAl alloys.
- Determine the mechanism by which yttrium influences the adherence of Al_2O_3 scales on these alloys and establish any effect of alloy microstructure.
- Determine the effect of an oxide dispersion on the adherence of Al_2O_3 to these alloys and compare such effects to those produced by yttrium.
- Examine the effect of an externally applied stress on the oxidation of these alloys.

The program plan designed to achieve these objectives consisted of five sequential tasks. Task I involved obtaining and thoroughly characterizing the compositions and microstructures of NiCrAl(Y) and CoCrAl(Y) specimens. Task II involved obtaining isothermal and cyclic oxidation kinetics as well as determining the adherence of Al_2O_3 to these alloys. Task III involved obtaining scale thickness values as a function of time and performing detailed morphological examinations of the extracted Al_2O_3 scales and their corresponding substrates whenever possible. Task IV involved obtaining scale thickness values as a function of time for scales formed on alloys during oxidation under an applied stress. Task V involved obtaining specimens with an oxide dispersion, performing isothermal and cyclic oxidation tests on these specimens and examining the resulting Al_2O_3 scales. In this report, the results obtained from these tasks will be presented and discussed.

SECTION II

EXPERIMENTAL

1. MATERIALS

The nominal, base compositions of the alloys used in this program were Ni-15Cr-6Al and Co-25Cr-6Al. These base compositions were selected because continuous, external Al_2O_3 scales were formed on these alloys during oxidation in air or oxygen at temperatures of 1000°C and above. For those alloys containing yttrium, a nominal yttrium concentration of 0.1% was chosen because this amount was sufficient to affect the oxide adherence but not so large as to cause severe preferential oxidation of the yttride phases. In the alloys containing oxide dispersions, ThO_2 , Al_2O_3 or Y_2O_3 were used.

2. ALLOY FABRICATION AND CHARACTERIZATION

In order to include alloy fabrication condition as a variable, three fabrication conditions were studied in addition to the procedures used to prepare alloys containing the oxide dispersions, namely, as-cast (AC), hot-worked and annealed (HWA) and vapor-deposited (VD). These three fabrication conditions were selected in order to perform studies on alloys with different degrees of structural and chemical heterogeneity.

a. As-Cast Alloys

Cast alloys were prepared by vacuum induction melting and investment casting into specially designed molds to yield two 5/8 in. diameter x 8 in. long rods and two 5/8 in. x 1 in. x 8 in. bars of each alloy composition. A typical mold and resulting casting are shown in Figure 1. The rods from these ingots were used to obtain specimens in the as-cast condition. Chemical analyses of the as-cast alloys are presented in Table 1.

All the cast alloys had a dendritic structure, as shown in Figure 2. The microstructures of both NiCrAl and NiCrAlY were composed of fine γ' (Ni_3Al) particles in a matrix of the γ -phase (nickel solid solution), Figure 3. In addition, an yttride phase was present at grain boundaries as well as within the grains of the γ -phase of the NiCrAlY alloy, as shown in Figure 3b. Both CoCrAl and CoCrAlY alloys contained β -phase in a matrix of the α -cobalt solid solution, Figure 4, and yttride phases were also apparent in the CoCrAlY alloy, as shown in Figure 4b. Specimens of as-cast NiCrAl and CoCrAlY were examined with an electron beam microprobe for compositional gradients. Variations of the chromium and aluminum intensities across the dendrites in NiCrAl were just barely discernible, indicating a negligible composition gradient for this alloy. Examination of the CoCrAlY alloy, on the other hand, showed significant variations for Cr and Al upon traversing the β - and α -cobalt solid solution phases. The yttride phases observed within the CoCrAlY alloy by metallographic examination were verified by microprobe analysis.

TABLE I
CHEMICAL ANALYSES OF AS-CAST ALLOYS

Alloy Designation	Chromium (w/o)	Aluminum (w/o)	Yttrium (w/o)	Total* Impurity Limits (w/o)	Sample Location
NiCrAl (AC)	15.80	5.96	—	0.09-1.00	top of casting
	15.80	5.99	—	—	bottom of casting
NiCrAlY (AC)	15.74	5.98	0.12	0.14-1.45	top of casting
	15.74	6.04	0.11	—	bottom of casting
CoCrAl (AC)	25.03	6.05	—	0.18-1.85	top of casting
	25.04	6.07	—	—	bottom of casting
CoCrAlY (AC)	25.32	6.06	0.10	0.21-2.25	top of casting
	25.32	6.04	0.11	—	bottom of casting

*Emission spectrographic analysis of total impurity limits.

b. Hot-Worked and Annealed Alloys

The cast bars of each composition were hot-rolled to 60-70 percent reductions in order to obtain specimens in the hot-worked and annealed condition. Both the NiCrAl and NiCrAlY bars cracked during the hot-working operation. Additional castings of these alloys were subsequently prepared by nonconsumable arc melting the remaining bars and center cores of the investment castings (see Figure 1) and then drop casting to obtain a much finer grain size. These finer grained alloys were then successfully hot-rolled to the required 60-70% thickness reductions with only minor amounts of edge cracking. Results from chemical analyses of the hot-worked and annealed (48 hr in flowing argon at 1000°C) NiCrAl and NiCrAlY alloys are presented in Table II. Even though the yttrium content of these alloys was as low as 0.04%, microstructural analysis showed yttride precipitates were present. It therefore appears that the solubility limit of yttrium in the Ni-15Cr-6Al alloy is less than 0.04 wt.%.

The microstructures of the hot-worked and annealed NiCrAl and NiCrAlY alloys are presented in Figure 5. These alloys contain the same phases as the as-cast NiCrAl and NiCrAlY alloys; however, no dendrites are present, the γ' (Ni₃Al) particles within the equiaxed grains appear to be slightly coarser and definitely much coarser at the grain boundaries where more γ phase (nickel solid solution) is evident. The yttride phases observed metallographically at the grain boundaries and within the grains were verified by electron beam microprobe analysis.

TABLE II
CHEMICAL ANALYSES OF HOT-WORKED AND
ANNEALED NiCrAl AND NiCrAlY

Alloy Designation	Chromium (w/o)	Aluminum (w/o)	Yttrium (w/o)	Total* Impurity Limits (w/o)
NiCrAl (HWA)	15.89	6.02	—	0.16-1.65
NiCrAlY (HWA)	15.79	5.98	0.04-0.07	0.16-1.65

*Emission spectrographic analysis of total impurity limits.

The cast bars from the investment castings of CoCrAl and CoCrAlY were successfully hot-rolled to 60-70% reduction and the compositions of these alloys were the same as those given in Table I for the as-cast CoCrAl and CoCrAlY alloys. Typical microstructures for the hot-worked and annealed (48 hr in flowing argon at 1000°C) CoCrAl and CoCrAlY alloys are presented in Figure 6. The phases present in these alloys are the same as those in as-cast CoCrAl and CoCrAlY but only remnants of the original dendritic structure were evident. In addition, substantial amounts of particulate β -phase (CoAl) were found to be somewhat uniformly distributed within these alloys.

In order to avoid the possibility of any surface contamination due to the hot-rolling operation or during the subsequent annealing treatment, approximately 0.010-inches of material was removed from the surface of all alloys prior to use.

c. Vapor-Deposited Alloys

Plane-front solidification was originally selected as a fabrication technique for the alloys of interest to suppress dendritic growth in cast alloys. Dendritic growth can be suppressed via a steep thermal gradient and a low solidification rate and the change in solidification mode from dendritic to either cellular or plane front has been observed to occur when the ratio of gradient to rate exceeds the ratio of alloy melting range to liquid diffusion coefficient. Some very limited successes were obtained for the rod castings of Ni-15Cr-6Al and Co-25Cr-6Al alloys processed in this manner. However, the alloys containing yttrium were totally inadequate when fabricated by this technique due to loss of the yttrium from the alloy. This condition was caused by the low solidification rate which resulted in reaction between the melt and the Al_2O_3 mold to form a complex Y-Al-O phase as a skin around the casting. A NiCrAlY alloy containing 3% yttrium was plane-front solidified and although the yttrium reacted with the mold, a substantial amount of yttrium was retained within the alloy. This alloy was not suitable for oxidation testing since an yttride phase was formed as a continuous network along grain boundaries and would result in preferential, internal oxidation.

Vapor-deposited coatings are known to contain fine, uniformly distributed yttrides in a dendrite-free matrix and thus vapor deposition was an attractive fabrication method for the required alloys in lieu of plane-front solidification. Vapor-deposited alloys were prepared by using the electron-beam vapor deposition process to form thick (70 mils) coatings of the alloys on 3 in. x 2 in. x 1/8 in. Hastelloy X sheets. This process depends upon a continuous feeding of an ingot at a rate consistent with the evaporation rate of the liquid in order to control the composition of the deposit. For example, an alloy ingot of composition X is fed upward through a water-cooled crucible (Figure 7). As the ingot emerges at the top of the crucible, a high-powered, focused electron-beam is played on the emerging end, causing local melting and forming a liquid pool contained by the walls of the crucible and solid ingot below. Elements of higher vapor pressures begin to evaporate immediately, while those with lower vapor pressures are accumulated in the liquid pool and become more concentrated with time, leading to increased amounts of these elements in the vapor phase. Under constant conditions, the liquid inventory of composition Y will approach equilibrium with a gaseous phase of composition X. Normally, with a finite supply of alloy for the molten pool, the composition X and Y would exist only momentarily. In this case, more ingot material of composition X is fed into the molten pool and at precisely the same rate as vapors of composition X leave the pool. The result is a condition in which all three phases are in equilibrium with each other and the composition of the resulting coating can be kept constant, provided the process is maintained under constant conditions. Thus control of composition is accomplished mainly in the casting process used to produce the ingot feed stock. The Hastelloy X sheets were removed from the vapor-deposited alloys as well as any contamination from the substrates by sufficient surface grinding and the alloys were then annealed 48 hours at 1000°C in flowing argon. The chemical analyses of the vapor-deposited alloys are presented in Table III.

TABLE III
CHEMICAL ANALYSES OF VAPOR-DEPOSITED ALLOYS

Alloy Designation	Chromium (w/o)	Aluminum (w/o)	Yttrium (w/o)	Total* Impurity Limits (w/o)
NiCrAl (VD)	13.95	6.22	—	0.01-0.10
NiCrAlY (VD)	13.87	5.68	0.14	0.01-0.10
CoCrAl (VD)	23.01	5.96	—	0.06-0.60
CoCrAlY (VD)	22.10	6.08	0.54	0.06-0.60

*Emission spectrographic analysis of total impurity limits.

Typical microstructures of these alloys are presented in Figure 8. The phases present in these alloys are the same as those that were present in the as-cast and hot-worked and annealed conditions; however, the structures of the vapor-deposited alloys are extremely uniform and the yttride phases in the NiCrAlY and CoCrAlY alloys are fine and uniformly distributed. Electron beam microprobe analysis was used to verify the presence of the small yttride phases observed metallographically and to determine how much of the alloy was contaminated by the Hastelloy X substrate in order to determine the amount of material to be removed prior to annealing.

d. Alloys Containing Oxide Dispersions

In order to study the effect of dispersed oxide particles within alloys on the oxidation of NiCrAl and CoCrAl alloys, three alloys were used, specifically, NiCrAl-ThO₂, CoCrAl-Al₂O₃ and CoCrAl-Y₂O₃. The NiCrAl-ThO₂ was selected since it was commercially available (TD NiCrAl™, Fansteel Corporation) and was obtained as 0.053-inch thick sheet. This alloy contained 15.34% Cr and 3.72% Al, Table IV. The aluminum content was low but previous studies (ref. 8) showed that an Al₂O₃ scale should be developed on an alloy with this composition during oxidation. The CoCrAl-Al₂O₃ alloy was prepared by hot isostatically pressing blended powders of cobalt and a 76 Cr-24 Al alloy. The blended powders were sealed in an evacuated (5 x 10⁻⁶ mm Hg) 304 stainless steel cylinder and then hot isostatically pressed at 2225°F for 3 hours under 15,000 psi. After a vacuum heat treatment at 2200°F for 24 hours the canned specimen was hot swaged at 2100°F to approximately 25% reduction. The stainless steel can and some of the alloy surface were removed by centerless grinding to provide a 0.250-inch diameter specimen rod. Sections of the rod were hot-rolled at 2100°F to sheet specimens approximately 0.050-0.060-inches thick (75-80% reduction). Chemical analysis of this alloy showed that it contained about 18.75% Cr and 4.75% Al as indicated in Table IV. Isothermal oxidation of specimens of this alloy showed that continuous Al₂O₃ scales were formed over the major portion of the alloy surface. In localized regions, however, it was evident that oxides other than Al₂O₃ were present. Such localized, but excessive, transient oxidation has been observed for the oxidation of certain NiCrAl alloys (ref. 8). In these studies it appeared as though continuous Al₂O₃ scales would be developed beneath these transient oxides providing the oxidation time was sufficiently long. The CoCrAl-Y₂O₃ alloy* was prepared by attrition milling (mechanical alloying)(ref. 23). This alloy, which contained 20% Cr, 6% Al and 2 v/o Y₂O₃, was used to attempt to compare the effects produced by Y₂O₃ particles to those of Al₂O₃ particles in the CoCrAl-Al₂O₃ alloy.

*This alloy was supplied by I. G. Wright, Battelle Columbus Laboratories (ref. 22).

TABLE IV
CHEMICAL ANALYSES OF OXIDE DISPERSION
STRENGTHENED NiCrAl-ThO₂ AND CoCrAl-Al₂O₃

Alloy Designation	Chromium (w/o)	Aluminum (w/o)	ThO ₂ (w/o)
NiCrAl-ThO ₂	15.34	3.72	1.99
CoCrAl-Al ₂ O ₃	18.75	4.75	—

Microstructural photomicrographs of the three alloys with an oxide dispersion are presented in Figure 9.

3. DESCRIPTION OF EXPERIMENTS

The experiments performed to study the oxidation of the alloys, as well as the adherence of the Al₂O₃ scales consisted of both isothermal and cyclic oxidation experiments. Experiments were also performed to examine the effect of externally applied tensile and compressive stresses, during oxidation, upon the oxidation kinetics and oxide morphological features of some of the alloys. The details of these experiments are discussed in the following.

a. Isothermal Oxidation

Isothermal oxidation experiments were performed in 1 atmosphere of dry air at temperatures of 1000°, 1100° and 1200°C. Alloys in the hot-worked and annealed condition were studied at all three temperatures whereas alloys in the other three fabrication conditions were studied only at 1100°C. The oxidation of the hot-worked and annealed alloys was also studied at 1100°C in 0.2 atmosphere of oxygen. The results obtained with 0.2 atmosphere were similar to those obtained in dry air which showed that the nitrogen in the air was not significantly affecting the oxidation of the alloys. The air and oxygen was dried by passing it over anhydrous magnesium perchlorate. The oxygen was also passed over Ascarite (sodium hydroxide on an asbestos base) to remove CO₂.

The oxidation kinetics were obtained by measuring specimen weight-gains and the thicknesses of Al₂O₃ scales as a function of time. An Ainsworth type FV-AU-2 vacuum microbalance was used to obtain continuous weight-gain versus time data. Specimens were inserted into the bottom of an enclosure that contained the microbalance and a high temperature Marshall furnace. The enclosure was first evacuated and after introduction of the desired environment the specimens were raised from the cold zone to the hot zone. To terminate an experiment, the reverse procedure was used. Specimens were raised to the hot zone, or lowered to the cold zone, in less than 15 seconds. A more detailed description of this apparatus has been presented previously (ref. 24). Duplicate experiments were performed to obtain the weight-change versus time data. These experiments were performed

for 48 and 100 hours which also provided specimens for thickness measurements. Experiments were also performed in this apparatus for oxidation times of 2, 8, 16, 24 and 74 hours to provide additional specimens for thickness measurements. The thicknesses of the scales were determined by using the scanning electron microscope. This procedure consisted of obtaining scanning micrographs of transverse sections through at least three different oxide scales from a given specimen and then determining the average scale thickness.

During the course of this program it became evident that it was necessary to perform some isothermal oxidation experiments longer than 100 hours (e.g., ~ 500, 1000 and 3700 hrs). Such experiments were performed in laboratory air within a box furnace that was left undisturbed except for periodic temperature determinations. The oxidized specimens were suspended within Al_2O_3 crucibles by using Al_2O_3 (sapphire) rods which rested in slots cut into the walls of the Al_2O_3 crucibles.

At times in this program it was useful to oxidize specimens at reduced oxygen pressures. These were achieved by using flowing CO_2 - CO gas mixtures and the apparatus by which the gases were cleaned and mixed has been described previously (ref. 25).

b. Cyclic Oxidation

The cyclic oxidation experiments performed for this program consisted of three different types; discontinuous cyclic weight-change, continuous cyclic weight-change and automatic, discontinuous cyclic weight-change which are described individually in the following.

All of the discontinuous cyclic weight change experiments were performed with a laboratory box furnace in air at temperatures of 1000°C , 1100°C , and 1200°C . Alloys in the hot-worked and annealed condition were tested at all three temperatures, whereas alloys in all three of the fabrication conditions were only studied at 1100°C . These cyclic tests were performed in duplicate for a total time of 30 hours and the specimens were cooled to room temperature every two hours. The specimens were suspended from Al_2O_3 (sapphire) rods which lay in diametrical slots cut into the walls of Al_2O_3 crucibles. The crucibles were placed in a box furnace for two hours, then removed and put into a desiccator. Alumina covers were placed upon the crucibles as they were transferred to the desiccator. The specimens cooled from the test temperature to about 100°C in approximately ten minutes. After about three hours the crucibles containing the specimens, as well as the individual specimens, were weighed and the weight-changes of the crucibles with the specimens were used to determine the amount of oxide formed as a function of time. The difference between the weight-change of individual specimens was used to determine the amount of oxide spallation.

The continuous cyclic weight-change oxidation tests were performed at 1100°C in 1 atmosphere of dry air for 30 hours and only those alloys in the hot-worked and annealed condition were tested. These experiments were performed by using the same microbalance utilized for the isothermal oxidation tests except that continuous weight-change versus time data was only taken for 2-hour periods, after which the specimens were cooled to room temperature before the next cycle.

The automatic discontinuous weight-change experiments were performed at 1100°C in air for 1000 hours. In this test the specimens were automatically cycled between 1100°C and the apparatus cold zone at 30°C once every hour (50 minutes in furnace hot zone, 10 minutes in cold zone). The specimens were suspended by quartz hooks and were moved into and out of the vertical furnace by using a pneumatic cylinder and an electronic timer. The hot zone of the furnace was of sufficient length to permit eight specimens to be tested simultaneously. Periodically during the test the specimens were removed from the apparatus, weighed and examined optically.

c. Oxidation Under Externally Applied Compressive Stress

Experiments were performed on the hot-worked and annealed alloys to examine the effects of an externally, applied compressive stress on their oxidation. These experiments were performed in a Materials Testing System unit (MTS Model 502.03) using parallelepiped specimens having dimensions of 0.15 x 0.15 x 0.45 inches as shown in Figure 10. The conditions of the tests were such that creep type deformation occurred normal to the square cross section of the specimens at a constant strain rate and the strain rates utilized for this program were 0.042, 0.208, 0.417 and 0.625 %/hr. All experiments were performed in air at 1100°C for time periods up to 24 hours. It was necessary to insert specimens into a cold furnace, heat the furnace to 1100°C, soak at temperature to achieve thermal equilibrium and then initiate the experiment by application of the loads. The slow heating of the specimens to temperature caused more transient oxidation to occur than was observed for unstressed specimens which were inserted into a furnace at the test temperature. In addition, a significant amount of oxidation occurred prior to the application of the applied loads. In view of these conditions, argon was passed over the specimens during heating the furnace to temperature and during part of the soak period. The flow of argon over the specimens was then terminated and the specimens were soaked in air for an additional hour after which the loads were applied. This procedure considerably reduced the amount of transient oxidation. Some oxidation did occur, of course, prior to the application of the loads.

d. Oxidation Under Externally Applied Tensile Stress

Each of the hot-worked and annealed alloys was subjected to externally applied tensile stresses during oxidation at 1100°C in air in order to examine the effects of such stresses upon their oxidation properties. These experiments were to be performed in an Instron tensile machine using specimens having a one inch gage length as shown in Figure 10. It was found, however, that the Instron tensile machine could not impose the small strain rates that were desired. For example, an experiment was performed using NiCrAl (HWA) in which it was attempted to have strain rates of about 0.042 to 0.083%/hr. After 21 hours of testing 17.4% strain had occurred or 0.83%/hr. Under such strains grain boundary separation or cracks in the substrate were evident and contained oxidation products. Such a condition showed that the external Al₂O₃ scale must have fractured at least in some areas during test. Since the development of cracks in the Al₂O₃ scale prevented examining the effect of stress on the growth of this scale, it was decided to apply smaller tensile strains by using a standard one-to-one creep machine.

The shapes of the specimens used in the creep machine were the same as those used in the Instron machine, Figure 10. In using the creep machine, it was also necessary to use flowing argon to inhibit transient oxidation during heating and soaking of the specimens. The soak period consisted of one-half hour in argon followed by one-half hour in air. In these tests constant strain rates were not used. Creep curves (% strain versus time) were obtained and the tests were terminated after a given amount of total strain. In all of these tests the tertiary stage of creep was not achieved. In a few of the creep tests where the total strain was small, the specimens were used again in a subsequent test and whenever the oxide spalled profusely, the specimens were repolished prior to testing.

e. Specimen Geometry and Preparation

Specimens in the hot-worked and annealed or the vapor-deposited conditions for both the isothermal and cyclic oxidation tests were in the shape of rectangular coupons having dimensions of approximately 1 cm x 1 cm x 0.1 cm. Specimens in the as-cast condition were in the shape of discs about 0.1 cm thick and 1.3 cm in diameter.

Unless noted otherwise, all specimens were polished through 600-grit SiC abrasive paper, ultrasonically agitated in ethylene trichloride and rinsed with ethyl alcohol.

f. Examination of Oxidized Specimens

All of the oxidized specimens were examined in detail by means of standard techniques which included the following.

- Examination of the oxide in situ as well as the alloy surface, where possible, by using light and scanning electron microscopes.
- Examination of transverse sections through the oxide and substrate by using the light microscope and electron beam microprobe.
- X-ray diffraction analyses of the oxides scales.
- Examination of replicas stripped from the surface of adherent oxide scales as well as the replicas stripped from the bare substrate, when possible, with the electron microscope.
- Examination of small, localized areas of oxide scales and substrates by X-ray energy spectroscopy to detect the presence of various elements.

SECTION III

RESULTS AND DISCUSSION

1. INTRODUCTION

In this section the results obtained from the program will be used first to examine the oxidation rates, growth mechanisms and adhesion of Al_2O_3 for NiCrAl and CoCrAl alloys. The effects produced by yttrium on the oxidation rate, growth mechanism and adherence of the scales will then be considered and the results obtained with alloys containing oxide dispersions will then be compared to those obtained with the yttrium-containing alloys. Finally, the effects produced by externally applied loads on the growth and adhesion of Al_2O_3 scales will be examined.

2. THE RATES AND MECHANISMS OF OXIDE GROWTH ON NiCrAl AND CoCrAl ALLOYS

a. Oxide Formation

Continuous layers of Al_2O_3 were eventually developed on the surfaces of NiCrAl and CoCrAl alloys in all three fabrication conditions throughout the temperature interval studied. In all cases, the continuity of the Al_2O_3 scales was developed over a period of time during which other oxides in addition to Al_2O_3 (e.g., Cr_2O_3 , NiO or CoO, $NiCr_2O_4$ or $CoCr_2O_4$) were formed. The sequence of steps leading to the development of continuous Al_2O_3 scales on these alloys are illustrated schematically in Figure 11 for the NiCrAl alloy (ref. 8). Similar conditions prevail during the oxidation of the CoCrAl alloy but the transient period involves the formation of more transient oxides, perhaps due to the faster growth rate of CoO than NiO.

Examination of thin oxide films removed from the NiCrAl alloy after five minutes of oxidation at $1100^\circ C$ by transmission electron microscopy showed that oxidation did not occur uniformly over the entire alloy surface. At what appeared to be grain boundaries of the substrate, the oxide was thin and fine-grained whereas in other areas the film was thicker, Figure 12a, and coarser-grained. Electron diffraction analyses showed the thicker regions of the film contained NiO, Cr_2O_3 and Al_2O_3 whereas in the thinner regions only Cr_2O_3 and Al_2O_3 were usually present. X-ray diffraction analyses of oxide films removed from NiCrAl and CoCrAl alloys after oxidation at temperatures between 1000° and $1200^\circ C$ showed continuous layers of Al_2O_3 were developed over the major portions of the surfaces of these alloys after only 30 minutes of exposure. In some localized areas, however, transient oxidation was evident. This transient oxidation was easily discernible since the alloy surfaces contained depressions and mounds of transient oxide were evident on the surface of the Al_2O_3 scale at the gas interface, Figure 12b. In addition, the oxide scale adjacent to the alloy surface beneath the transient oxide mounds was composed of large, uneven Al_2O_3 crystals, Figure 12c.

The amount of localized, transient oxidation was dependent upon the fabrication condition of the alloys and the temperature. Usually alloys in the as-cast condition contained more localized areas of transient oxides than either hot-worked and annealed or vapor-deposited alloys. The number of localized areas with observable transient oxides also appeared to decrease as the oxidation temperature was increased in the temperature interval between 1000° and 1200°C. Even under the conditions most favorable for the formation of localized patches of transient oxides, however, continuous layers of Al_2O_3 eventually developed beneath these oxides after about eight hours of oxidation.

b. Morphologies of Al_2O_3 Scales and Substrate Surfaces

The morphologies of the Al_2O_3 scales and the substrate surfaces from which the Al_2O_3 had spalled, are of value not only in discussing the rates and mechanisms of Al_2O_3 growth but also in developing models to account for the spalling of Al_2O_3 from NiCrAl and CoCrAl alloys. In this section only features of the Al_2O_3 which are relevant to the growth mechanism of this oxide will be presented. In a subsequent section of this report additional morphological features of the Al_2O_3 scales related to spalling of the Al_2O_3 will be presented.

In studying the morphological features of the Al_2O_3 scales, it was necessary to differentiate between the features of continuous Al_2O_3 scales and features of scales where the Al_2O_3 was still in the process of developing continuity. This differentiation was easy to accomplish since the features typical of localized transient oxidation, Figure 12, were readily apparent upon examining specimens with the light and scanning electron microscopes.

The morphological features of the Al_2O_3 scales which were formed on the NiCrAl and CoCrAl alloys were similar and these features were not dependent upon the fabrication condition of the alloys. The features were dependent upon the oxidation time and temperature. At 1000°C the Al_2O_3 scales were flat, Figure 13a, whereas at 1200°C these scales were highly wrinkled, Figure 13b. At all temperatures the surfaces of the Al_2O_3 scales at the oxide-gas interface contained a fine network of dimpled depressions and filamentary growths, Figure 13c. Wrinkling of the oxide was not observed during the initial stages of oxidation but it was observed as the oxidation time was increased as shown in the photographs presented in Figure 14.

At 1000°C the substrate surface from which the Al_2O_3 had spalled contained grooves at grain boundaries of the substrate and isolated imprints of oxide grains, Figure 15a. The surfaces of the substrates away from these imprints were smooth and it appeared that the oxide and substrate had not been in intimate contact during oxidation. At higher temperatures, the substrate surfaces contained numerous smooth areas as well as mounds of metal that were highly imprinted from oxide grains, Figures 15b and 15c. These smooth areas usually contained numerous thermal facets, Figure 16a, and were not confined only to the grain boundaries of the alloy. In the case of the CoCrAl alloy, however, the smooth areas were almost always coincidental with sites where the β -phase had resided in the alloy at the beginning of oxidation, Figure 16b.

The Al_2O_3 surfaces adjacent to the substrates contained features matching those observed on the substrates. For example, under conditions where the oxide had not wrinkled, protrusions of oxide were observed to extend from the scale into the alloy, Figures 17a and 17b. The position of these oxide protrusions in relation to the continuous oxide scale and the imprinted substrate, Figures 17a and 17b, showed that the oxide away from the protrusions was not in contact with the substrate. Under conditions where wrinkles were observed in the oxide scales, these wrinkles were always coincidental with smooth areas on the substrate surfaces, Figure 18a, and protrusions of oxide were evident extending from the oxide toward the smooth substrate, Figure 18b.

The morphological features of the Al_2O_3 scales at the oxide-gas interface did not change significantly with oxidation times up to 100 hours. Only a few specimens were examined for oxidation times greater than 100 hours and such specimens were oxidized only at 1200°C . After 1000 hours of oxidation the features of the Al_2O_3 scales at the gas interface had not changed significantly from those for shorter times except that wrinkles in the Al_2O_3 were less evident after 1000 hours of oxidation, Figure 19a.

The morphological features of the Al_2O_3 scales at the substrate interfaces did vary not only with time but also with location on specimen surfaces for a constant oxidation time. Under conditions where the Al_2O_3 was not profusely wrinkled (e.g., 1000°C and short oxidation times at 1100°C), the surface of the Al_2O_3 scales at the substrate interfaces was frequently composed of large, widely-spaced crystals, Figure 20a. As oxidation was continued the spaces between these oxide crystals became smaller and in some cases scales of uniform thicknesses were developed. The filling of the spaces between these oxide crystals occurred more rapidly at 1100°C , Figure 20b, than 1000°C , Figure 20c. While morphologies such as those shown in Figures 20a and 20c were common, scales of uniform thicknesses without oxide protrusions were also abundant, Figure 20d. Under conditions where the Al_2O_3 scales contained numerous wrinkles, Figure 13b, the surfaces of the scales at the substrate interfaces contained depressions and large areas of oxide crystallites, Figures 21a and 21b. The patterns of these depressions were identical to those of the wrinkles and it was obvious that the depressions were the undersides of the wrinkles. In the case of the CoCrAl alloy the depressions formed a pattern identical to that of the β -phase in this alloy, Figure 21a. Within the depressions on scales removed from either CoCrAl or NiCrAl alloys, large irregular grains of oxide were evident whereas the oxide in other areas had a fine granular texture, Figure 21b. After 1000 hours of oxidation at 1200°C , depressions in the surfaces of scales at the substrate interfaces were as numerous as what was observed for shorter times, Figure 19b. This surface was not flat but contained continuous undulations and had a well defined grain structure, Figure 19c. The substrate surface also contained these undulations and was almost completely covered with the imprints of oxide grains.

The nonuniformity of the scales at the substrate interface, Figures 17, 20a and 20c, is a feature common to the transient stage of oxidation during which the continuity of the Al_2O_3 is being developed. During the transient stage of oxidation mounds of external oxides, Figure 12b, above discontinuous Al_2O_3 crystals, Figure 12c, that extend deeply into the alloy are usually evident. The mounds of external oxide typical of transient oxidation are not evident in Figures 17, 20a and 20c. The lack of imprints between the imprints of

the large crystallites, Figure 15a, as well as features such as those shown in Figure 17, indicate the oxide was not in intimate contact with the substrate. Such a condition is also not compatible with the transient oxidation process. It therefore is not readily apparent that the irregular features of the Al_2O_3 which are developed at the substrate interface are due to transient oxidation. On the other hand, such a possibility also cannot be ruled out.

The surfaces of the Al_2O_3 scales exposed by cracking on CoCrAl and NiCrAl alloys frequently had structures such as that shown in Figure 20b. Small equiaxed grains were evident in the scale near the Al_2O_3 -gas interface whereas coarser, columnar-shaped grains were developed beneath this zone of small grains. Numerous Al_2O_3 flakes were mounted in STYCAST, polished, removed from the mounting material, examined with the scanning electron microscope, (SEM) etched, and examined once again with the SEM. Typical structures are presented in Figure 22. It can be seen that the oxide scales were composed of smaller grains near the oxide-gas interface. As one proceeds toward the substrate interface, the grains become larger and more columnar in shape but the columnar pattern is not usually as complete as indicated by the structure shown in Figure 20b.

c. Mechanism of Al_2O_3 Growth

In discussing the mechanism of Al_2O_3 growth on NiCrAl and CoCrAl alloys, it is first necessary to determine whether this growth occurs by the diffusion of aluminum outward through the scale, the diffusion of oxygen inward, or a combination of both aluminum and oxygen diffusion. The results obtained from morphological observations of the Al_2O_3 scales indicate the following:

- The morphologies of the surfaces of the Al_2O_3 scales at the Al_2O_3 -gas interfaces did not change significantly with oxidation time.
- The spaces between the large oxide crystals, Figure 20a, which extended from the scales at the Al_2O_3 -substrate interfaces were filled with oxide as oxidation was continued, Figure 20b.
- The columnar grains of the Al_2O_3 adjacent to the alloy appeared to grow with time rather than the more equiaxed grains which were observed in the Al_2O_3 near the Al_2O_3 -gas interface.

All three of these conditions indicate that the Al_2O_3 growth involves a significant amount of oxygen diffusion inward through the scale. Subsequently in this report more convincing data will be presented to show that the growth of Al_2O_3 on NiCrAlY and CoCrAlY alloys occurs via the inward diffusion of oxygen. There are also data in the literature (ref. 19 and 26) which indicate that Al_2O_3 scales are developed during high temperature oxidation via the inward diffusion of oxygen.

If it is assumed that the Al_2O_3 scales are formed by the inward diffusion of oxygen, the morphological features which have been observed can be used to develop the following description for the growth of Al_2O_3 on NiCrAl and CoCrAl alloys. During the initial stages of oxidation, continuous layers of Al_2O_3 are developed over these alloys as illustrated schematically in Figure 11. Since the formation of the Al_2O_3 scale involves the inward diffusion of oxygen, the Al_2O_3 scale is in compression as indicated in Figure 23a.

Subsequent growth of the Al_2O_3 results in the formation of voids at the Al_2O_3 -substrate interfaces, Figure 23b. These voids may have rather random shapes but those developed at grain boundaries of the alloys usually have a groove-like configuration. The origin of the voids is not known. They may be formed as a result of interdiffusion within the alloy which occurs because of the selective oxidation of aluminum (ref. 19). It is also possible, as will be discussed subsequently, that such voids are developed in response of the alloy to the stresses generated by the Al_2O_3 growth. The formation of these voids at the Al_2O_3 -substrate interface causes the oxide to buckle under the action of the compressive stresses in the oxide and the area of detachment between the oxide and the substrate is increased, Figure 23c.

The features of the subsequent oxidation are dependent upon temperature. At temperatures of 1000°C , the oxidation rate is relatively slow and the alloy is not as easily plastically deformed as at higher temperatures. Subsequent oxidation at 1000°C , therefore causes even larger areas of detachment to be developed, Figure 23d. In addition, in those areas where the oxide has become detached, aluminum vapor presumably diffuses across the void and reacts with oxygen to form large distinct crystals of Al_2O_3 , Figure 23d. At higher temperatures, such as 1200°C , wrinkles in the oxide are developed due to the formation of oxide crystals on the surface of the oxide exposed to the void, Figure 23e, which impinge upon one another.* The aluminum which is necessary for this process is transported across the void supposedly as a vapor. At these higher temperatures the previously, planar, oxide-substrate interface is apparently unstable and stresses in the oxide and the alloy are partially relieved by the formation of undulations at this interface, Figure 23e. As the thickness of the scale is increased, the voids at the bottom of the wrinkles become filled with oxide and contact between the oxide and the substrate is re-established, Figure 23f. In addition, it appears that the frequency of the undulations at the oxide-substrate interface is decreased supposedly as a result of the further relief of stresses in the oxide and the alloy. During growth of the Al_2O_3 scales, the orientations of some oxide grains are apparently more favorable for growth than others and the oxide grains therefore become larger and more columnar as growth is continued.

d. Rate of Al_2O_3 Growth

For oxidation times up to about 100 hours the weight-changes and thicknesses as a function of time could be approximated by the parabolic rate law. Typical results are presented in Figure 24 and the parabolic rate constants obtained from such data are presented in Table V where the rate constants determined from the thickness measurements have been converted to units of $\text{gm}^2/\text{cm}^4\text{-sec}$.

*Such a condition was first suggested to the authors by J. Stringer, University of Liverpool, Liverpool, England.

TABLE V
 PARABOLIC RATE CONSTANTS FOR THE OXIDATION OF NiCrAl,
 CoCrAl, NiCrAlY AND CoCrAlY ALLOYS IN AIR

Alloy Designation	Weight-Change Measurements $k_p(\text{gm}^2/\text{cm}^4\text{-sec})$			Thickness Measurements* $k_p(\text{gm}^2/\text{cm}^4\text{-sec})$		
	1000°C	1100°C	1200°C	1000°C	1100°C	1200°C
NiCrAl(AC)	—	$3.0 \cdot 10^{-13}$	—	—	$3.2 \cdot 10^{-13}$	—
NiCrAl(HWA)	$3.9 \cdot 10^{-14}$	$2.4 \cdot 10^{-13}$	$3.0 \cdot 10^{-12}$	$5.1 \cdot 10^{-14}$	$4.3 \cdot 10^{-13}$	$1.6 \cdot 10^{-12}$
NiCrAl(VD)	—	$19.0 \cdot 10^{-13}$	—	—	$9.6 \cdot 10^{-13}$	—
CoCrAl(AC)	—	$15.0 \cdot 10^{-13}$	—	—	$8.4 \cdot 10^{-13}$	—
CoCrAl(HWA)	$1.4 \cdot 10^{-13}$	$9.9 \cdot 10^{-13}$	$5.4 \cdot 10^{-12}$	$8.5 \cdot 10^{-14}$	$6.1 \cdot 10^{-13}$	$4.9 \cdot 10^{-12}$
CoCrAl(VD)	—	$16.0 \cdot 10^{-13}$	—	—	$13.5 \cdot 10^{-13}$	—
NiCrAlY(AC)	—	$11.0 \cdot 10^{-13}$	—	—	$5.0 \cdot 10^{-13}$	—
NiCrAlY(HWA)	$4.9 \cdot 10^{-14}$	$4.2 \cdot 10^{-13}$	$2.9 \cdot 10^{-12}$	$8.6 \cdot 10^{-14}$	$7.6 \cdot 10^{-13}$	$3.2 \cdot 10^{-12}$
NiCrAlY(VD)	—	$3.8 \cdot 10^{-13}$	—	—	$3.3 \cdot 10^{-13}$	—
CoCrAlY(AC)	—	$5.5 \cdot 10^{-13}$	—	—	$6.4 \cdot 10^{-13}$	—
CoCrAlY(HWA)	$1.0 \cdot 10^{-13}$	$8.8 \cdot 10^{-13}$	$3.3 \cdot 10^{-12}$	$13.9 \cdot 10^{-14}$	$8.6 \cdot 10^{-13}$	$3.7 \cdot 10^{-12}$
CoCrAlY(VD)	—	$6.5 \cdot 10^{-13}$	—	—	$5.7 \cdot 10^{-13}$	—

*In the case of scales which contained large irregular oxide crystals, Figure 20 a, the thickness of the continuous layer α oxide was used.

A significant difference between specimens with different fabrication conditions is not evident. The data presented in Table V have also been plotted versus reciprocal temperature. There was scatter of the data points but the data could be fitted with a straight line. An activation energy of 70 kcal/mole was calculated from the slope of this curve. In Figure 25 some of the data obtained for the hot-worked and annealed alloys are plotted in different ways to illustrate certain points. In Figure 25a it can be seen that rate constants obtained from weight-change measurements and thickness measurements are in reasonable agreement. In Figure 25b it can be seen that the rate constants for the nickel-base alloys are slightly less than those for the cobalt-base alloys. The rate constants for the nickel-base alloys are generally less than those for the cobalt alloys by a factor of about 2, Table V. This difference between parabolic rate constants for nickel and cobalt-base alloys is small but it is consistently observed.

The parabolic rate constants which have been obtained for NiCrAl and CoCrAl alloys are consistent with those obtained in previous studies for the growth of Al_2O_3 on alloys (ref. 8). Reliable data for the diffusion of oxygen or aluminum in Al_2O_3 at temperatures between 1000° and 1200°C are not available. Oishi and Kingery (ref. 27) have determined the self-diffusion coefficients for oxygen in single crystal and polycrystalline Al_2O_3 at temperatures up to 1780°C . Paladino and Kingery (ref. 28) have determined the self-diffusion coefficients of aluminum in polycrystalline Al_2O_3 at temperatures between 1670° and 1905°C . At temperatures where data exist for both aluminum and oxygen, the self-diffusion coefficients for oxygen in single crystals are more than an order of magnitude less than those for aluminum. Mistler and Coble (ref. 29) have proposed that aluminum diffusion is the same in polycrystalline and single-crystal Al_2O_3 and that oxygen diffusion is enhanced by the presence of grain boundaries. The enhanced transport of oxygen at a grain boundary is presumed to take place either because the jump frequency of the types of defects present at the grain boundary is greater than in the lattice, or the concentrations of defects in the boundary are higher than those in the lattice. Mistler and Coble have shown that the self-diffusion coefficients for oxygen are greater than those for aluminum when the grain size of the Al_2O_3 is 3 microns or less. For all of the processes involving transport parallel to grain boundaries, the product of diffusivity times boundary width appears as a contributor to the overall flow of atoms. Mistler and Coble (ref. 30) have determined the diffusion coefficients for oxygen along grain boundaries in Al_2O_3 at temperatures between 1650° and 1900°C . These authors have also shown the widths of the grain boundaries in Al_2O_3 at these temperatures are on the order of 100\AA .

If the data obtained by Mistler and Coble (ref. 30) for the diffusion of oxygen along grain boundaries are extrapolated to 1200° and 1000°C and a grain boundary width of 100\AA is used, it is possible to calculate the parabolic rate constants for the growth of Al_2O_3 in the case where this growth is controlled by diffusion of oxygen along grain boundaries. The results obtained, assuming that 1) the diffusion coefficients at a given temperature are constant, 2) the grain size of the Al_2O_3 is one micron, 3) the activity of aluminum at the alloy- Al_2O_3 interface is 0.1, and 4) the oxygen pressure in the gas is 0.2 atm, are $1.7 \cdot 10^{-13}$ and $6.8 \cdot 10^{-16}$ ($\text{gm}^2/\text{cm}^4 \cdot \text{sec}$) at temperatures of 1200° and 1000°C , respectively. The experimental values obtained at 1200° and 1000°C are $3 \cdot 10^{-12}$ and $7 \cdot 10^{-14}$ ($\text{gm}^2/\text{cm}^4 \cdot \text{sec}$), respectively. The agreement between the calculated and experimental values is not good but it is not considered to be unreasonable. The main source of error in the calculated

values arises because of the extrapolation used to obtain the diffusion coefficients. Oishi et al (ref. 27) have found that at temperatures above 1650°C the diffusion of oxygen is controlled by intrinsic defects whereas at temperatures below 1650°C extrinsic defects produced by impurities were important and caused the self-diffusion coefficients for oxygen to be increased. It is proposed that the difference between the calculated and experimental parabolic rate constants and the difference between the rate constants for the cobalt and nickel-base alloys is caused by impurities in the Al₂O₃ scales.

In view of the data available for the diffusion of oxygen in Al₂O₃, as well as the results obtained in this program for the growth of Al₂O₃ scales, it is proposed that the growth of the Al₂O₃ scales on NiCrAl and CoCrAl alloys is controlled by the diffusion of oxygen along grain boundaries in the Al₂O₃ scales. As will be shown subsequently in this report, the growth of Al₂O₃ on NiCrAlY and CoCrAlY alloys takes place at rates similar to those for the growth of Al₂O₃ on NiCrAl and CoCrAl alloys; however, voids are not formed at the Al₂O₃-substrate interfaces of the former alloys. It therefore appears that the voids at the Al₂O₃-substrate interfaces of NiCrAl and CoCrAl alloys do not affect the oxidation kinetics since the transport of aluminum across these voids is rapid in comparison to the diffusion of oxygen through the oxide layer. The evaporation rates of aluminum from an alloy into a vacuum are about $2.5 \cdot 10^{-7}$ and $7.1 \cdot 10^{-7}$ gm/cm²-sec, at 1000° and 1200°C, respectively, assuming an aluminum activity in the alloy of 0.1. After one hour of oxidation the amounts of aluminum required to combine with the oxygen diffusing through the scale are $5.3 \cdot 10^{-9}$ and $3.5 \cdot 10^{-8}$ gm/cm²-sec at 1000° and 1200°C, respectively. The results from these calculations show that the rate of supply of aluminum across the voids is probably rapid in comparison to the diffusion of oxygen through the Al₂O₃ scale. The observed lack of any influence of the voids on the oxidation kinetics is therefore reasonable.

3. THE ADHESION OF Al₂O₃ ON NiCrAl AND CoCrAl ALLOYS

a. Experimental Results

The continuous weight-change versus time data obtained for the isothermal oxidation of NiCrAl and CoCrAl alloys at temperatures between 1000° and 1200°C showed that cracking or spalling of the Al₂O₃ did not occur at temperature. The results obtained from cyclic oxidation tests showed cracking or spalling of the Al₂O₃ occurred after the first cycle to room temperature. Typical cyclic data are presented in Figure 26 where the difference between the cyclic and isothermal weight-change data shows that cracking and spalling of the Al₂O₃ in the cyclic tests are taking place. Such results indicate that the growth stresses are not sufficient to produce spalling of the scale; however, when thermally induced stresses are superimposed upon the growth stresses, spalling of the Al₂O₃ scales always occurs. Spalling of the Al₂O₃ was not observed to be affected by the fabrication condition of the NiCrAl or CoCrAl alloys.

b. Morphological Features of Al₂O₃ Scales

The features of the Al₂O₃ scales which formed on the NiCrAl and CoCrAl alloys have been described previously in this report. In view of the results which were presented, it would seem reasonable to propose that spalling of the Al₂O₃ occurs because the thermally induced stresses are concentrated at locations where voids exist between the scale and the substrate, Figure 23.

It was observed that the voids at the Al_2O_3 -substrate interface were developed not only at grain boundaries and chemical heterogeneities (e.g., β -phase in CoCrAl) in the substrates but also at the edges of specimens and at locations where polishing marks had been present on the surfaces of the specimens. In order to determine if the adhesion of the Al_2O_3 to the substrate could be improved by having fewer voids at the Al_2O_3 -substrate interface, specimens of NiCrAl were electropolished prior to oxidation to remove polishing marks. The surfaces of the oxide scales and substrates after oxidation of an electropolished (1 min. at 8V in a 10 vol. % solution of H_2SO_4 in methyl alcohol contained in an ice bath) specimen and a specimen polished through 600-grit SiC abrasive paper are compared in Figure 27. The surface of the oxide formed on the specimen with the 600-grit finish is highly wrinkled, Figure 27a, whereas the oxide on the electropolished specimen was much smoother except for isolated patches of wrinkles, Figure 27b. The substrate surface of the specimen with the 600-grit finish contained numerous smooth areas, Figure 27c. The surface of the electropolished specimen contained virtually no smooth areas except at the edges of the specimen and was highly imprinted by oxide grains, Figure 27d. Even though many more voids had been present at the interface between the Al_2O_3 and the substrate with the 600-grit finish than at this same interface on the electropolished specimen, the Al_2O_3 spalled profusely from both specimens during cooling.

In a previous study concerned with the spalling of Al_2O_3 from an Fe-25Cr-4Al alloy (ref. 19), void formation was proposed as the cause of oxide scale spalling. An electropolished specimen of this alloy was therefore oxidized and examined. The Al_2O_3 scale spalled but perhaps not as extensively as that observed with specimens polished through 600-grit. No smooth areas were observed on the substrate surface, Figure 28, and the substrate was totally covered with imprints of oxide grains, Figures 28b and 28c. The oxide scale was not wrinkled, Figure 28a, and the oxide surface at the substrate interface contained only a few, isolated voids, Figure 28d.

During this program oxidation experiments were performed in a CO_2 -CO gas mixture with $\text{CO}_2/\text{CO} = 3$ in order to examine the oxidation of NiCrAl and the CoCrAl alloys at an oxygen pressure below that required to form NiO or CoO. The morphological features of the Al_2O_3 scales and substrates on specimens after oxidation in the CO_2 -CO mixture were the same as those observed after oxidation in air with one exception: fewer voids were evident at the oxide-substrate interfaces of specimens oxidized in the CO_2 -CO gas mixture. In the case of the NiCrAl alloy, voids were only evident near the edges of the specimens oxidized in the CO_2 -CO gas mixture. On such specimens the Al_2O_3 scales and the substrate surfaces had a fine orange peel texture, Figure 29a, and the substrate surface also contained a continuous network of imprints of oxide grains, Figure 29c. In comparison, the NiCrAl specimens after oxidation in air had highly wrinkled oxide flakes, Figure 29b, and the substrates contained numerous smooth areas, Figure 29d. The Al_2O_3 was observed to spall profusely from the NiCrAl specimens after oxidation in air or in the CO_2 -CO mixture. Similar results were obtained with the CoCrAl alloy but even after oxidation in the CO_2 -CO gas mixture, some voids had been formed at the oxide-substrate interface at sites where the β -phase was present on specimen surfaces.

Specimens of NiCrAl and CoCrAl were oxidized in the CO_2 -CO mixture for 2 hours and then oxidized 20 hours in air. The specimens were not cooled to room temperature upon

changing from the CO₂-CO mixture to air. The thickness of the Al₂O₃ scales were equivalent to those formed in air after 20 hours of oxidation. Virtually no smooth areas were evident on the NiCrAl specimen except at the edges of the specimen, Figure 30a. The alloy surface contained numerous undulations and was highly imprinted, Figures 30a and 30b. The Al₂O₃ surface at the substrate interface contained ridges and valleys, Figure 30c, corresponding to the features observed on the substrate. These depressions in the Al₂O₃ at the substrate interface did not contain large, protruding crystals of oxide, Figure 30c, and the mating mounds on the substrate were always totally covered with the imprints of oxide grains. These results show that the Al₂O₃ and the substrate were in intimate contact with one another during oxidation except at the edges of the specimen. The Al₂O₃ spalled profusely upon cooling of the specimen to room temperature.

c. Mechanism For Spalling From NiCrAl and CoCrAl Alloys

The results obtained from the studies concerned with the adhesion of Al₂O₃ on NiCrAl and CoCrAl alloys indicate that spalling of the Al₂O₃ scales occurs because of the effects produced by thermally induced stresses. The thermally induced stresses, which are generated during cooling of specimens are distributed in a fashion similar to that for the growth stresses illustrated in Figure 23a. It is not clear if superposition of the growth and thermally induced stresses is required for spalling of the Al₂O₃ scales. It is apparent that the compressive stresses which exist in the oxide during cooling are greater than the strength of the Al₂O₃-substrate interfacial bond. In addition, voids at the Al₂O₃-substrate interface are not required to initiate fracture along this interface. For example, even on specimens where void formation had occurred only at the edges of specimens, spalling of the Al₂O₃ was observed to begin at locations far removed from the edges of the specimens.

While void formation at the Al₂O₃-substrate interface is not a necessary precursor for spalling of Al₂O₃ scales from NiCrAl, CoCrAl or FeCrAl alloys, it appears that the initiation of spalling does occur at locations where voids are present. For example, the initial sites of oxide spallation were often marked by tarnish colors on the substrate (due to exposure of the substrate at a comparatively higher temperature. These tarnish color markings were observed to be invariably at locations where voids had been developed along the Al₂O₃-substrate interface.

It appears as though the formation of the voids along the oxide-substrate interface must involve, in some way, the diffusion of vacancies to this interface. The fact that voids are frequently observed at the edges of specimens indicates that some configurations of the Al₂O₃-substrate interface are more favorable for void formation than others. Other factors also appear to influence void formation. The lack of voids on specimens prepared by electropolishing indicates that residual stresses on the substrate surface may play some role in void formation. The absence of voids on specimens which were oxidized in the CO₂-CO mixture indicates that the transient oxides which are formed during oxidation in air may favor void formation. Finally, voids were observed at the Al₂O₃-substrate interfaces at grain boundaries in the alloys and where the β -phase had been present in the CoCrAl alloy. The reason that voids are associated with the β -phase is not known.

In summary, the mechanism by which voids are initiated at the Al_2O_3 -substrate interfaces is not known. These voids do serve as sites for the initiation of oxide spallation but they are not required for spalling of Al_2O_3 scales.

4. THE EFFECT OF YTTRIUM ON THE RATE OF GROWTH AND THE GROWTH MECHANISM OF Al_2O_3

a. Oxide Formation

Continuous layers of Al_2O_3 were developed on the NiCrAlY and CoCrAlY alloys during a transient period of oxidation where processes similar to those illustrated in Figure 11 for NiCrAl and CoCrAl alloys took place. Transmission electron micrographs of oxide films formed on the NiCrAlY alloy after 5 minutes of oxidation, Figure 31a, showed that the film was more uniform than films formed on the NiCrAl alloy after a similar treatment, Figure 12a. Electron diffraction analyses of the films removed from the NiCrAlY alloy detected Al_2O_3 , Cr_2O_3 and NiAl_2O_4 . Nickel oxide was not detected as in the case of the NiCrAl alloy. In addition, the size of the grains in the oxide film on the NiCrAlY specimen were about an order of magnitude smaller than those in the film removed from the NiCrAl specimen. While the grain size of the initial oxide films formed on NiCrAlY and NiCrAl were different, it must be emphasized that these films were composed of different phases. It appeared that the transient oxidation period required for the formation of an Al_2O_3 layer on the NiCrAlY and CoCrAlY alloys was shorter than that for NiCrAl and CoCrAl alloys. Nevertheless, it was not unusual to observe localized patches of transient oxides on the NiCrAlY and CoCrAlY alloys, similar to those shown in Figure 12b, for oxidation times up to about 8 hours. This condition was especially true for alloys in the as-cast condition.

While the development of Al_2O_3 scales on the NiCrAlY and CoCrAlY alloys appeared to occur by a mechanism similar to that for the NiCrAl and CoCrAl alloys, the oxidation of yttrium in the former alloys did occur during and after the development of the continuous Al_2O_3 scales. Examination of NiCrAlY and CoCrAlY alloys after oxidation showed that the surfaces of the Al_2O_3 scales at the gas interface contained a network of oxide which was rich in yttrium, Figure 31b. At points where spalling of the Al_2O_3 had occurred, this same network was evident in the substrate, Figure 31b, and it appeared as though the yttrium-rich portions extended completely through the oxide scale to the substrate. This condition indicated that yttrides, which were known to be present at grain boundaries of the NiCrAlY and CoCrAlY alloys, were being preferentially oxidized. The conditions which developed in the oxide scale as a result of the oxidation of yttrium will be described in detail in the following section.

b. Morphologies of Al_2O_3 Scales

The Al_2O_3 scales which developed on the NiCrAlY and CoCrAlY alloys were much more adherent than the Al_2O_3 formed on NiCrAl and CoCrAl alloys. On the NiCrAlY and CoCrAlY alloys the surfaces of the Al_2O_3 at the oxide-gas interface did not contain wrinkles, Figure 32a. The surfaces of the Al_2O_3 at this interface otherwise contained features similar to those observed with NiCrAl and CoCrAl alloys except for the network of yttrium-rich oxides and the absence of filamentary protrusions. At locations

where the Al_2O_3 scales had spalled, the substrate surfaces were relatively flat, Figure 32b, and completely covered with imprints from oxide grains, Figure 32c. These substrate surfaces, however, did contain grooves, Figure 32b, at sites where protrusions of oxide had extended into the alloys, Figure 32d.

Since the Al_2O_3 scales which formed on the NiCrAlY alloys were frequently adherent, the surfaces of these scales at the substrate interface were examined by dissolving the alloys in a 10 percent bromine-methanol solution. The extracted oxide flakes were separated from the solution by filtering and subsequently were washed in pure methanol. Typical features of the Al_2O_3 at the substrate interface are presented in Figure 33. The oxide contained a network of oxide protrusions, Figure 33a, which extended into grain boundaries of the alloy, Figure 33c. Electron-beam microprobe analyses showed that these protrusions contained predominantly yttrium and were probably Y_2O_3 , except at locations where reaction with Al_2O_3 had occurred to form a double oxide. The Al_2O_3 surface contained well defined oxide grains, Figure 33b. Examination of transverse sections through the Al_2O_3 scales showed that the yttrium-rich protrusions extended completely through the oxide scale. This condition was especially obvious after long periods of oxidation where some of these protrusions were totally incorporated into the Al_2O_3 scales, Figure 34a, whereas others still extended into the alloy and were partially enveloped with Al_2O_3 , Figure 34b. The incorporation of the yttria stringers into the Al_2O_3 scales is considered to be conclusive proof that the Al_2O_3 is formed predominantly via the inward diffusion of oxygen. Even after 1000 hours of oxidation, remnants of the yttria stringers were evident on the surface of the Al_2O_3 at the oxide-gas interface, Figures 34c and 34d, which shows that virtually no outward growth of the Al_2O_3 takes place.

The surfaces of extracted Al_2O_3 flakes at the substrate interface always exhibited the coarse network of oxide protrusions, Figure 35a. On numerous flakes extremely small oxide protrusions were also evident, Figures 35b and 35c. The density of these smaller protrusions was observed to vary from flake to flake. On some flakes particle densities such as those shown in Figures 35b and 35c were observed. Other flakes appeared to contain only a small number of these particles. It was attempted to determine the composition of these particles by using an energy dispersive technique. Yttrium was detected in large particles. Yttrium was not detected in the smaller particles, but it is believed that these particles may have been too small to generate detectable intensities. Electron-beam microprobe analyses of alloys with the oxide scales in situ were also performed. Numerous analyses were performed normal to the oxide-substrate interface and typical results are presented in Figure 36. The yttrium concentration frequently was observed to increase near the oxide-substrate interface. However, in some analyses no intensity increase for yttrium was observed whereas in others the yttrium intensity peaked in the oxide scale. Analyses were also performed parallel to the oxide-substrate interfaces at depths of 3 and 30 microns within the alloy. The results obtained at a depth of 3 microns are presented in Figure 37. It can be seen that the yttrium concentration varies in a fashion that would be expected for the small particles shown in Figures 35b and 35c. At a depth of 20 microns in the alloy, Figure 37, no such variations in the yttrium concentration were observed. It is believed that these results indicate small particles of Y_2O_3 are formed within these alloys and that these particles become incorporated within the inward growing Al_2O_3 scales along with the more coarse protrusions.

Since the formation of the network of coarse oxide protrusions appeared to be related to the oxidation of yttrides in the alloy, a Ni-15Cr-6Al-3Y alloy, which contained a continuous network of an yttride, Figure 38a, was oxidized in order to examine the oxidation behavior of yttrides in more detail. The surface of this alloy after 30 minutes of oxidation at 1200°C is shown in Figure 38b. This oxidized surface contained an oxide network with a pattern similar to that of the yttride phase in this alloy. A transverse section through a specimen after 1 hour of oxidation, Figure 38c, showed that the alloy surface was covered with a thin layer of Al_2O_3 except at the oxide network where preferential oxidation of the yttride had occurred. The results obtained from examining one of these sites of preferential oxidation with the electron-beam microprobe are presented in Figure 39. It can be seen that the oxidation front is not in contact with the yttride, Figure 39a; a zone denuded of yttrium, Figures 39a and 39c, has developed between the yttride and the zone of yttrium oxide particles. It is also to be noted that the oxide formed by the preferential oxidation of the yttride is completely separated from the alloy by an oxide rich in aluminum, Figure 39b, probably Al_2O_3 . Chromium and nickel were also detected in the oxide formed by preferential oxidation of the yttride. The nickel was usually concentrated in the outer portions of the oxide near the surface of the specimen. Chromium was detected in the oxide and also in the zone of alloy between the oxide protrusion and the retreating yttride, Figure 39d.

The results obtained with the Ni-15Cr-6Al-3Y alloy show that the yttrides on the surfaces of NiCrAlY and CoCrAlY alloys are preferentially oxidized. This preferential oxidation of yttrides occurs because the yttrides in NiCrAlY and CoCrAlY alloys contain in addition to yttrium predominantly nickel and cobalt, respectively, and transport through the oxides of these metals takes place at rates much greater than those for transport through Al_2O_3 . The extent of this preferential oxidation is dependent upon the size of the yttrides and temperature. In NiCrAlY and CoCrAlY alloys preferential oxidation of yttrides does not necessarily continue indefinitely, however, since a continuous layer of Al_2O_3 can be developed between the alloy and the area of preferential oxidation, Figure 39b. The formation of the Al_2O_3 at the front of the zone of preferential oxidation occurs because a diffusion zone is developed between the yttride and the zone of preferential oxidation, Figure 39a. Particles of yttrium oxide are formed within this diffusion zone, Figures 38c and 39c. In addition, aluminum and chromium from the surrounding alloy diffuse into this zone and a continuous layer of Al_2O_3 can be developed. After a continuous layer of Al_2O_3 is developed at the site of preferential oxidation, yttrium from the yttride continues to be oxidized internally because yttrium has a greater affinity for oxygen than aluminum. It appears that yttrium diffuses from the yttride to the zone of internal oxidation at which a stringer of yttrium oxide, probably Y_2O_3 , is developed, Figure 38d. These stringers of yttrium oxide are then incorporated into the Al_2O_3 scale since the Al_2O_3 is formed by the inward diffusion of oxygen. These stringers or protrusions of yttrium oxide are usually located at the grain boundaries of the alloys, Figure 33c. This condition is reasonable since the yttrides in NiCrAlY and CoCrAlY alloys are located at the grain boundaries of these alloys. It also appears, however, that only those yttria stringers at grain boundaries grow to any significant extent which indicates that yttrium diffusion in the alloys occurs predominantly along grain boundaries in the alloys.

Transverse sections through Al_2O_3 scales from NiCrAlY and CoCrAlY alloys were examined to compare the structures of these scales to those from NiCrAl and CoCrAl alloys. A photograph of a polished section through an Al_2O_3 scale from a CoCrAlY alloy is presented in Figure 40a. The incorporation of the yttria stringers is readily apparent and in some instances the stringers were observed to extend completely through the Al_2O_3 scale and emerge at the oxide-substrate interface as a protrusion, Figure 40b. Photographs which show microstructural features of etched Al_2O_3 scales are presented in Figures 40c and 40d. The oxide grains appear to be smaller near the oxide-gas interface and more coarse and columnar near the oxide-substrate interface. The grain structure of the Al_2O_3 -scales which formed on the alloys that contained yttrium is not markedly different from those formed on alloys without any yttrium.

c. The Effect of Yttrium on the Growth Rate of Al_2O_3

The oxidation kinetics which were obtained for the NiCrAlY and CoCrAlY alloys conformed to the parabolic rate law. As can be seen in Table V and Figure 25c, the parabolic rate constants obtained for the alloys which contained yttrium were not affected by alloy fabrication conditions and were similar to those for alloys which did not contain any yttrium. It therefore appears that the growth rates of Al_2O_3 scales on NiCrAl, NiCrAlY, CoCrAl and CoCrAlY alloys are controlled by the diffusion of oxygen along grain boundaries in the Al_2O_3 scales and that yttrium does not influence these growth rates. Such a proposal is consistent with the observation that the grain size of the Al_2O_3 scales was not substantially modified by yttrium in the alloys. Voids were developed at the Al_2O_3 -substrate interfaces during oxidation of NiCrAl and CoCrAl alloys but no voids were observed at these interfaces on NiCrAlY and CoCrAlY alloys. Previous considerations in this report have shown, however, that such voids apparently do not affect the growth rates of the Al_2O_3 scales. It is also worth noting that the yttria protrusions which were formed at the oxide-substrate interfaces on the NiCrAlY and CoCrAlY alloys did not affect the magnitude of the parabolic rate constants. These protrusions would not be expected to affect the rate constants determined from thickness measurements of the Al_2O_3 scales. The fact that the rate constants determined from the weight-change measurements are also not influenced by the formation of these protrusions indicates that the amount of oxygen combined with yttrium is small in comparison to that combined with aluminum.

In this program the weight-change and thickness measurements were usually obtained for oxidation times up to 100 hours. At 1200°C , however, oxide thickness measurements were also performed on scales removed from some alloys after approximately 3700 hours of oxidation. The results from these measurements are presented in Figure 41. A significant difference between the thicknesses of scales removed from cobalt or nickel base alloys was not evident. Furthermore, the thicknesses of the scales were not influenced by yttrium within the alloys. These thicknesses conformed to the parabolic rate law up to about 400 hours. For longer periods of oxidation, the oxidation rate is smaller than that required for conformance with the parabolic rate law. The initial parabolic rate constant, k_p^0 , is about five times larger than the rate constant obtained by drawing a straight line through the longer-time data points, K_p^{3700} . Since the growth rate of the Al_2O_3 is believed to be controlled by the diffusion of oxygen along grain boundaries, the observed decrease of the parabolic rate constant should be accompanied by an increase in the size of the grains in

the oxide scale. Moreover, if the widths of the grain boundaries in the oxide are not assumed to change with time, the oxide grains should increase by about a factor of five. The oxide grains in the Al_2O_3 scales after approximately 3700 hours of oxidation were about a factor of 2 greater than the grains in scales formed by oxidation up to 100 hours. The agreement between the ratio of parabolic rate constants and the ratio of the sizes of the grains in the Al_2O_3 scales is not good enough to conclude that the decreased rate after long periods of oxidation has been caused by grain growth, but at the present time such a proposal seems to be a reasonable one.

d. The Effect of Yttrium on the Growth Mechanism of Al_2O_3

The results obtained from the studies with NiCrAl, NiCrAlY, CoCrAl and CoCrAlY alloys show that yttrium does not affect the growth rate nor the growth mechanism of Al_2O_3 on NiCrAlY or CoCrAlY alloys. Even though the growth of Al_2O_3 on alloys with or without yttrium occurs by the diffusion of oxygen along grain boundaries in the Al_2O_3 scales, there are certain features of the oxidation mechanism for the alloys containing yttrium which are worth further discussion.

In discussing the oxidation mechanism for NiCrAlY and CoCrAlY alloys it is convenient to use the schematic diagrams presented in Figure 42. The solubility of yttrium in NiCrAl and CoCrAl alloys is less than 0.04 percent and therefore all of the NiCrAlY and CoCrAlY alloys, used in this program, contained yttride precipitates at grain boundaries of these alloys as illustrated in Figure 42a. The sizes and shapes of these yttride precipitates were dependent on the fabrication condition of the alloys. These precipitates were much smaller in the hot-worked and annealed and vapor-deposited alloys compared to those in as-cast alloys. In many cases, however, these precipitates were formed as elongated stringers at grain boundaries. It therefore is not practicable nor necessary to specify the different sizes and shapes of these precipitates. It is sufficient to consider these alloys as having discontinuous precipitates of yttrides at grain boundaries as illustrated in Figure 42a. Finally, the composition of these yttrides has not been determined. It has been found that they contain primarily nickel or cobalt in addition to yttrium and they probably are compounds such as Ni_{17}Y_2 (ref. 31).

As alloys such as that illustrated in Figure 42a are oxidized, a continuous layer of Al_2O_3 is developed over the alloy surface except at areas where yttrides are exposed to the oxidizing environment, Figure 42b. In such areas preferential oxidation of yttrides occurs and NiO or CoO and yttrium oxides are formed. Since these oxides do not afford as much protection to the alloy as Al_2O_3 , the amount of oxidation is more extensive at the yttrides than where the continuous Al_2O_3 layer has been developed. As oxidation is continued, zones, denuded of yttrium but containing yttrium oxide particles, are developed between the yttrides and the oxides formed as a result of preferential oxidation of the yttrides. Aluminum and chromium from the alloy diffuse into this zone and Al_2O_3 and Cr_2O_3 particles are developed. Eventually the volume fraction of the Al_2O_3 particles becomes sufficient to allow the development of a continuous layer of Al_2O_3 around the oxides formed by preferential oxidation of the yttrides. The Al_2O_3 layers which have enveloped these oxides formed by preferential oxidation of the yttrides, however, do contain stringers of yttrium oxide, Figure 42c, that developed in the diffusion zone. In addition, these stringers of yttrium oxide grow into the alloy as yttrium is supplied by yttrides located on grain boundaries deeper

within the alloy, Figure 42c. In cases where yttrides are not exposed on the alloy surface, yttrium oxide stringers are developed beneath the continuous Al_2O_3 layer at grain boundaries in the alloy, Figure 42b. As oxidation continues, such stringers are incorporated into the inward growing Al_2O_3 scale, but they also grow deeper into the alloy as yttrium is supplied from yttrides deeper in the alloy via grain boundary diffusion, Figure 42c.

As in the case of NiCrAl and CoCrAl alloys, the formation of the Al_2O_3 layers on NiCrAlY and CoCrAlY results in the development of compressive stresses in the Al_2O_3 and the alloy adjacent to the Al_2O_3 scale is in tension, Figures 42b and 42c. The formation of the large yttrium oxide pegs at grain boundaries, as well as the formation of smaller particles of yttrium oxides due to oxidation of yttrium in solution in the alloy, Figure 42d, may cause the alloy to deform such that these stresses are at least partially relieved. As the Al_2O_3 scale continues to grow inward, the coarse protrusions and the particles of yttrium oxide are incorporated into the Al_2O_3 scale, Figure 42e. In addition, these protrusions continue to grow deeper into the alloy and new particles of yttrium oxide are developed within the alloy for reasons discussed previously, Figure 42e.

After long periods of oxidation, grain growth in the alloy does occur and some grain boundaries are annihilated. Under such conditions, the protrusions of yttrium oxide over the annihilated grain boundaries cease to grow and are completely incorporated into the Al_2O_3 scale. Figure 42f.

In this mechanism which has been proposed for the oxidation of NiCrAlY and CoCrAlY alloys, the amount and distribution of yttrides in the alloys is important. If the yttrides are large and continuous, the development of conditions, whereby an Al_2O_3 layer is developed with subsequent oxidation of only yttrium from the yttride, may require long periods of oxidation. During these longer periods of oxidation severe oxidation of the yttrides occurs and therefore large, continuous precipitates of yttrides in these alloys are an undesirable condition. On the other hand, if the yttrides are small and discontinuous and the grain size of the alloy is small, numerous coarse protrusions of yttrium oxide will extend as pegs from the oxide into the alloy. The effects produced by such pegs will be considered subsequently as the effects of yttrium on the adhesion of Al_2O_3 are examined.

In comparing the proposed mechanisms for the growth of Al_2O_3 on alloys with and without yttrium, Figures 23 and 42, it is apparent that voids or separations are not supposed to be formed at the Al_2O_3 -substrate interfaces of alloys containing yttrium. There are a number of possible reasons as to why this condition should prevail. First, yttrium in solution in the alloy or the particles of yttrium oxide in the alloy may provide sinks for the vacancies required to form the void (ref. 19). Secondly, even if voids are formed at this interface, conditions are not favorable for their growth. Yttrium oxide would be formed in the void due to oxidation of yttrium in the alloy. Finally, in order to form separations of the size observed on NiCrAl and CoCrAl alloys, some detachment of the Al_2O_3 from the alloy is required. Conditions for the detachment of the Al_2O_3 from NiCrAlY and CoCrAlY alloys are less favorable than those developed on these alloys without yttrium for reasons which will be discussed subsequently.

The proposed mechanism for the growth of Al_2O_3 on NiCrAl and CoCrAl alloys does not account for the formation of filamentary protrusions at the Al_2O_3 -gas interface. Generally no such filamentary growths were observed on Al_2O_3 scales from the NiCrAlY and CoCrAlY alloys. At present, it is not known exactly how these whiskers are developed or why they usually are not formed on the alloys which contained yttrium.

5. THE EFFECT OF YTTRIUM ON THE ADHERENCE OF Al_2O_3

a. Cyclic Oxidation Test Results

The addition of yttrium to either NiCrAl or CoCrAl alloys resulted in a substantial increase in the adherence of the Al_2O_3 scales formed during oxidation. Continuous weight-change versus time data obtained for the cyclic oxidation of these alloys are presented in Figures 43 and 44. Thermal cycling of the NiCrAl and CoCrAl alloys resulted in cracking and spalling of the oxide scale as is evident from the shapes of the weight-change versus time curves, Figure 43. The weight changes obtained for NiCrAlY and CoCrAlY alloys in this test did not indicate that a significant amount of oxide cracking and spalling had occurred, Figure 44.

Yttrium was effective in improving the adhesion of Al_2O_3 on alloys in any of the three fabrication conditions used in this program. Yttrium was most effective, however, in developing resistance to spalling of Al_2O_3 when alloys were in the hot-worked and annealed or vapor-deposited conditions. The microstructures of as-cast and vapor-deposited CoCrAlY after cyclic oxidation testing at 1100°C are presented in Figure 45. After 500 hours of testing the specimen with the as-cast fabrication condition had been depleted of aluminum to the extent that internal, particulate Al_2O_3 is formed rather than a continuous, external scale of Al_2O_3 , Figure 45a. The specimen with the vapor-deposited fabrication condition still had an adherent, continuous, external layer of Al_2O_3 after 1000 hours of testing, Figure 45b. While the as-cast fabrication condition was not as effective as the other two fabrication conditions in permitting yttrium to be used to improve the adhesion of Al_2O_3 , it must be emphasized that the adhesion of Al_2O_3 to as-cast alloys which contained yttrium was still very much better than the adhesion of Al_2O_3 to alloys with no yttrium. Such a condition is clearly evident upon examining the cyclic oxidation data presented in Figure 46.

The adherence of Al_2O_3 to NiCrAl and CoCrAl alloys was not influenced by alloy microstructure. The Al_2O_3 always spalled from these alloys during cooling from the temperature of oxidation regardless of the fabrication condition and the morphological features of the spalled Al_2O_3 flakes from these alloys were similar. The morphological features of the Al_2O_3 flakes extracted from the yttrium-containing alloys were dependent upon the fabrication condition or, more accurately, upon the alloy microstructure. In Figure 47 photographs are presented which show the surfaces of Al_2O_3 flakes (oxide-gas interface) removed from alloys having different microstructures. The macropeg network on the flake removed from the as-cast alloy, Figure 47a, is much less extensive than the macropeg networks on the flakes removed from alloys in the hot-worked and annealed, Figure 47b, or vapor-deposited, Figure 47c, conditions. This difference between the macropeg networks has apparently resulted in the inferior adhesion of the Al_2O_3 on the as-cast alloys.

b. Mechanism By Which Yttrium Affects Adherence of Al_2O_3

In discussing the mechanism by which yttrium improves the adhesion of Al_2O_3 , it is convenient to consider the consistency of the results obtained in this program with the different mechanisms that have been proposed to account for the observed effects.

(1) Enhanced Oxide Plasticity — It has been proposed that elements such as yttrium may improve the adhesion of Al_2O_3 on alloys by causing the Al_2O_3 to be more easily deformed and thereby allowing the relief of growth and thermally induced stresses which would otherwise have caused spalling of the Al_2O_3 . In the present studies more apparent deformation of the Al_2O_3 has been observed on the alloys which did not contain yttrium than on those containing yttrium. It therefore is concluded that this proposed model can not be used to account for the effects produced by yttrium.

Deformation of the alloys is another means by which stress relief may occur. If the alloys that contain yttrium can be deformed at lower stress levels than those which do not contain yttrium, then the Al_2O_3 will be subjected to less stress on the systems that contain yttrium. In a later section of this report, where oxidation under externally applied loads will be discussed, it will be shown that at $1100^\circ C$, the loads required to deform the alloys are not significantly affected by yttrium concentration. It therefore is believed that deformation of the alloy is not a viable means to account for the effects produced by yttrium on oxide adhesion.

(2) Graded Seal Mechanism - The graded seal mechanism is based on the supposition that a layer of oxide is developed between the Al_2O_3 and the alloy which possesses thermal expansion coefficients that gradually change from values similar to those of the alloy to values close to those of Al_2O_3 as one proceeds through this layer from the alloy to the Al_2O_3 . In the present studies no such continuous layer has been observed. In addition, the interfaces between numerous Al_2O_3 scales and their substrates have been examined with sufficient detail to show that for the systems studied no such continuous, intermediate layer is developed. In the alloys which contain yttrium, immediately adjacent to the Al_2O_3 scale, oxide stringers and particles are present, Figures 33 and 35. The amount of oxide in this zone increases as one proceeds from the alloy towards the Al_2O_3 scale. This zone could therefore possess thermal expansion coefficients that gradually change from values similar to those of the alloy to values close to those of the Al_2O_3 .

The mechanisms proposing increased oxide or substrate plasticity, graded seals or modification of the thermal expansion coefficients of the alloys and/or the oxides are all based on the concept that the Al_2O_3 scales are adherent since less stress is developed at the Al_2O_3 - alloy interface. When oxidized specimens of CoCrAlY are bent at room temperature after oxidation, it is evident that rather severe stresses can be imposed on such specimens without producing the amount or type of oxide spalling that is observed on CoCrAl, as can be seen by comparing Figures 48 and 49. Such results show that any mechanism to account for the improved adhesion of the Al_2O_3 must involve an improvement of the bond (i.e. chemical and/or mechanical) between the scale and the substrate. In view of this condition it is believed that all models which propose improved adhesion because of stress relief or the absence of any stress development are not acceptable.

(3) Chemical Bonding — The adhesion of Al_2O_3 on alloys is dependent upon the nature of the atomic bonds which are developed across the oxide-substrate interface. It has been found that impurities which have a higher affinity for oxygen than the metals in which they are in solution can play a dominant role in the adhesion of oxides to metals by developing stronger atomic bonds across the oxide-substrate interface (ref. 32). The standard free energies of formation for Y_2O_3 are more negative than those for NiO , CoO , Cr_2O_3 and Al_2O_3 . It is therefore possible that yttrium may improve the adhesion of Al_2O_3 on $NiCrAl$ and $CoCrAl$ alloys by causing stronger chemical bonds to be developed across the oxide-substrate interface.

In a previous study it was determined that an adherent layer of Al_2O_3 was formed on a Fe-25Cr-4Al alloy which contained a dispersion of about two volume percent Al_2O_3 (ref. 19). In the present program it was also observed that Al_2O_3 particles in the $CoCrAl$ alloy caused the adherence of the Al_2O_3 scale to be increased significantly. Surface photographs of oxidized specimens are presented in Figure 50 which show that more spalling of Al_2O_3 occurs from the $CoCrAl$ alloy that did not contain any oxide particles. Examination of such specimens with the SEM showed that the Al_2O_3 scale did spall from the alloy with oxide particles, Figure 50c, but the degree of spalling was much less than that for an alloy that did not contain oxide particles or yttrium, Figure 50d.

The observation that Al_2O_3 particles can be used to improve the adhesion of Al_2O_3 scales to alloys cannot be explained in terms of a chemical bonding mechanism. These observations are consistent with models to be discussed subsequently. More work may be required before the chemical model can be eliminated. Nevertheless, based on the available data, it is reasonable to conclude that the formation of yttrium oxide particles and protrusions in the alloy are more critical in improving the adhesion of Al_2O_3 than are any chemical bonding effects.

(4) Vacancy Sink Mechanism — The vacancy sink model is based upon the assumption that the formation of voids at the Al_2O_3 -substrate interface leads to spalling of the Al_2O_3 . The results obtained in this program show that such void formation does result in less adherent scales. On the other hand, it has been observed that profuse spalling of Al_2O_3 from $NiCrAl$, $CoCrAl$ and $FeCrAl$ alloys can take place when voids are not present at the Al_2O_3 -alloy interface. It is also important to note that, when yttrium was present in $NiCrAl$ and $CoCrAl$ alloys, voids were not detected at the interfaces between the oxides and the alloys. The results which have been obtained therefore indicate that yttrium does prevent the formation of voids at the Al_2O_3 -alloy interface and this absence of voids does result in more adherent scales. However, the observed adherence of the scales on the yttrium-containing alloys was greater than that observed on alloys where voids were not present at the oxide-alloy interface and therefore yttrium must be affecting the adherence of Al_2O_3 by some other process in addition to that described by the vacancy sink mechanism.

(5) Mechanical Keying or Pegging Mechanism — In the pegging mechanism it is proposed that oxide pegs are developed at the Al_2O_3 -alloy interface which mechanically key the Al_2O_3 to the alloy and adherence of the Al_2O_3 to the alloy is therefore improved. In the present studies pegs extending into the alloy from the Al_2O_3 have been observed. The coarse network of yttrium — rich oxide protrusions can be considered as

macropegs whereas the smaller particles of yttrium rich oxide can be called micropegs. Since the Al_2O_3 scales are formed by inward growth, these macro and micropegs are effectively incorporated into the Al_2O_3 scale and the alloy. It is reasonable to suppose that this condition should improve the adherence of the Al_2O_3 .

In the experiments which were performed to obtain oxide thickness data for times beyond 100 hours, it was observed that the Al_2O_3 scales spalled from the NiCrAlY and CoCrAlY alloys much more extensively than after oxidation of these alloys for times up to 100 hours. Even though the spalling of the Al_2O_3 from these specimens was extensive after oxidation times greater than 100 hours, no evidence of void formation at the Al_2O_3 -substrate interface was observed. Metallographic examination of NiCrAlY and CoCrAlY specimens after 1000 hours of oxidation showed, Figure 51, that as a result of grain growth in these alloys the macropeg densities were much less than those observed in these alloys after oxidation for times less than 100 hours. These results indicate that spalling of the Al_2O_3 after long periods of oxidation may have occurred because of the smaller macropeg density. It is also possible, however, that larger stresses were developed at the oxide-substrate interface due to the thicker scales which are formed on these alloys.

Since the oxide scales that formed after 1000 hours of oxidation were thick, the NiCrAlY and CoCrAlY specimens were repolished and oxidized 24 hours at 1200°C in air in order to permit examination of the adhesion of Al_2O_3 on these alloys at a smaller oxide thickness. In polishing these specimens the amount of metal removed was less than the depth of the oxide pegs that were observed to extend into these specimens as a result of the previous 1000 hours of oxidation, Figure 51b. This procedure was used since it was desired to determine if thinner Al_2O_3 scales would spall from alloys with small macropeg densities. During the subsequent oxidation of these repolished specimens, new macropegs should not be formed since the yttride phases near the surfaces of these alloys had been consumed during the initial 1000 hours oxidation treatment. After the second oxidation treatment, the Al_2O_3 was adherent over a large fraction of the surfaces of these two alloys. Typical results are presented in Figure 52 for the NiCrAlY specimen. As shown in Figure 52, spalling of the Al_2O_3 was confined predominantly to the network of macropegs formed during the initial 1000 hours period of oxidation. Away from this network the oxide was adherent. In addition, no macropegs were observed to extend into the alloy from beneath the adherent oxide as shown in Figure 52b. While the oxide which formed on the reoxidized specimens did not appear to be as adherent as that formed on alloys which received no pretreatment, since some detachment of the oxide was evident after preparation for metallographic examination, there was no question that the oxide was much more adherent than that formed on alloys without yttrium after 24 hours of oxidation. The adherent Al_2O_3 on the repolished and subsequently oxidized NiCrAlY specimen, Figure 52a, was extracted by dissolving the alloy in a bromine-methanol solution and the surfaces of the extracted oxide were found to contain numerous micropegs of yttrium oxide at the oxide-substrate interface, Figure 52c.

The results obtained with these repolished and oxidized specimens show that micropegs can be effective in improving the adhesion of Al_2O_3 . The observed dependence of Al_2O_3 adherence on the fabrication condition indicates that the macropeg network also affects the scale adhesion. When the macropeg network was not extensive, as occurred in the case of

alloys with as-cast microstructures, Figure 47a, more spalling of the oxide was observed than for fabrication conditions such as hot-worked and annealed or vapor-deposited where more extensive macropeg networks were developed, Figures 47b and 47c.

In a previous study (ref. 19), specimens of Fe-25Cr-4Al-0.2Sc were oxidized for about 1000 hours at 1200°C and it was observed that the Al₂O₃ scale was adherent even though the macropegs had been incorporated into the scale. Based upon this condition it was concluded that the scandium improved the scale adhesion by preventing void formation at the oxide-alloy interface. Since it is now apparent that oxide particles are formed in such systems even after long periods of oxidation and that these particles are incorporated into the Al₂O₃ scale, the observed adherence of the Al₂O₃ on the FeCrAlSc alloy could have been due not only to the absence of voids at the oxide-alloy interface but also due to the mechanical keying effect produced by the micropegs.

(6) Summary -- Of the models which are available to account for the improved adhesion of Al₂O₃ on alloys that contain yttrium, the results obtained in this program support the pegging and vacancy sink models. It is proposed that yttrium causes the adherence of Al₂O₃ on NiCrAl and CoCrAl alloys to be improved since yttrium oxides are developed in these alloys beneath the Al₂O₃. These yttrium oxides are formed as fine particles, micropegs, and coarser protrusions, macropegs, both of which serve to mechanically key the Al₂O₃ to the substrate and which also serve as sites for vacancy condensation thereby preventing void formation at the oxide-alloy interface. Since the oxide particles and protrusions serve both as mechanical pegs and vacancy sinks, it is difficult to determine which of these effects is the more important to the adherence of the oxide scale. For the alloys studied in this program, rather extensive spalling of the oxide scale was observed even though voids were not evidently present at the oxide-substrate interface. It therefore appears as though the mechanical keying effect produced by the yttrium oxide particles is a critical part of the process.

6. THE EFFECT OF OXIDE DISPERSIONS IN ALLOYS ON THE ADHERENCE OF Al₂O₃

a. Introduction

Since it is now apparent that oxide particles can also be used to improve the adhesion of oxide scale on alloys (refs. 19 and 22), NiCrAl and CoCrAl alloys, which contained oxide particles as described in Section II, were included in the present program in order to compare any effects produced by the oxide particles and yttrium. In the following, the data obtained from experiments with the alloys containing oxide dispersions are presented and compared with results from experiments using alloys that contained yttrium. The mechanism by which oxide particles and yttrium influence the scale adherence is then discussed.

b. Experimental Results

Specimens of NiCrAl-ThO₂, CoCrAl-Al₂O₃ and CoCrAl-Y₂O₃ were oxidized in air at 1100°C. In the isothermal experiments parabolic rate constants were obtained that showed continuous layers of Al₂O₃ were developed on the NiCrAl-ThO₂ and CoCrAl-Y₂O₃

specimens. For example, specimens of these two alloys were oxidized for 100 hours and parabolic rate constants of $0.7 \cdot 10^{-12}$ and $1.0 \cdot 10^{-12}$ $\text{gm}^2/\text{cm}^4\text{-sec}$ were obtained from the weight-change versus time data for NiCrAl-ThO₂ and CoCrAl-Y₂O₃, respectively. These rate constants are in satisfactory agreement with those presented in Table V for NiCrAl, NiCrAlY, CoCrAl and CoCrAlY alloys. A continuous layer of Al₂O₃ was not developed on the CoCrAl-Al₂O₃ alloy during isothermal oxidation in air. The chromium and aluminum content of this alloy was insufficient to result in selective oxidation of the aluminum in this alloy. A specimen of this alloy was oxidized at 1100°C in a flowing CO-CO₂ gas mixture with CO₂/CO = 3 in order to attempt to develop a continuous layer of Al₂O₃ at a reduced oxygen pressure. Under such conditions continuous layers of Al₂O₃ were formed on this alloy but, in some localized areas on the specimen surface, the continuous Al₂O₃ scale was only developed after a substantial amount of transient oxidation had occurred.

The results obtained from cyclic oxidation testing at 1100°C in air of NiCrAl-ThO₂ and CoCrAl-Y₂O₃ are compared to results obtained for the cyclic oxidation of NiCrAl, NiCrAlY, CoCrAl and CoCrAlY in Figure 53. These results show that both oxide particles and yttrium are very effective in improving the adhesion of Al₂O₃ on NiCrAl and CoCrAl alloys. Metallographic examination of the specimens from this test showed that successive spalling of the Al₂O₃ from the NiCrAl and CoCrAl alloys had resulted in severe aluminum depletion followed by internal oxidation of the aluminum in these alloys. Photographs showing transverse sections through the NiCrAlY, CoCrAlY, NiCrAl-ThO₂ and CoCrAl-Y₂O₃ specimens from this test are presented in Figure 54. A small amount of spalling and cracking of the Al₂O₃ scales on these alloys has occurred but based on these microstructures, in general, the amount of oxidation is not markedly more than that expected for isothermal oxidation of these alloys. The oxide particles and the yttrium apparently have been equally effective in making the alloys resistant to the degradation caused by thermal cycling.

Since continuous layers of Al₂O₃ were not developed on the CoCrAl-Al₂O₃ alloy during oxidation in air, specimens of this alloy were not included in the cyclic oxidation test. Visual examination of the specimen of CoCrAl-Al₂O₃ after oxidation in the CO-CO₂ mixture showed that the Al₂O₃ scale was more adherent to this alloy than to a CoCrAl specimen which was oxidized under similar conditions, Figure 50.

The Al₂O₃ that formed on the TD NiCrAl after 100 hours of isothermal oxidation at 1100°C was adherent and normally spalling was observed only upon cutting specimens for examination. Typical morphological features of the Al₂O₃ which formed on this alloy are presented in Figures 55a and 55b. The modular appearance of the oxide surface, Figure 55b, is typical of that observed for Al₂O₃ scales formed on NiCrAlY and CoCrAlY alloys. Flakes of oxide removed from NiCrAl-ThO₂ by compressing to induce spallation were examined by using X-ray energy spectroscopy. As shown in Figure 55c, thorium was detected in the flake at the oxide-gas interface. Such a result is consistent with inward growth of the Al₂O₃ scale. The features of the Al₂O₃ at the substrate interface as well as the surface of the alloy where the oxide had spalled are shown in Figure 56. The Al₂O₃ at the substrate interface is irregular and contains numerous cusp-shaped grains as well as grains with deep depressions, Figures 56a and 56b. The imprints of the oxide on the substrate, Figures 56c and 56d, show that the substrate and oxide were in intimate contact and, in particular, that the cusps and depressions in the oxide were filled with alloy prior to spalling of the oxide.

Morphological features observed on the CoCrAl-Y₂O₃ specimen after 100 hours of isothermal oxidation were similar to those of NiCrAl-ThO₂. The Al₂O₃ was adherent to the substrate except for a small amount of spalling, Figure 57a, and the surface of the oxide at the gas interface had a nodular texture, Figure 57b. In locations where the oxide had spalled voids were not evident but the substrate surface was very irregular, Figures 57b and 58a, because crystallites of oxide extended into the alloy, Figure 58b, and portions of the alloy also protruded into the oxide, Figures 58c and 58d.

The morphological features observed with the CoCrAl-Al₂O₃ specimen that was oxidized in the CO-CO₂ gas mixture were similar to those described for NiCrAl-ThO₂ and CoCrAl-Y₂O₃. The surface of the Al₂O₃ at the gas interface was nodular, Figure 59a, and where spalling of the Al₂O₃ had occurred the exposed substrate was completely covered with imprints from oxide grains, Figure 59b. No evidence was observed that voids had been present at the Al₂O₃-substrate interface. The surface of the oxide at the substrate interface, Figure 59c, was not quite as irregular as such surfaces observed for NiCrAl-ThO₂ and CoCrAl-Y₂O₃ but cusping of the oxide grains was obvious and large imprints of isolated oxide grains were evident, Figure 59b.

c. Comparison of Mechanisms by which Oxide Particles and Yttrium Improve Adherence of Al₂O₃

The results which have been obtained with oxide particles and yttrium show that the same conditions are probably responsible for improving the adherence of the Al₂O₃ scales. In both cases vacancy sinks are provided to prevent the formation of voids at the Al₂O₃-substrate interface and oxide particles are available in the alloy to be incorporated into the inward growing Al₂O₃ scale and thereby act as micropegs. The Al₂O₃ which develops on alloys with oxide dispersions does not contain macropegs of oxide as does the Al₂O₃ formed on the yttrium-containing alloys. It has been observed, however, that macropegs may be developed in the Al₂O₃ on the alloys with dispersions by the alloy extending out into the oxide, Figures 54b, 57 and 58. In summary, oxide particles and oxygen active elements such as yttrium produce similar effects on the adhesion of Al₂O₃ apparently because both conditions establish vacancy sinks in the alloys and mechanically key the Al₂O₃ to the substrate. It is not possible to state which of these two techniques is the more effective in improving the adhesion of Al₂O₃. It appears that both techniques can be equally effective and that the factor which determines the efficiency of either technique is the distribution of the oxide particles or the oxygen active element in alloys. The more uniform the distribution, the more effective yttrium additions or oxide particles are in improving oxide scale adherence.

7. OXIDATION OF NiCrAl(Y) AND CoCrAl(Y) ALLOYS WITH EXTERNALLY APPLIED LOADS

a. Introduction

The purpose of the oxidation experiments using externally applied loads was to study the oxidation of NiCrAl, NiCrAlY, CoCrAl and CoCrAlY alloys under conditions where creep type deformation of specimens was occurring coincidental with the oxidation

process. Very little research data are available on this subject. The experimental procedure that was followed to perform these studies was described in Section II. All experiments were performed at 1100°C in air. In these experiments, since slow heating to temperature and soaking at temperature was necessary prior to application of the external load, in most cases a continuous Al₂O₃ scale had been developed on the specimens prior to their deformation. The oxidation process which took place along with the creep of the specimen was therefore growth of the Al₂O₃ scales. In the following, the results obtained from experiments with applied compressive and tensile loads are presented and discussed sequentially. Before presenting these results, it is worth noting that all of the alloys were found to be weak and ductile at 1100°C. For example, in the compression tests using strain rates between 0.4 and 0.6% per hour, the yield point of NiCrAl and NiCrAlY alloys was observed to be less than about 1000 psi whereas that for CoCrAl and CoCrAlY was less than about 700 psi. In the creep tests about 100 psi would cause 1-2% strain of CoCrAl or CoCrAlY over a 24-hour period while about 600 psi was required to achieve the same results for NiCrAl and NiCrAlY alloys.

b. Oxidation in the Presence of Externally Applied Compressive Loads

The oxidation kinetics of specimens with externally applied loads were determined by measuring the thicknesses of the Al₂O₃ scales as a function of time. The results obtained with specimens strained at a rate of 0.042% per hour are compared to data for unstressed specimens in Figures 60 and 61. In the case of the CoCrAl and CoCrAlY alloys, Figure 60, a difference between the thicknesses of oxides formed on stressed and unstressed specimens is not evident. The results obtained with the NiCrAl and NiCrAlY, Figure 61, alloys indicate that the thicknesses of the stressed specimens may be somewhat greater than those of unstressed specimens. The observed difference is small but does appear to be real for the NiCrAl alloy since the scatter in data points for stressed specimens should not be significantly greater than for unstressed specimens.

Specimens were also oxidized with loads producing strain rates greater than 0.042% per hour. These experiments were usually performed for 16 hours. The oxide thicknesses obtained after oxidation with the different strain rates are presented in Table VI.

These data indicate that there is a trend for the thickness of the Al₂O₃ to increase as the specimen is strained during oxidation. The difference between strained and unstrained specimens is not large and no dependence of oxide thickness on strain rate is evident.

The morphological features of the Al₂O₃ scales and substrates from the oxidation experiments with externally applied compressive loads were not markedly different from those observed on unstressed specimens. This was especially true for specimens that had not undergone a large amount of deformation. In the case of NiCrAl and CoCrAl alloys partially adherent Al₂O₃ was observed on specimen surfaces, Figures 62a and 63a, and the substrate surfaces exposed by spalling of the Al₂O₃ contained smooth areas and numerous imprints from oxide grains, Figures 62b and 63b. The oxide surfaces adjacent to the substrates contained well defined oxide grains and cavities that matched with the smooth areas on the substrate surfaces, Figures 63c and 63d. These morphological features were virtually identical to those observed with unstressed specimens as can be seen upon comparing the scanning micrographs presented in Figure 64.

TABLE VI
OXIDE THICKNESS MEASUREMENTS FOR THE OXIDATION
OF SPECIMENS AT 1100°C IN AIR FOR 16 HRS
WITH COMPRESSIVE LOADING AND NO LOADING

Compressive Strain Rate (%/hr)	Oxide Thickness (μ)			
	NiCrAl	NiCrAlY	CoCrAl	CoCrAlY
0	1.0	1.2	1.1	1.2
0.042	2.1	1.1	1.7	1.1
0.208	2.2		1.9	
0.417	2.4	1.5	1.7	1.8
0.625		1.7	-	1.6

As the amount of compressive strain was increased, evidence for grain boundary sliding, Figures 65a and 65b, as well as possible extruded metal, Figure 65c, were observed on alloys that did not contain yttrium. Even though a substantial amount of deformation of these alloys had occurred, the Al_2O_3 scale appeared in many instances to deform also rather than crack, Figures 65b and 65c.

The alloys which contained yttrium showed very little effect of compressive loads that produce about 1-2% strain over a period of 24 hours (0.042%/hr), Figure 66. Loads that produced larger strains resulted in wrinkles being developed in the alloy, Figures 67a, 68a, and 69a, and cracking of the Al_2O_3 at these locations was evident, Figures 67b, 68b and 69b. It was apparent that this cracking of the Al_2O_3 had occurred at temperature since sites at which the exposed alloy had been oxidized were clearly evident, Figures 67c and 68d. At locations where the substrate surface could be observed the imprints of oxide grains were apparent, but smooth areas indicative of void formation were also obvious, Figures 67d, 68c and 69c. In some instances, the voids developed between the Al_2O_3 and the substrate were clearly visible, Figure 69d. The oxide surface adjacent to these voids contained the typical features, Figure 70, observed previously at voids on unstressed specimens.

Transverse sections through specimens of NiCrAlY and CoCrAlY were helpful to examine the deformation of specimens and the adhesion of the oxide. Even when the substrate had been severely deformed, cracking and spalling of the oxide scale was not extensive, Figure 71. Cracking of the oxide appeared to occur at sites of extreme curvature where contact between the oxide and the substrate could not be maintained, Figure 71c. At areas where cracks had developed in the oxide, it was not uncommon for oxide (Al_2O_3) to be evident on the substrate beneath the cracks, Figure 72. Such a condition is consistent with the proposal that cracking of the oxide had occurred at temperature.

c. Oxidation in the Presence of Externally Applied Tensile Loads

The oxide thickness as a function of time for specimens oxidized with externally applied tensile loads is presented in Figures 60 and 61. The results obtained with tensile loads are similar to those obtained with compressive loads. It appears as though the growth of Al_2O_3 scales on CoCrAl and CoCrAlY alloys is not affected by the applied tensile load. In the case of NiCrAl and NiCrAlY, the oxide thicknesses appear to be greater for stressed specimens.

Only two specimens were oxidized with tensile loads that produced more than 2% strain after 24 hours other than those described in Figure 60. A NiCrAl specimen was oxidized for 21 hours and had a tensile strain of 17.4% and the thickness of the oxide formed on this specimen was about 1.5μ compared to 1.3μ for an unstressed specimen oxidized for a similar time. A CoCrAl specimen was oxidized for 16 hours with a total strain of 8%. The oxide thickness was determined to be 1.8μ compared to an unstressed value of 1.1μ .

The morphological features of the Al_2O_3 scales and the substrate surfaces after oxidation with applied tensile loads that produced small strains (e.g. 1-2% after 24 hours) were usually similar to those described previously for the compressive loads. The oxide surfaces at the gas interface had nodular textures, Figure 73a, and filamentary protrusions were evident, Figure 73b, on scales formed on CoCrAl and NiCrAl alloys. The substrate surfaces of NiCrAl alloys from which the scales had spalled contained numerous imprints of oxide grains and smooth areas where voids had been developed at the oxide-substrate interface, Figure 74. The oxide scales formed on the NiCrAlY and CoCrAlY alloys contained features at the oxide-substrate interfaces very similar to those observed for unstressed specimens, Figure 75, of these alloys.

When specimens were oxidized with tensile loads that produced strains of about 20% in 24 hours, separation of the alloy grain boundaries occurred, Figure 76. Examination of such specimens by using the SEM showed that the alloy adjacent to these areas of grain boundary separation was smooth, Figures 76b and 76c, and it was evident that the oxide had not been in intimate contact with the substrate at such smooth areas. Numerous flakes of Al_2O_3 were observed to overlay these areas of grain boundary separation. It was determined that these flakes were not oxide debris formed on cooling but rather Al_2O_3 in situ. While in situ Al_2O_3 flakes, spanning the points of grain boundary separation in the alloy, indicate that the Al_2O_3 may not have cracked as these openings in the alloy were developed, a significant amount of oxidation was observed within these openings. Such results clearly show that the Al_2O_3 scale must have fractured, at least in some areas, during the test.

d. Effect of Externally Applied Stress on the Oxidation of NiCrAl(Y) and CoCrAl(Y) Alloys at 1100°C

The results obtained by oxidizing specimens with applied loads at 1100°C have shown that at this temperature and with strain rates of about 0.042%/hr the Al_2O_3 scales are apparently deformed plastically rather than cracked under the influence of the load.

In the case of strain rates on the order of 1%/hr, the Al_2O_3 scales also appear to be capable of accommodating a very large amount of deformation, however, cracking of the Al_2O_3 does occur. In cases where cracking of the Al_2O_3 takes place, a protective layer of Al_2O_3 is developed on the alloys beneath the cracks. The observation that stresses imposed upon Al_2O_3 scales at 1100°C can be relieved by deformation, indicates that oxide growth stresses probably do not have any effect on the spalling of the Al_2O_3 from specimens oxidized at temperatures of 1100°C and above.

Oxidation of NiCrAlY and CoCrAlY alloys with compressive loads that caused cracking of the Al_2O_3 scales also resulted in the development of voids at the Al_2O_3 -alloy interfaces. These results indicate that the formation of such voids may be related to a stress relief mechanism which involves detachment at the alloy-oxide interface (ref. 21). Since the formation of such voids were commonplace for unstressed NiCrAl and CoCrAl specimens, it is possible that the void development on these alloys may occur as a means of stress relief rather than from vacancy condensation occurring as a result of diffusion processes established within the alloy by the oxidation reaction.

The data which has been obtained for the growth of Al_2O_3 on CoCrAl and CoCrAlY alloys with applied loads indicates that the applied loads have not significantly affected the growth rates of these scales. The data for the NiCrAl and NiCrAlY alloys are less clear. There does appear to be a small increase in the growth rate for specimens with applied loads. This observed effect does not appear to be experimental error since the scanning electron microscope was calibrated and the error in thickness measurements was less than $\pm 0.2\mu$. The thicknesses which were taken from the data were average values. It is possible that the flakes used for these measurements in the case of the specimens under consideration were not representative. Previous results obtained with the unstressed specimens has indicated that the growth of the Al_2O_3 is controlled by diffusion of oxygen along grain boundaries in the scales. The grain sizes of the Al_2O_3 from stressed and unstressed specimens of NiCrAl and NiCrAlY were about the same. In view of this condition, and since no effect of applied load was observed for the growth of Al_2O_3 on CoCrAl and CoCrAlY alloys, it is believed that the indicated dependence of Al_2O_3 scale thickness on applied load for NiCrAl and NiCrAlY alloys is not significant.

SECTION IV

SUMMARY AND CONCLUDING REMARKS

In this program a number of conditions which are important to the development of oxidation resistance in alloys has been studied by examining Al_2O_3 formation, growth and adhesion on NiCrAl and CoCrAl alloys at temperatures between 1000° and 1200°C . In the following, the important results which have been obtained in this program are briefly summarized.

1. CONCERNING THE RATES AND MECHANISMS OF Al_2O_3 GROWTH ON NiCrAl AND CoCrAl ALLOYS

- The growth mechanism of Al_2O_3 on these alloys consists predominantly of the inward diffusion of oxygen along grain boundaries in the Al_2O_3 .
- The rate of growth of the Al_2O_3 is controlled by the diffusion of oxygen along grain boundaries in the Al_2O_3 scales.
- During growth of Al_2O_3 scales on these alloys voids are usually formed at the Al_2O_3 -alloy interface.
- The growth rate of the Al_2O_3 is not affected by the formation of the voids since it appears that aluminum is rapidly transported across the voids as a vapor.
- Void formation does affect the morphology of the Al_2O_3 at the Al_2O_3 -substrate interface; large crystals of Al_2O_3 are formed at this interface when voids are present and impingement of these Al_2O_3 crystals on one another causes wrinkles to be developed in the Al_2O_3 scales.

2. CONCERNING THE ADHESION OF Al_2O_3 TO NiCrAl AND CoCrAl ALLOYS

- The Al_2O_3 scales are adherent to these alloys during oxidation under isothermal conditions.
- The Al_2O_3 spalls from these alloys because of stresses induced during cooling; growth stresses in the Al_2O_3 apparently can be relieved by plastic deformation.
- Spalling of the Al_2O_3 scales occurs because the applied stresses exceed the strength of the Al_2O_3 -alloy interfacial bond; the development of voids at the Al_2O_3 -alloy interface is not necessary in order to have spalling of the Al_2O_3 scales; however, such voids when present do result in more extensive spalling of Al_2O_3 scales.

3. CONCERNING THE EFFECT OF YTTRIUM ON THE RATE OF GROWTH AND GROWTH MECHANISM OF Al_2O_3

- Yttrium does not influence the growth rate nor the growth mechanism of Al_2O_3 on NiCrAl and CoCrAl alloys.
- The growth of Al_2O_3 on NiCrAlY and CoCrAlY alloys occurs predominantly by the inward diffusion of oxygen along grain boundaries in the Al_2O_3 scale.
- While yttrium does not directly affect the growth mechanism of Al_2O_3 , the oxidation of yttrium in these alloys results in the formation of yttrium oxide particles and stringers in these alloys beneath the Al_2O_3 scales.
- The yttrium oxide is incorporated into the inward-growing Al_2O_3 scale and macro- and micropegs are developed at the Al_2O_3 -alloy interface; voids are apparently not formed at this interface.

4. CONCERNING THE EFFECT OF YTTRIUM ON THE ADHESION OF Al_2O_3

- Yttrium improves the adherence of Al_2O_3 to NiCrAl and CoCrAl alloys.
- Yttrium improves the adhesion of Al_2O_3 to NiCrAl and CoCrAl alloys by two processes, namely, by providing sinks for vacancies which prevent void formation at the alloy- Al_2O_3 interface and by providing macro- and micropegs which mechanically key the Al_2O_3 to these alloys.

5. CONCERNING THE EFFECTS OF OXIDE PARTICLES ON THE ADHERENCE OF Al_2O_3 TO NiCrAl AND CoCrAl ALLOYS

- Oxide particles such as ThO_2 , Y_2O_3 and probably Al_2O_3 dispersed in these alloys can be equally effective as yttrium in improving the adhesion of Al_2O_3 scales.
- The mechanism by which oxide particles and oxygen active elements such as yttrium affect Al_2O_3 adherence is the same; both techniques involve the presence of sinks for vacancies and mechanical keying of the Al_2O_3 to the alloys.

6. CONCERNING THE EFFECT OF ALLOY MICROSTRUCTURE ON THE ADHESION OF Al_2O_3

- The microstructure of NiCrAl and CoCrAl alloys does not affect the adhesion of Al_2O_3 .

- The effectiveness of yttrium, and probably dispersed oxide particles, in improving the adhesion of Al_2O_3 is dependent upon alloy microstructure; optimum results are obtained with uniform distributions of the oxygen active element or the oxide particles.
- In the case of oxygen active elements such as yttrium, alloys with a small grain size give an additional advantage by providing conditions which lead to uniform networks of macropegs.

7. CONCERNING THE EFFECT OF APPLIED STRESS ON THE OXIDATION OF THESE ALLOYS

- An externally applied stress does not have a significant effect on the growth rate of Al_2O_3 on these alloys.
- At a temperature of 1100°C and low strain rates the Al_2O_3 scales on these alloys can relieve imposed stresses via plastic deformation rather than cracking or spalling.
- When the externally applied loads result in strain rates sufficient to cause cracking of the Al_2O_3 at temperature, extensive spalling of the oxide scale does not occur and a new protective layer of oxide is developed at the base of the crack.
- Deformation of specimens during oxidation resulted in development of voids at the alloy- Al_2O_3 interface which suggests that such void formations on unstressed specimens may result from a deformation process rather than from a reaction-induced diffusion process.

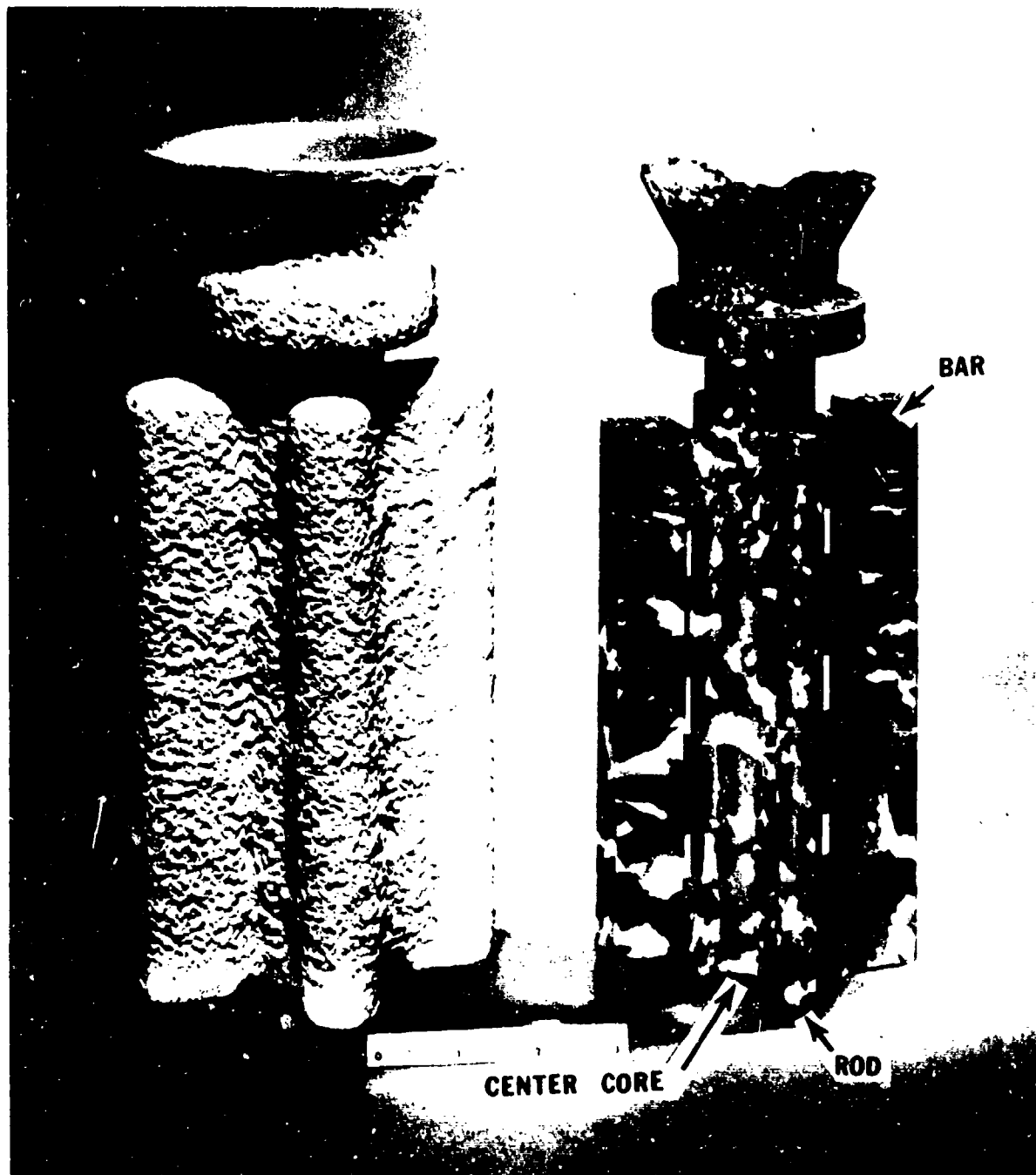


Figure 1 Typical Mold and the Resulting Investment Casting Used to Produce Specimens for the Oxidation Experiments. These castings were composed of two bars, two rods and a central core.



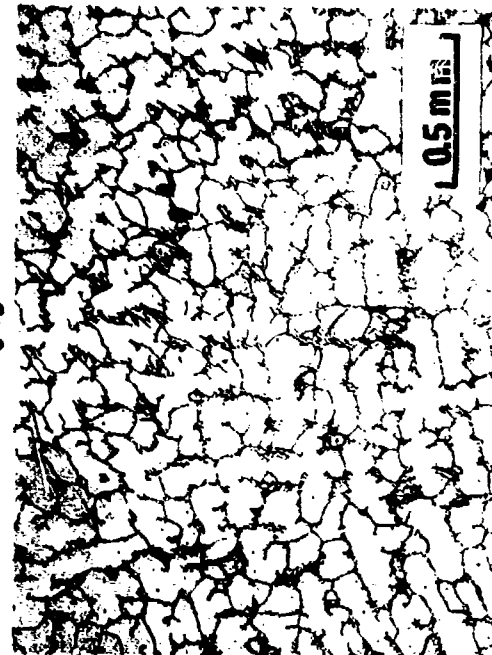
(a)



(b)

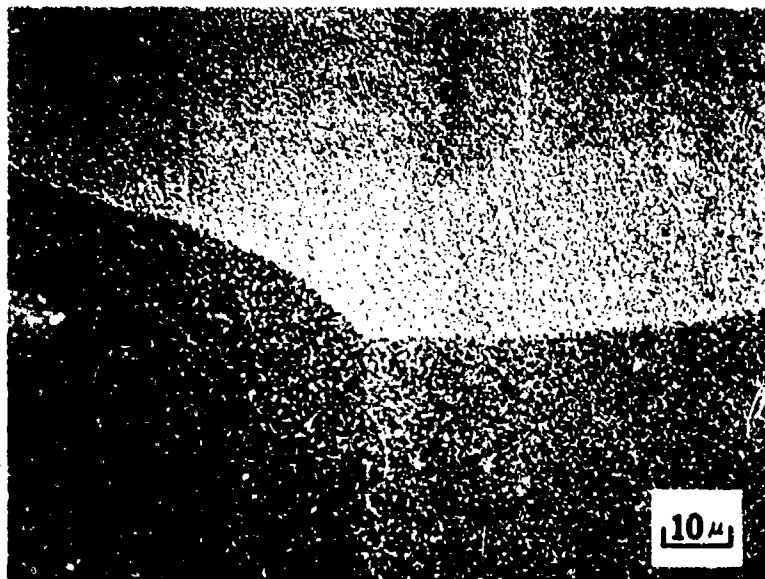


(c)

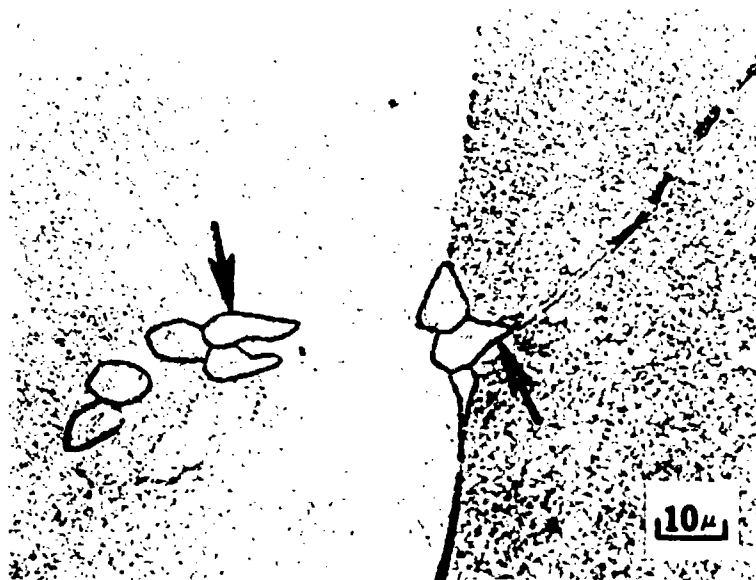


(d)

Figure 2. Photographs Showing the Microstructures of the As-Cast Alloys. All of these castings, (a) NiCrAl, (b) NiCrAlY, (c) CoCrAl and, (d) CoCrAlY exhibit a dendritic structure.



(a)



(b)

Figure 3 Photographs Showing the Details of the Microstructures of As-Cast NiCrAl and NiCrAlY Alloys in the Etched Condition. The microstructures of both alloys are composed of fine γ' (Ni_3Al) particles in a matrix of the γ -phase (nickel solid solution). In addition, an yttride phase is present at grain boundaries as well as within the grains of the NiCrAlY alloy (arrows).

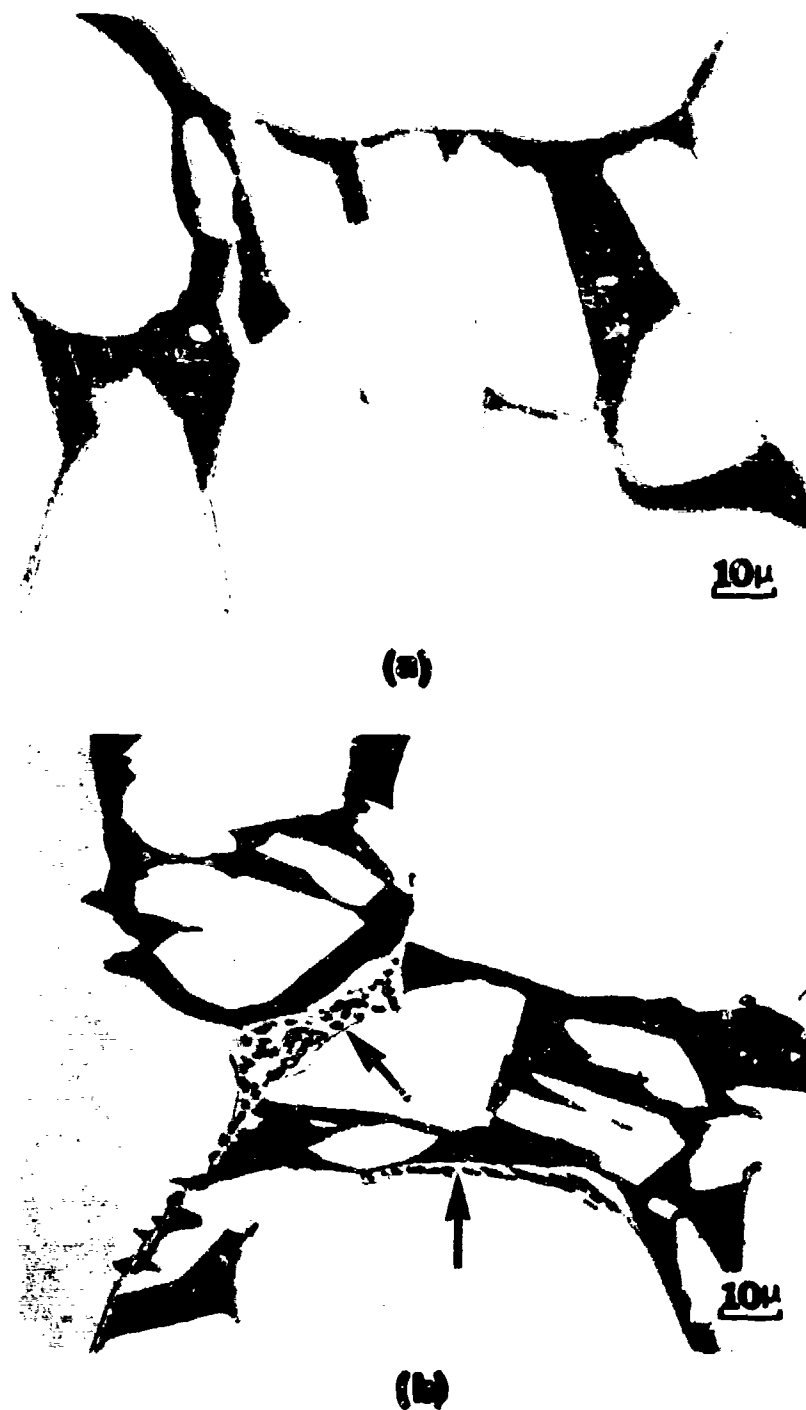


Figure 4 Photographs Showing the Details of the Microstructures of As-Cast CoCrAl and CoCrAlY Alloys in the Etched Condition. The microstructures of both alloys are composed of β -phase (CoAl) in a matrix of the α -cobalt solid solution. The microstructure of the CoCrAlY alloy also exhibits yttide precipitates (arrows) at the phase boundaries of the α -cobalt solid solution phase.



(a)



(b)

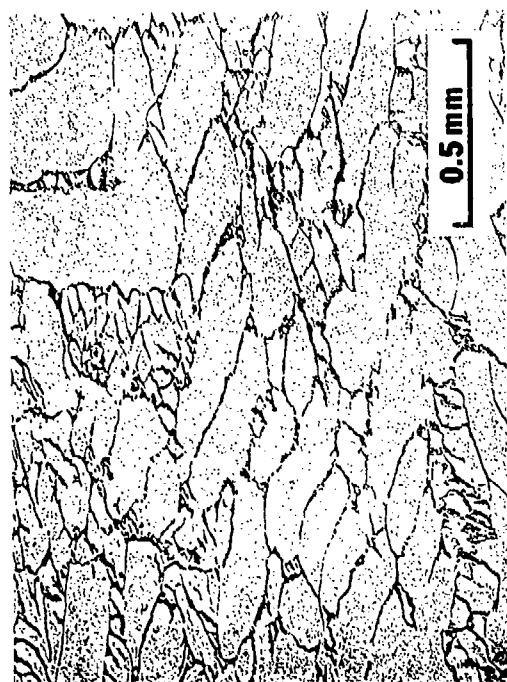


(c)



(d)

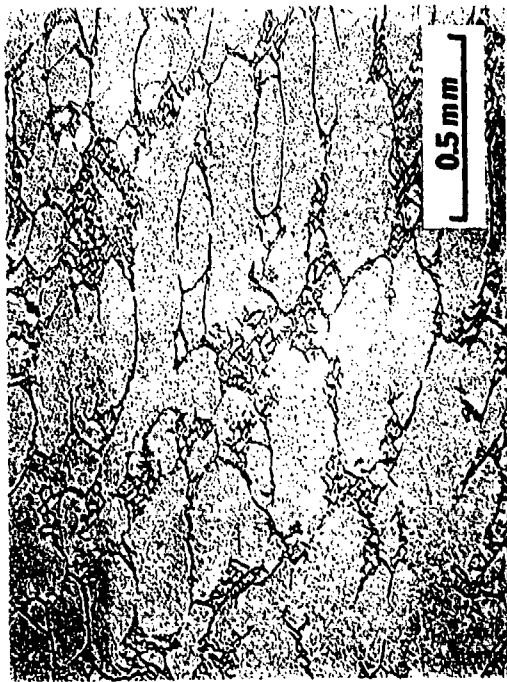
Figure 5 Microstructures of Hot-Worked and Annealed NiCrAl and NiCrAlY Alloys in the Etched Condition. Both the NiCrAl [(a), (b)] and NiCrAlY [(c), (d)] alloys exhibited precipitates of γ in a γ -phase matrix and the NiCrAlY alloy also contains yttride precipitates (arrows).



(a)



(b)



(c)



(d)

Figure 6 Microstructures of Hot-Worked and Annealed CoCrAl and CoCrAlY Alloys in the Etched Condition. Both the CoCrAl [(a), (b)] and CoCrAlY [(c), (d)] alloys show particles of β -phase at the phase boundaries of the α -cobalt solid solution and within the interiors of the grains. The CoCrAlY also contains yttride precipitates (arrows).

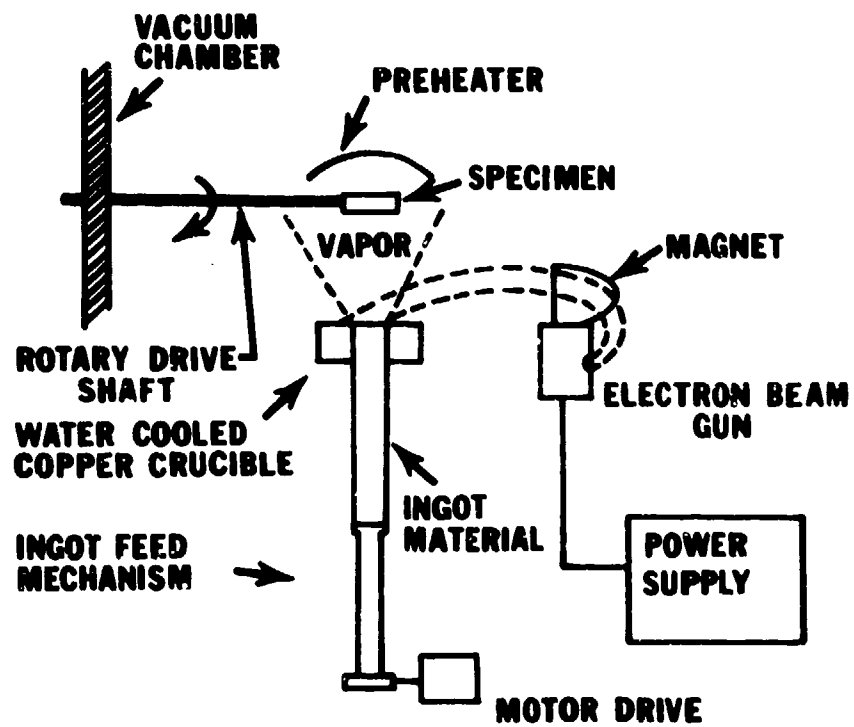


Figure 7 Schematic Diagram of the Electron Beam Evaporation Apparatus Used to Produce Vapor-Deposited Alloys.



(a)



(b)



(c)



(d)

Figure 8 Microstructure of Vapor-Deposited NiCrAl, NiCrAlY, CoCrAl and CoCrAlY Alloys in the Etched Condition. The NiCrAl (a) and NiCrAlY (b) alloys contain γ' particles in a γ -phase matrix, whereas the CoCrAl (c) and CoCrAlY (d) alloys contain particles of β -phase in a matrix of α -cobalt solid solution. Arrows indicate yttride phases in the alloys containing yttrium.

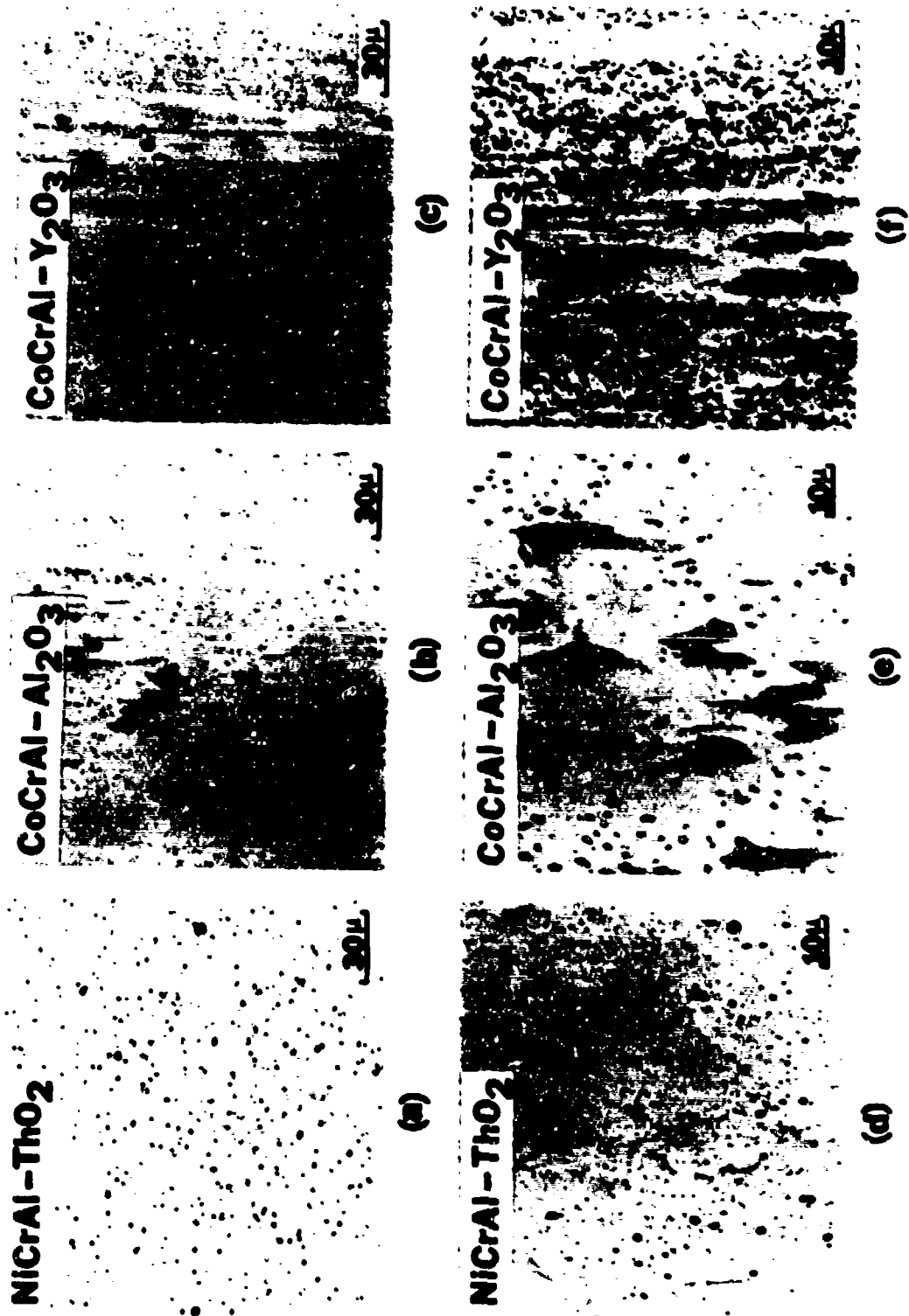


Figure 9 Microstructures of NiCrAl - ThO₂, CoCrAl - Al₂O₃ and CoCrAl - Y₂O₃ in the As-Polished and Etched Conditions. Corresponding higher magnification photographs show coarse γ (Ni₃Al) at grain boundaries of a γ -phase matrix in NiCrAl-ThO₂ and the distribution of β (CoAl) in an α -phase matrix for CoCrAl-Al₂O₃ and CoCrAl-Y₂O₃. Inert particle distribution is evident in all of these alloys.

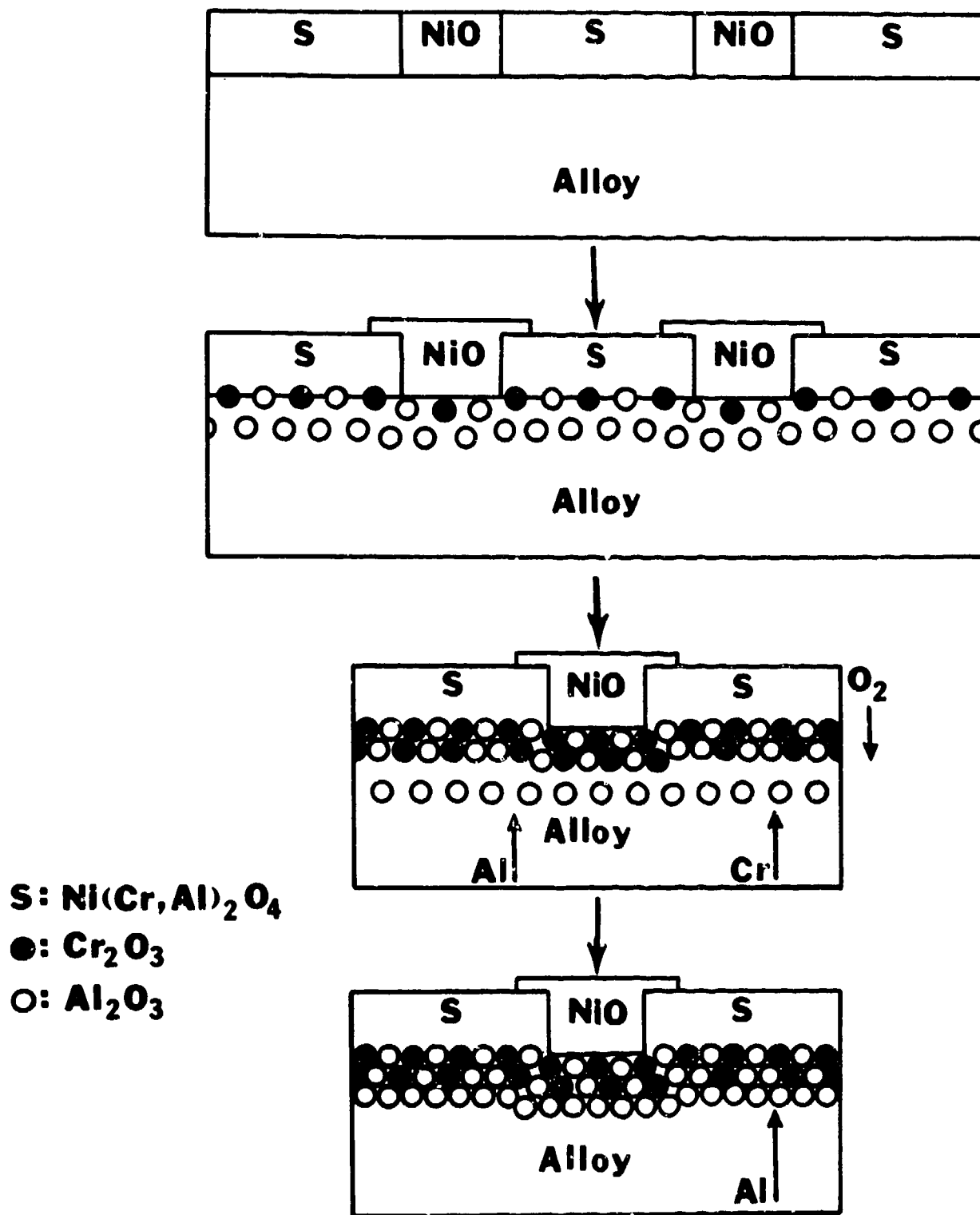
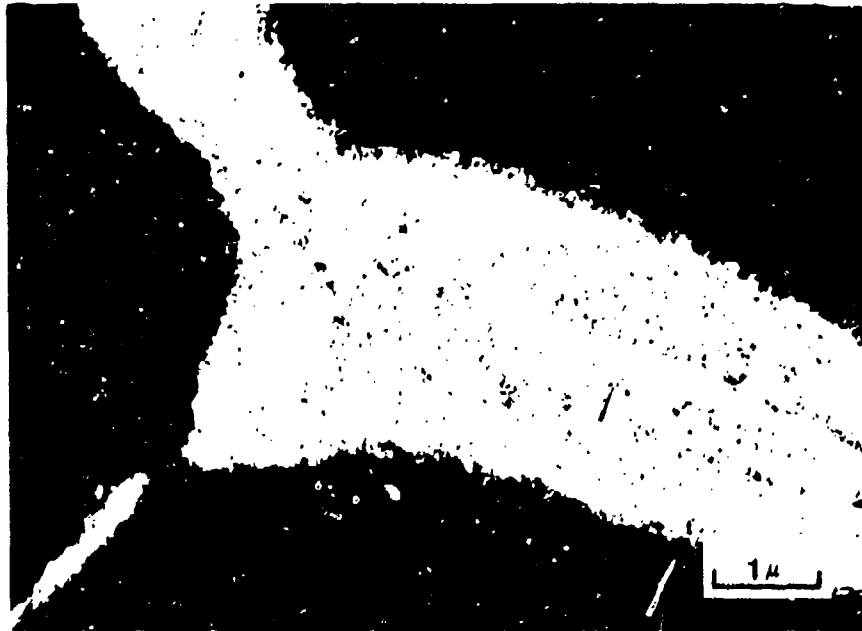


Figure 11 Schematic Diagram Illustrating the Processes by Which Continuous Al₂O₃ Layers Are Developed on NiCrAl Alloys.



(a)



(b)



(c)

Figure 12 Typical Transient Oxidation Features Developed During Oxidation of the NiCrAl Alloy. (a) Bright field transmission electron micrograph of oxide film formed on NiCrAl (VD) after 5 min. of oxidation at 1100°C in 1 atm of dry air. The oxide film is thinner (lighter area) over alloy grain boundaries. (b) and (c) Morphological features on NiCrAl (HWA) after 2 hrs of oxidation at 1100°C in 1 atm of dry air. The surface of the oxide contains mounds of transient oxides (arrows) and the substrate contains depressions where the mounds of oxide are evident (b). Numerous oxide crystals are evident at the oxide-substrate interface beneath these mounds of transient oxides (c).

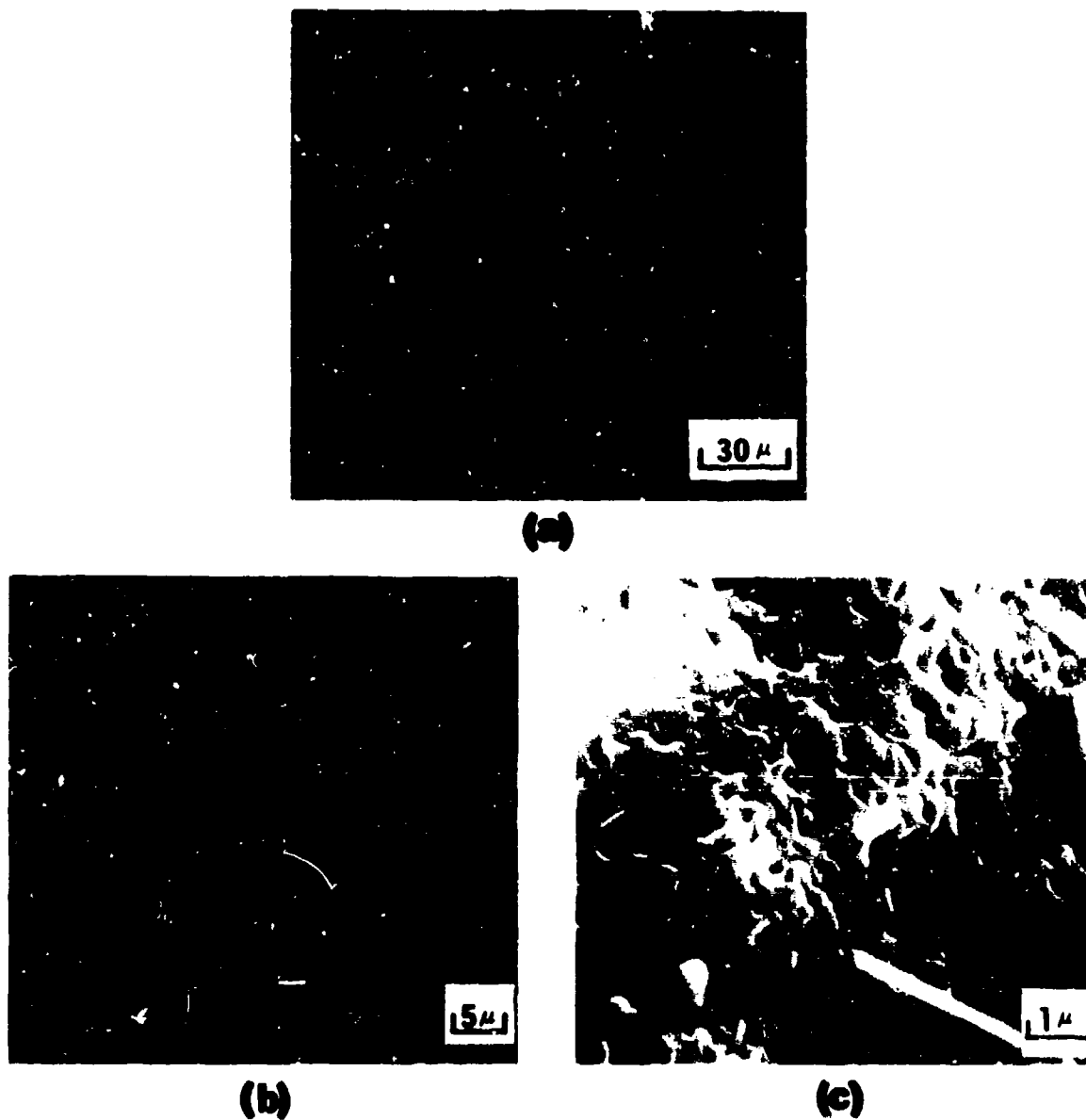
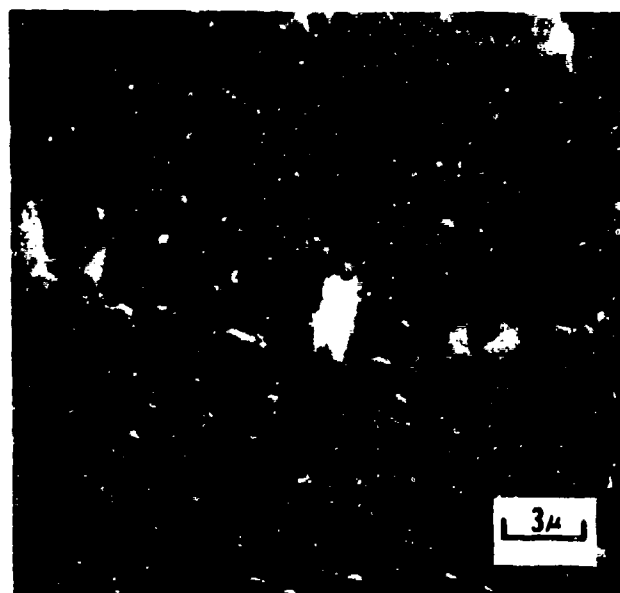
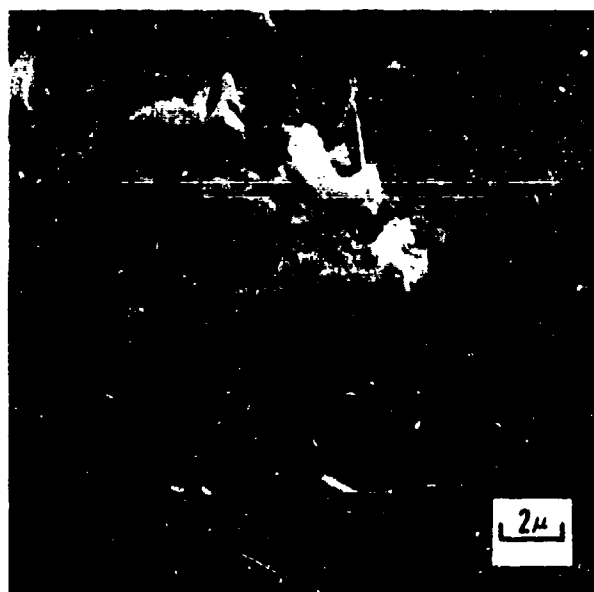


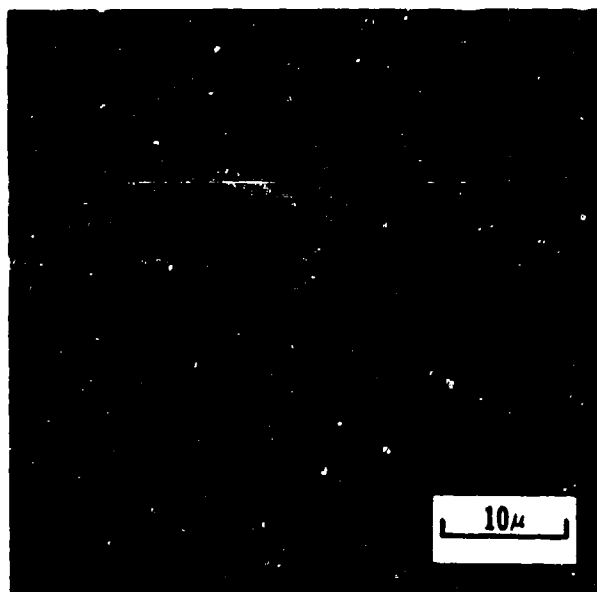
Figure 13 Typical Morphological Features Developed at the Al_2O_3 -Gas Interface of Al_2O_3 Scales on NiCrAl and CoCrAl Alloys. (a) After oxidation at 1000°C the oxide surface is flat [NiCrAl (HWA), 100 hrs in 1 atm of dry air]. (b) After oxidation at 1200°C the oxide surface contains numerous wrinkles [NiCrAl (HWA), 100 hrs in 1 atm of dry air]. (c) At all temperatures the Al_2O_3 exhibited a fine dimpled texture and contained filamentary growths [CoCrAl (HWA), 100 hrs in 1 atm dry air at 1100°C].



(a)



(b)



(c)

Figure 14 Photographs Showing Development of Wrinkles in Oxide Formed on CoCrAl (AC) During Oxidation at 1100°C in 1 atm of Dry Air. (a) 30 min, (b) 2 hrs (some bare substrate is evident in this photograph), (c) 16 hrs (in all photographs the arrows indicate aligned protrusions.)

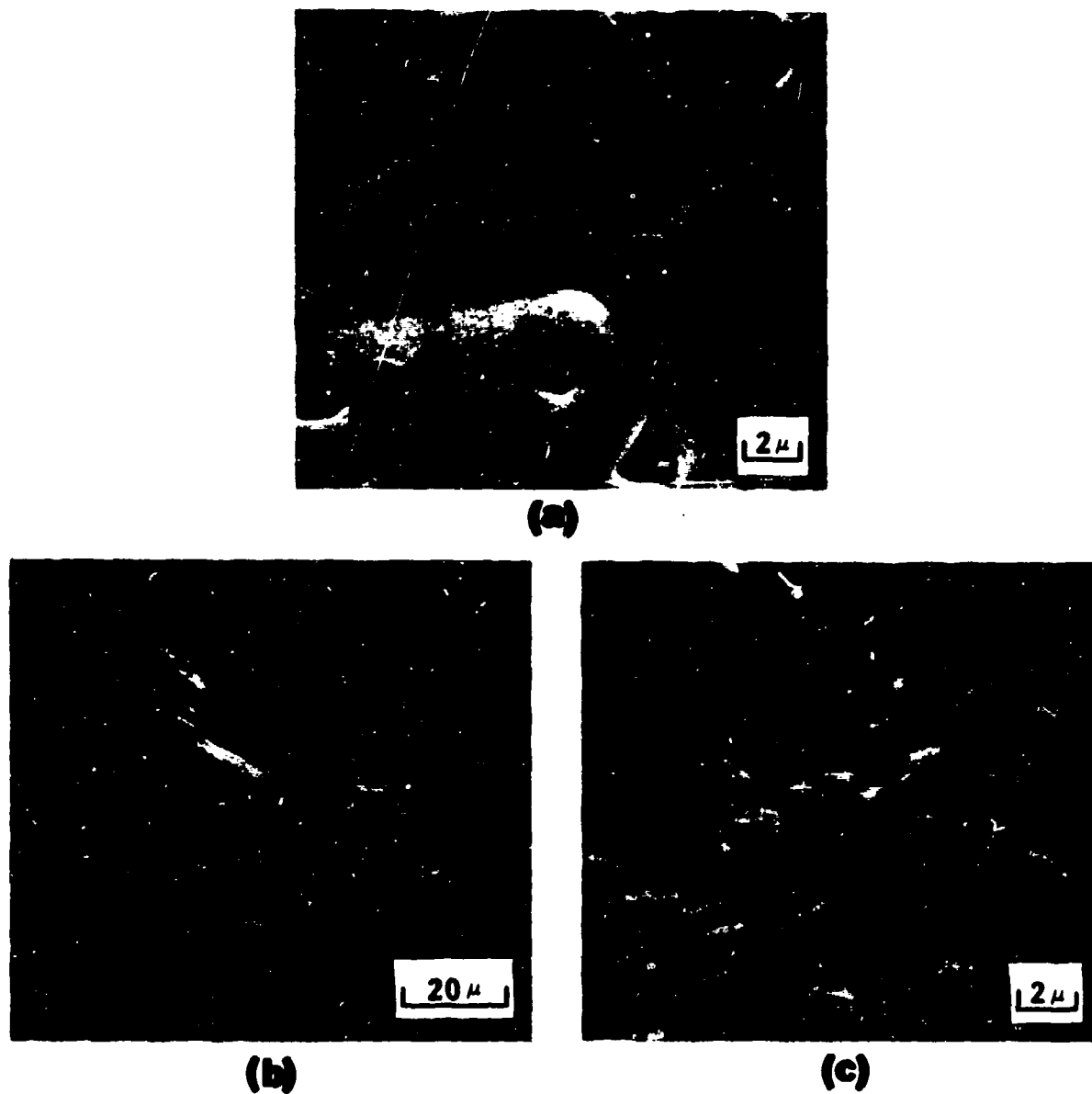


Figure 15 Morphological Features Typical of NiCrAl and CoCrAl Alloys From Which the Al_2O_3 Scales Had Spalled. (a) After oxidation at 1000°C the alloy surfaces contained grooved boundaries with isolated oxide imprints [NiCrAl (HWA), 100 hrs in 1 atm dry air]. (b) and (c) After oxidation at 1200°C the alloy surfaces contained localized smooth areas and rough, imprinted regions [NiCrAl (HWA), 100 hrs in 1 atm dry air].

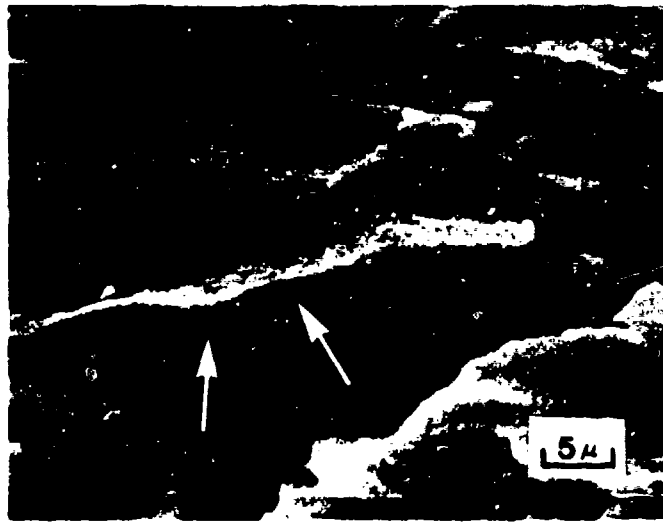


(a)

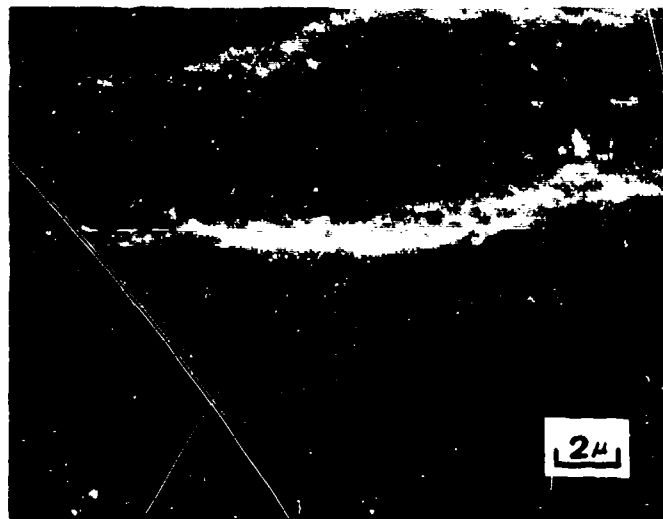


(b)

Figure 16 Photographs Showing Details of NiCrAl and CoCrAl Alloys From Which The Al_2O_3 Had Spalled. (a) The smooth areas on the alloy surfaces contained thermal facets (black arrows) whereas the rough areas contained the imprints of oxide grains (white arrows) [NiCrAl (AC), 100 hrs at 1100°C in 1 atm dry air]. (b) On the CoCrAl alloys the wrinkles in the oxide (black arrows) and the smooth areas on the alloy surface (white arrows) exhibited the same pattern as the distribution of the β -phase in the alloy [CoCrAl (AC), 100 hrs at 1100°C in 1 atm of dry air].

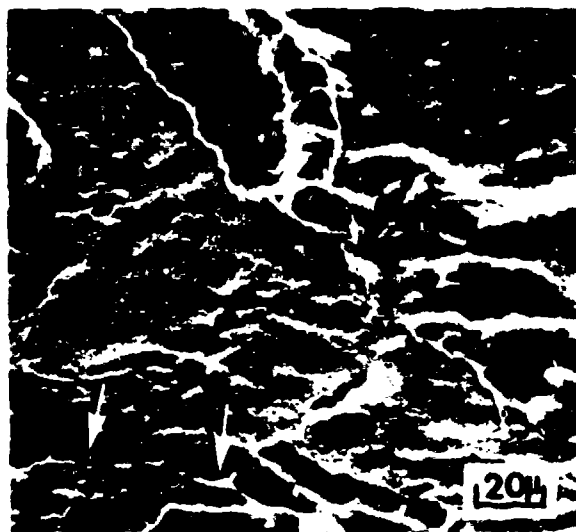


(a)



(b)

Figure 17 Photographs Showing Al_2O_3 Crystals In Situ on Alloy Surface and Position of Continuous Al_2O_3 Layer. The Al_2O_3 crystallites caused imprints to be developed in the substrate surfaces (a) (arrows) and the continuous layer of Al_2O_3 was not in intimate contact with the substrates (b) [NiCrAl (HWA), 8 hrs at 1100°C in 1 atm of dry air].

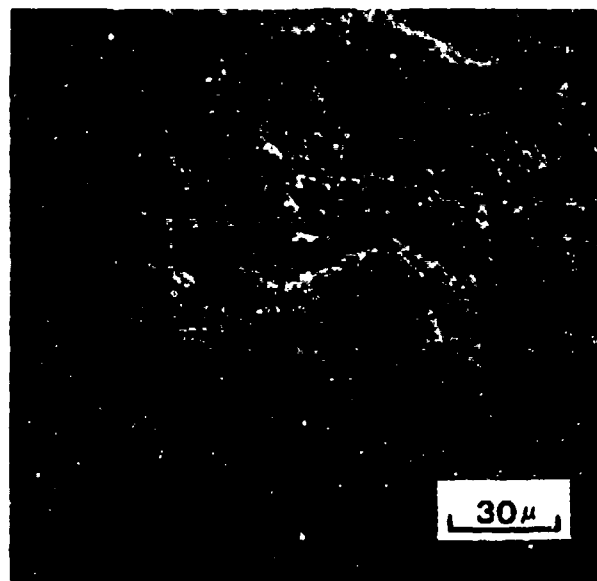


(a)

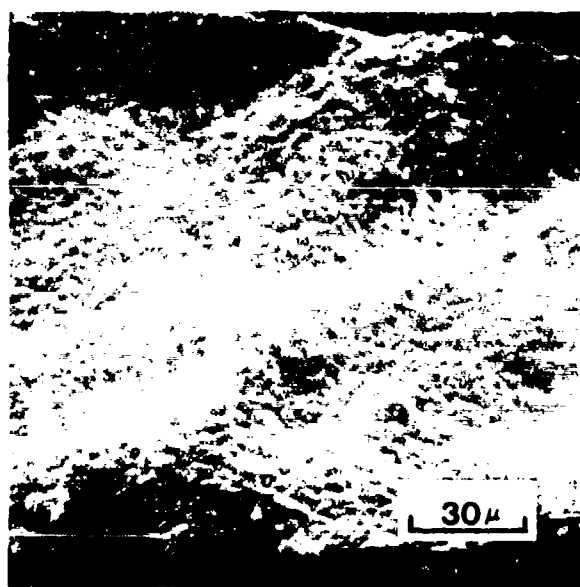


(b)

Figure 18 Photographs Showing Details of Wrinkles in Al_2O_3 Scales on NiCrAl and CoCrAl Alloys. (a) The wrinkles in the Al_2O_3 coincided with the smooth areas on the alloy surfaces and voids (arrows) were occasionally observed in these smooth areas [CoCrAl (AC) 100 hrs at 1100°C in 1 atm of dry air]. (b) The surfaces of these wrinkles adjacent to the substrate surfaces contained large, protruding, oxide crystals [NiCrAl (HWA) 100 hrs at 100°C in 1 atm of dry air].



(a)



(b)



(c)

Figure 19 Morphological Features Observed on Surfaces of Oxide Flakes Which Spalled From CoCrAl (HWA) After 100 hrs of Oxidation at 1200°C in Air. The surfaces of the oxide flakes at the oxide-gas (a) and the oxide-substrate (b) interfaces did not contain wrinkles but wavy or undulating features were evident. The surfaces of these flakes at the oxide-substrate interface contained well-defined oxide crystals (c).

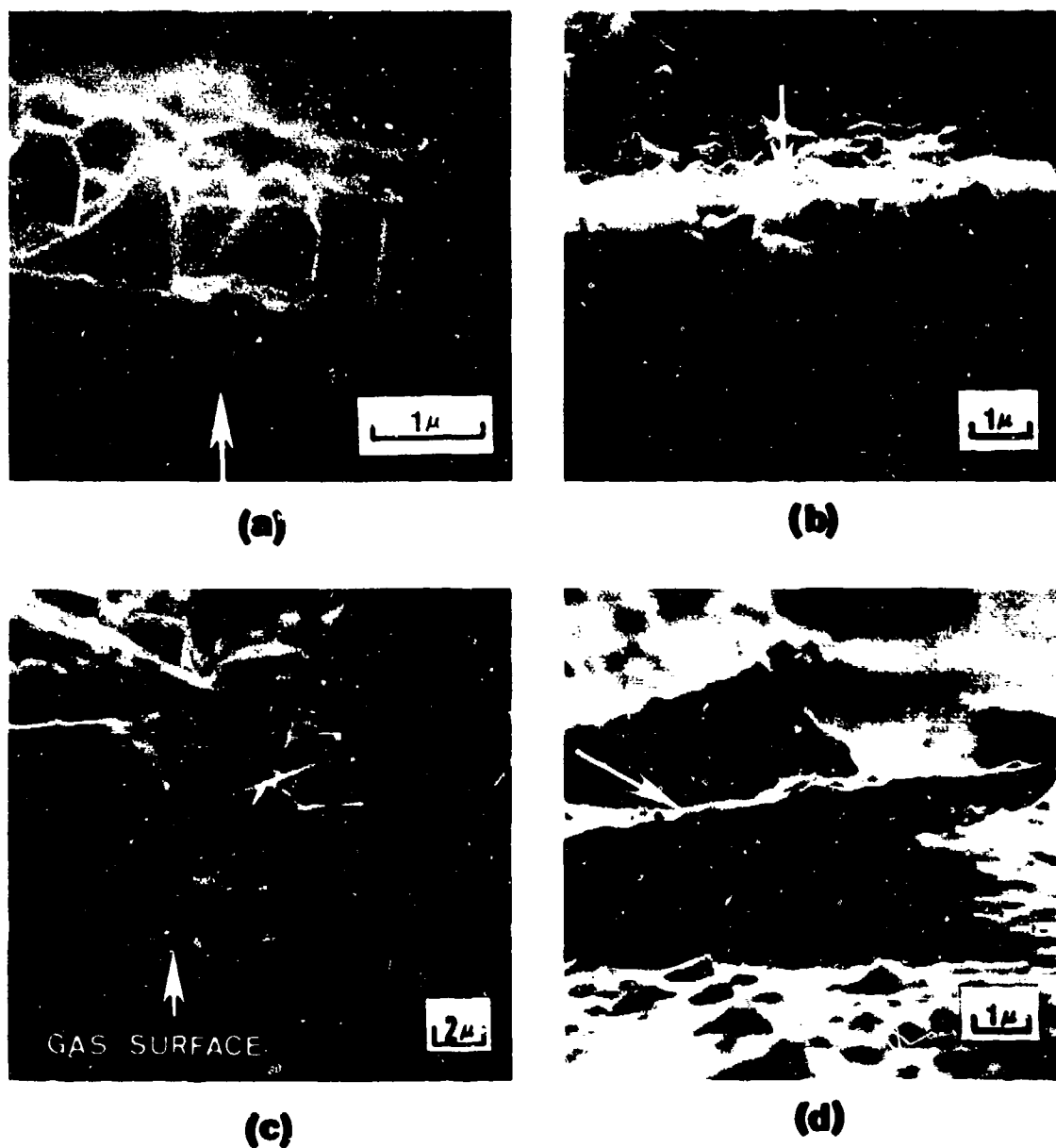
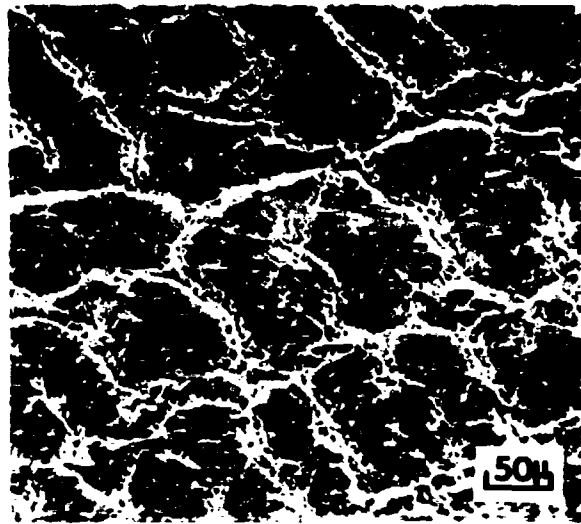
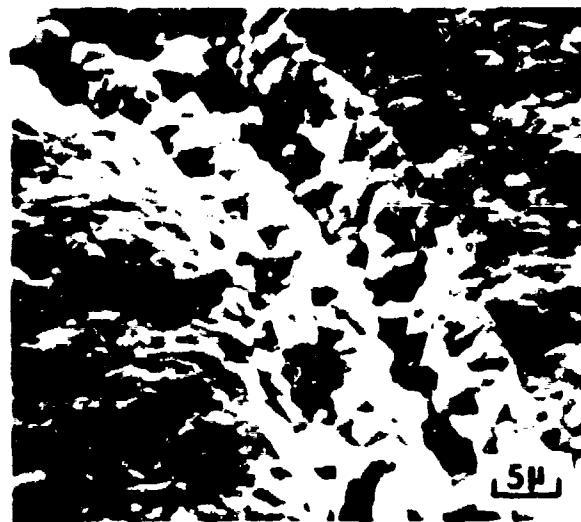


Figure 20 Photographs Showing Details of Al_2O_3 Scales Which Spalled From NiCrAl and CoCrAl Alloys. After 2 hrs of oxidation at 1100°C the Al_2O_3 frequently contained large, distinct crystallites at the Al_2O_3 -alloy interface (a) whereas after 100 hours (b) these crystals of oxide appeared to have grown together [CoCrAl (HWA) oxidized in 1 atm of dry air]. At 1000°C even after 100 hrs of oxidation the oxide crystals had not grown together (c) (CoCrAl oxidized in 1 atm of dry air). While Al_2O_3 scales with large crystals of oxide (a), (c) were common, more uniform scales which did not contain these crystallites were also abundant (d) [NiCrAl (HWA), 16 hrs at 1000°C in 1 atm of dry air]. In all the photographs the white arrows point to the oxide-gas interface and the black arrow indicates the zone of smaller oxide grains.



(a)



(b)

Figure 21 Depressions in Al_2O_3 Scales at the Al_2O_3 -Substrate Interface. In the case of the CoCrAl alloy the depressions formed a pattern identical to that of the β -phase in this alloy (a) [CoCrAl (AC), 100 hrs at 1100°C in dry air]. Within the depressions in the oxide, large oxide crystallites were evident (b) [CoCrAl (AC), 100 hrs at 1100°C in 1 atm dry air].

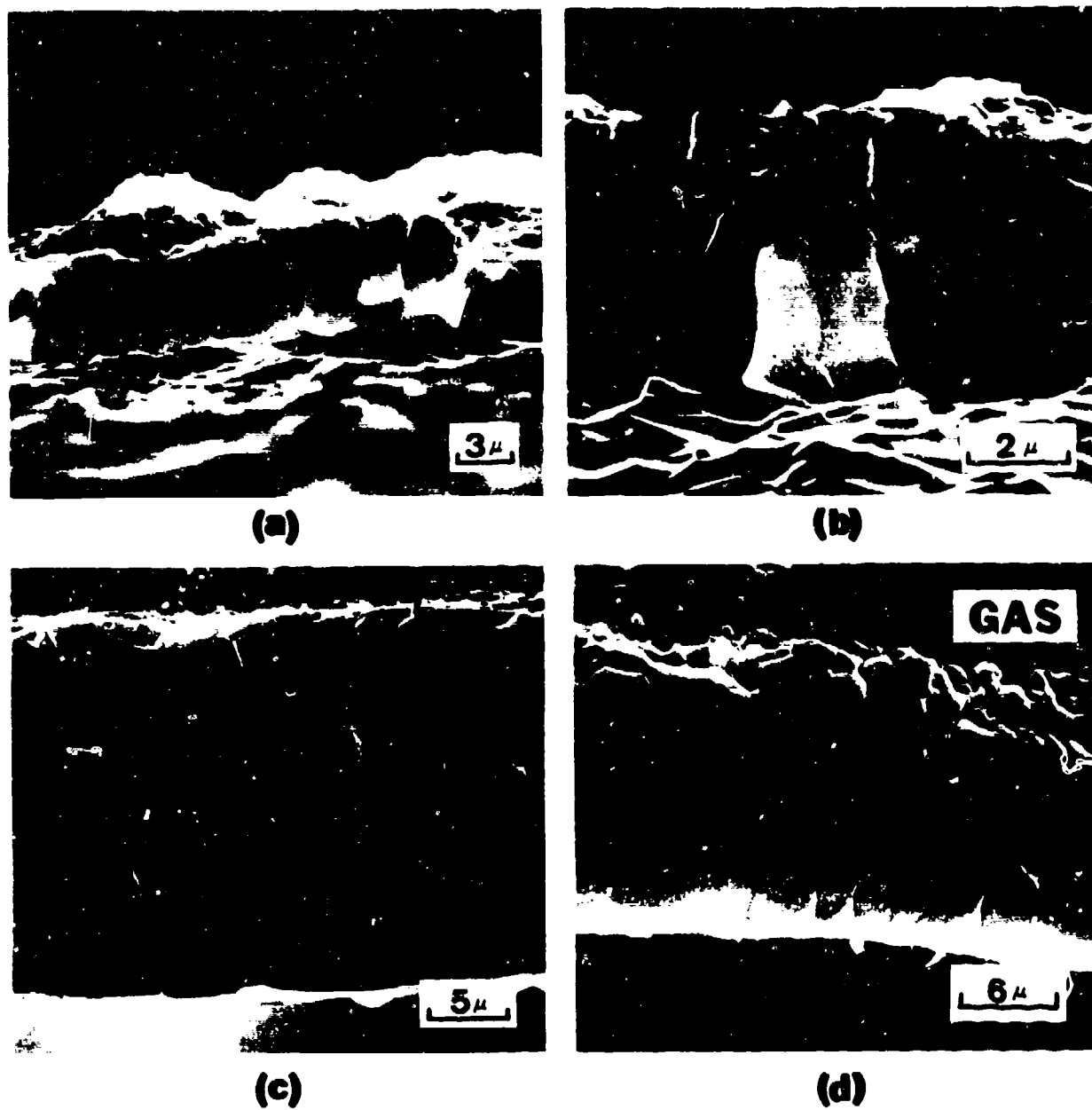


Figure 22 Scanning Micrographs Showing Microstructural Features of Polished and Etched (10 Minutes in Hot Phosphoric Acid), Transverse Sections Through Al_2O_3 Scales Formed on NiCrAl and CoCrAl Alloys After Oxidation at 1200°C in Air. (a) and (b) NiCrAl (HWA) after 100 hrs, (c) NiCrAl (VD) after 1000 hrs, (d) CoCrAl (HWA) after 1000 hrs.

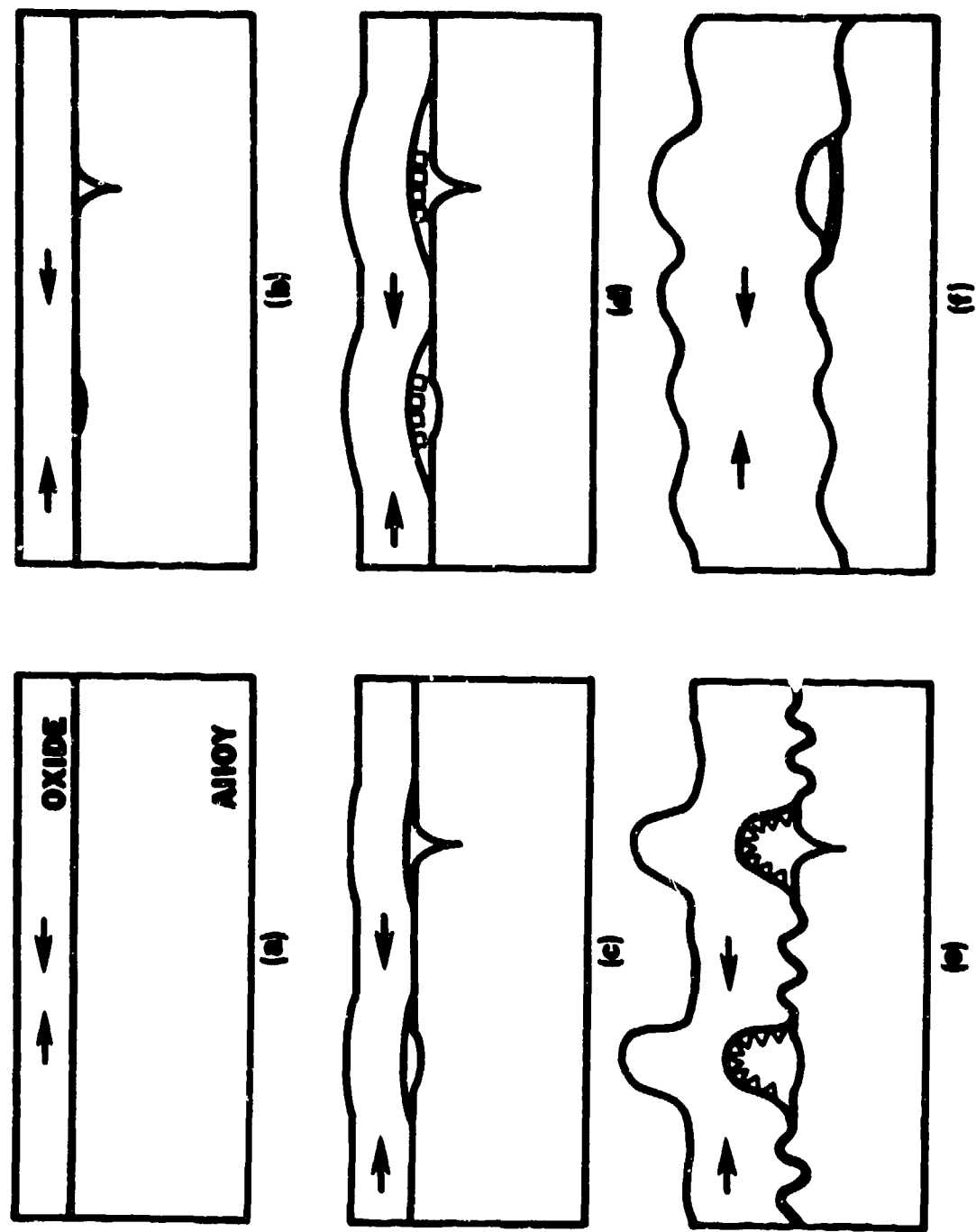


Figure 23. Schematic Diagram Illustrating the Formation of Voids at the Al_2O_3 - Substrate Interfaces of Al_2O_3 Scales Formed on NiCrAl and CoCrAl Alloys.

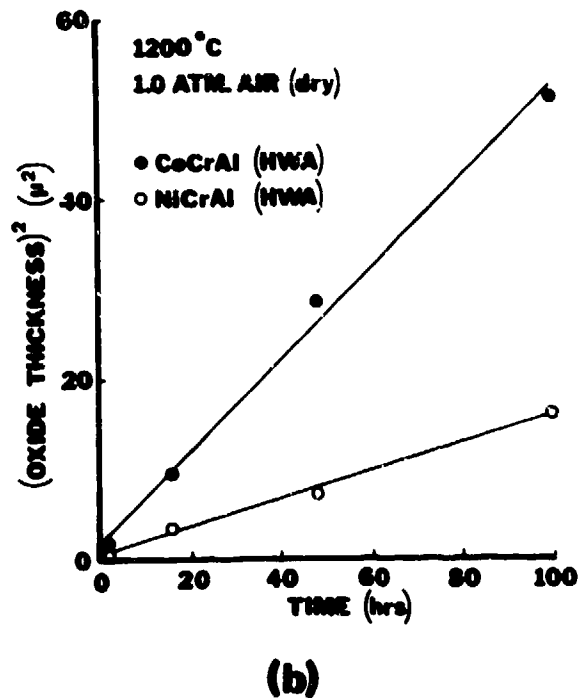
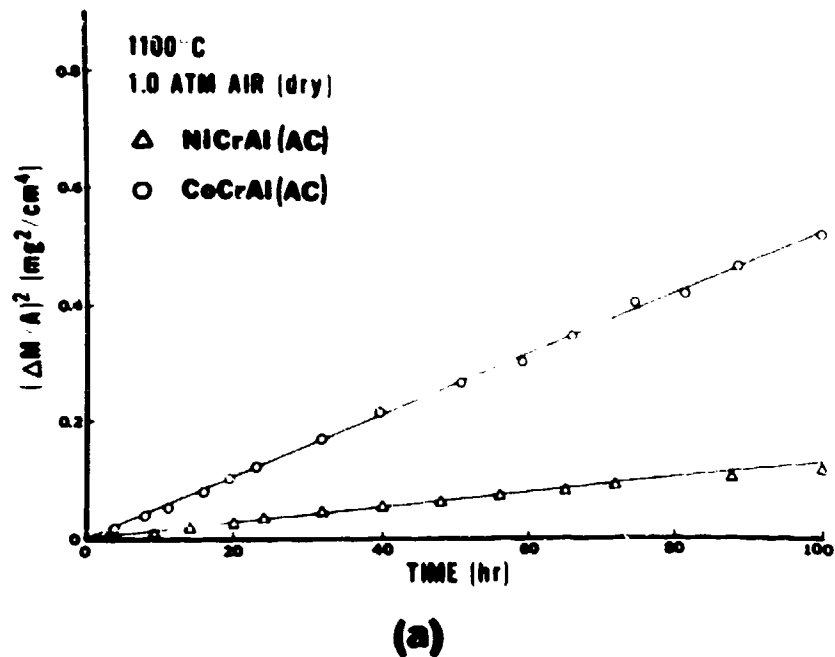


Figure 24 Typical Kinetic Data Obtained for the Oxidation of NiCrAl (Y) or CoCrAl (Y) Alloys. Both the weight-change versus time data (a) and the oxide thickness versus time data (b) conformed to the parabolic rate law for periods up to 100 hours.

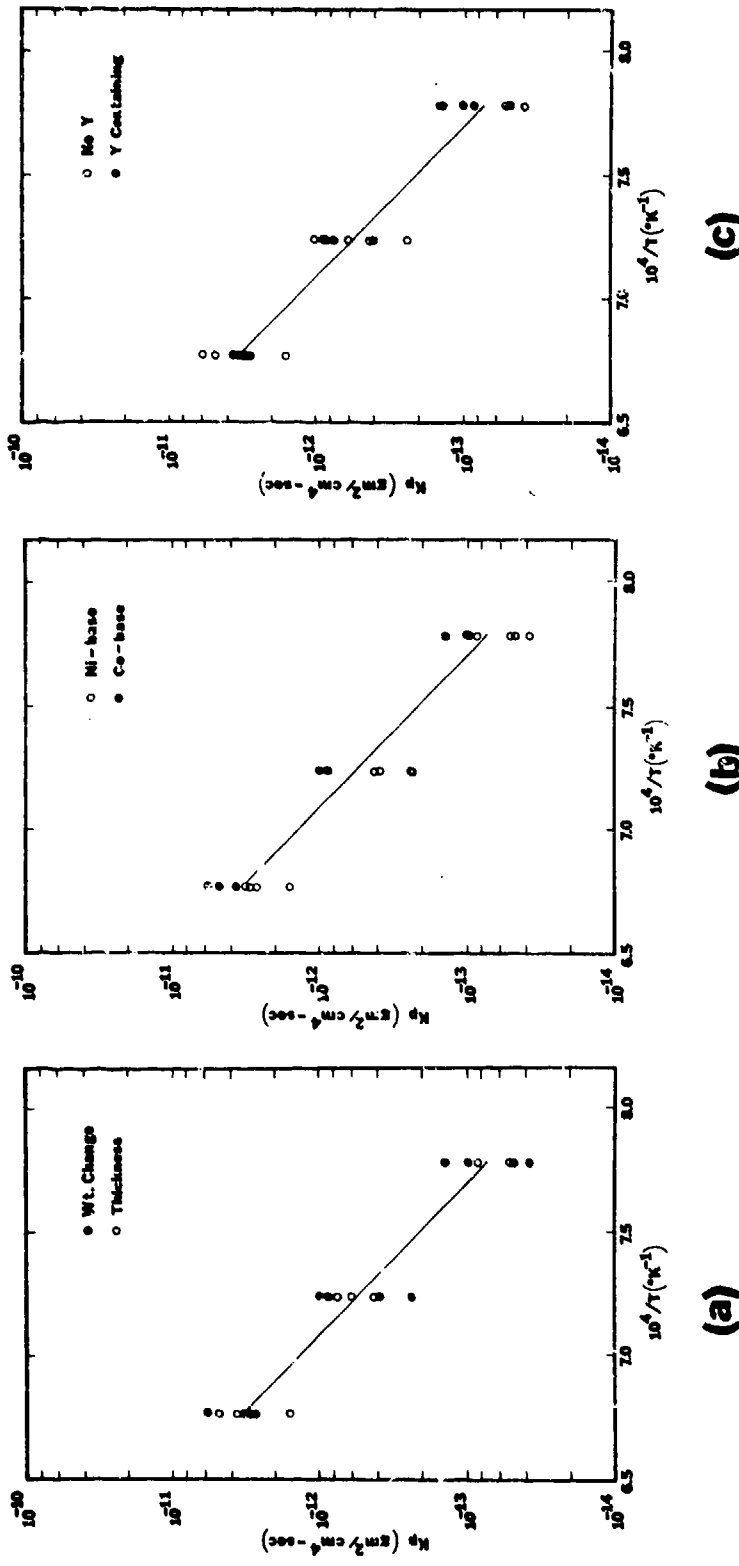


Figure 25 Arrhenius Plots of Parabolic Rate Constants Obtained From the Oxidation of Hot-Worked and Annealed NiCrAl, CoCrAl, NiCrAlY and CoCrAlY Alloys in 1 atm of Dry Air. (a) A significant difference between rate constants determined from weight-change and thickness measurements was not evident. (b) The rate constants for the cobalt-base alloys were consistently slightly greater than those for nickel-base alloys. (c) Yttrium in the alloys did not affect the rate constants.

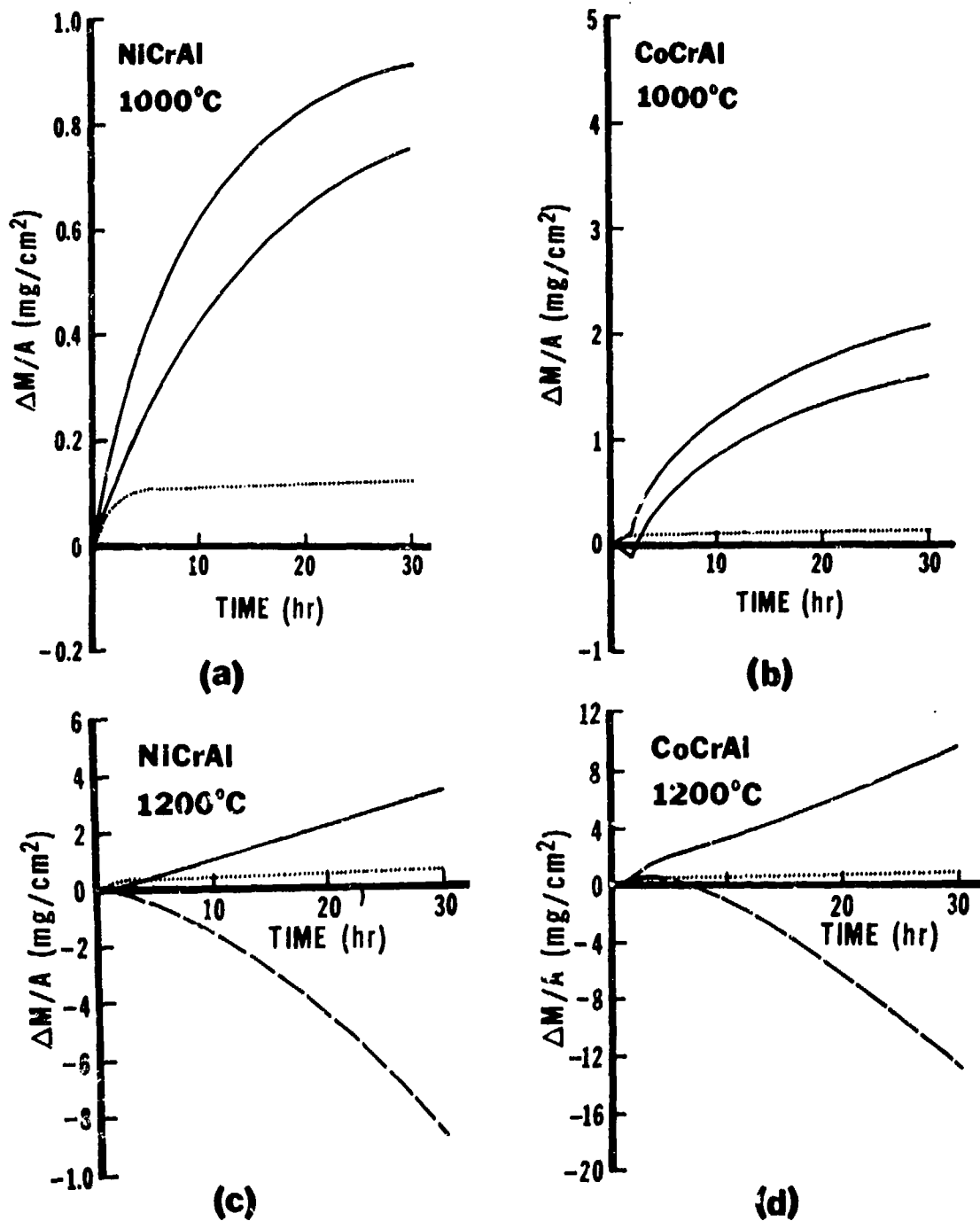


Figure 26 Weight-Change Versus Time Data for the Discontinuous Cyclic Oxidation (2-hr Cycles) of Hot-Worked and Annealed Alloys in Air. The solid curve represents total amount of oxygen consumed (i.e., weight of specimen plus spalled oxide). The dashed curve represents specimen weight. The dotted curve represents specimen weight-gain during isothermal oxidation. At 1000°C the specimen weight and the amount of oxygen consumed were not significantly different and two solid curves were therefore used to indicate the band within which all data points lie.

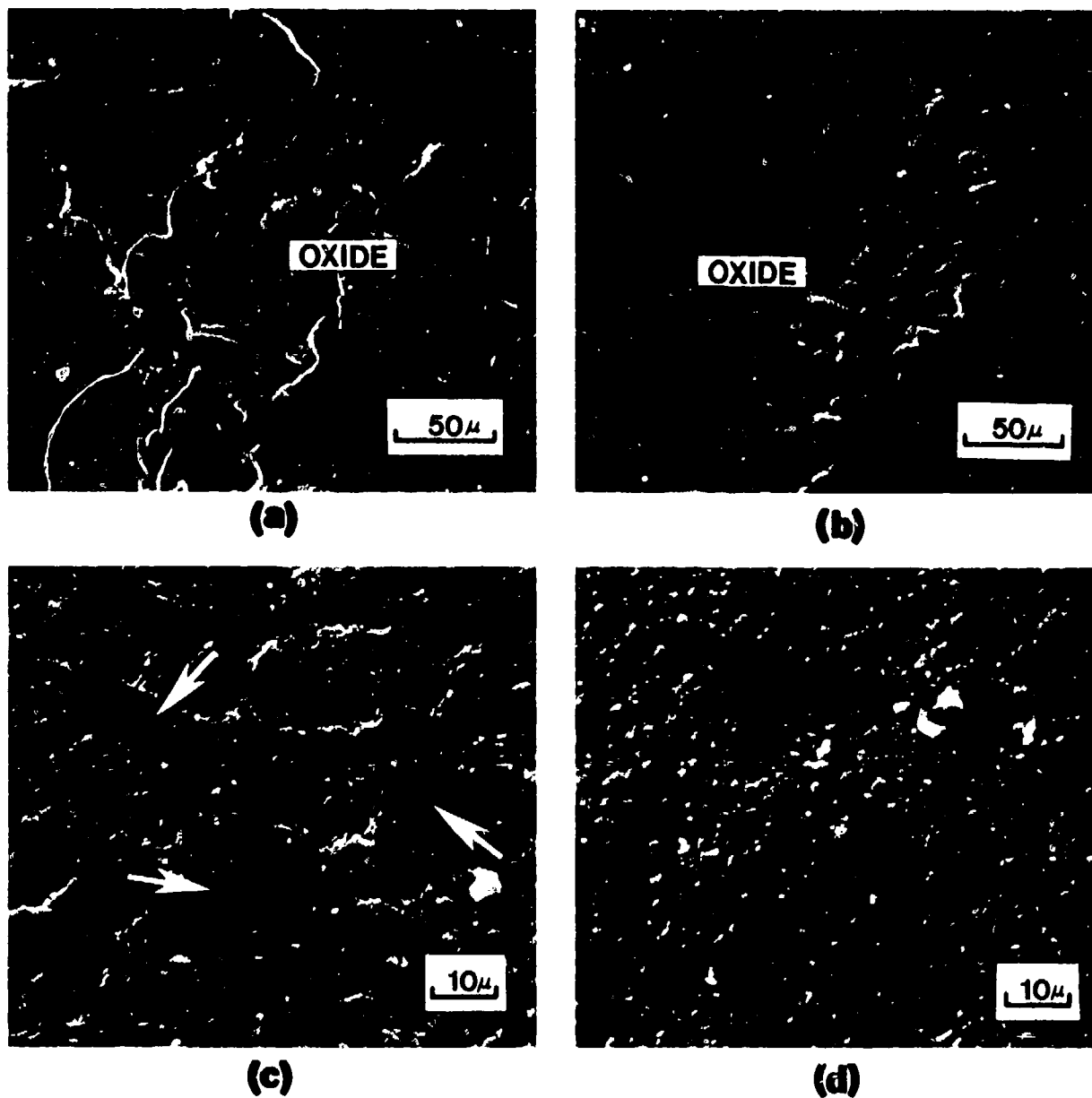
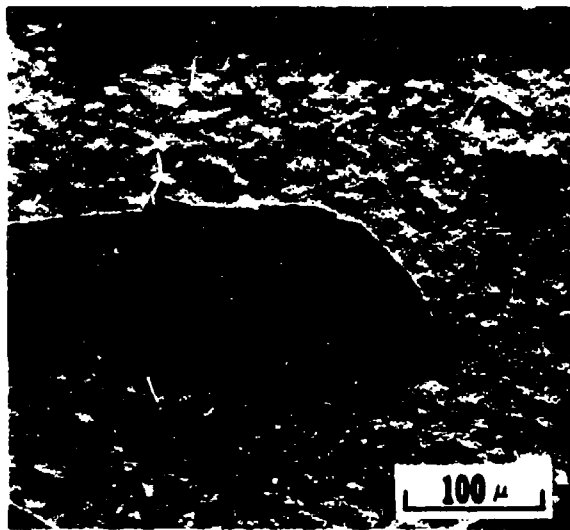
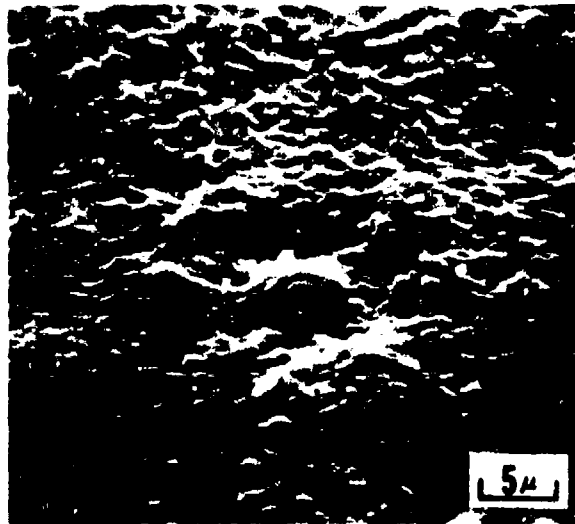


Figure 27 Photographs Showing the Effects of Specimen Surface Preparation on the Oxide and Substrate Morphological Features of NiCrAl (AC) After 24 hrs at 1200°C In 1 atm of Dry Air. The oxide which formed on the specimen polished through 600 grit SiC abrasive paper was wrinkled (a) and the substrate contained many smooth areas (c) (arrows). The oxide which developed on the electropolished specimen (1 min at 8V in a 10 v/o solution of H₂SO₄ in methyl alcohol contained in an ice bath) was not wrinkled in most areas (b) and the substrate beneath such areas contained only imprints from oxide grains (d).



(a)



(b)



(c)



(d)

Figure 28 Oxide Scale and Alloy Surface Morphologies of Electropolished Fe-25Cr-4Al After Isothermal Oxidation at 1200°C for 24 hrs in 1 atm of Air. (a) General structure of oxide flakes and bare alloy surface. (b) and (c) Low and high magnification of alloy surface specifically showing that the mounds of alloy were not smooth but faceted completely by imprints of the oxide grains. (d) Only a few regions of the oxide surface at the alloy interface contained voids.

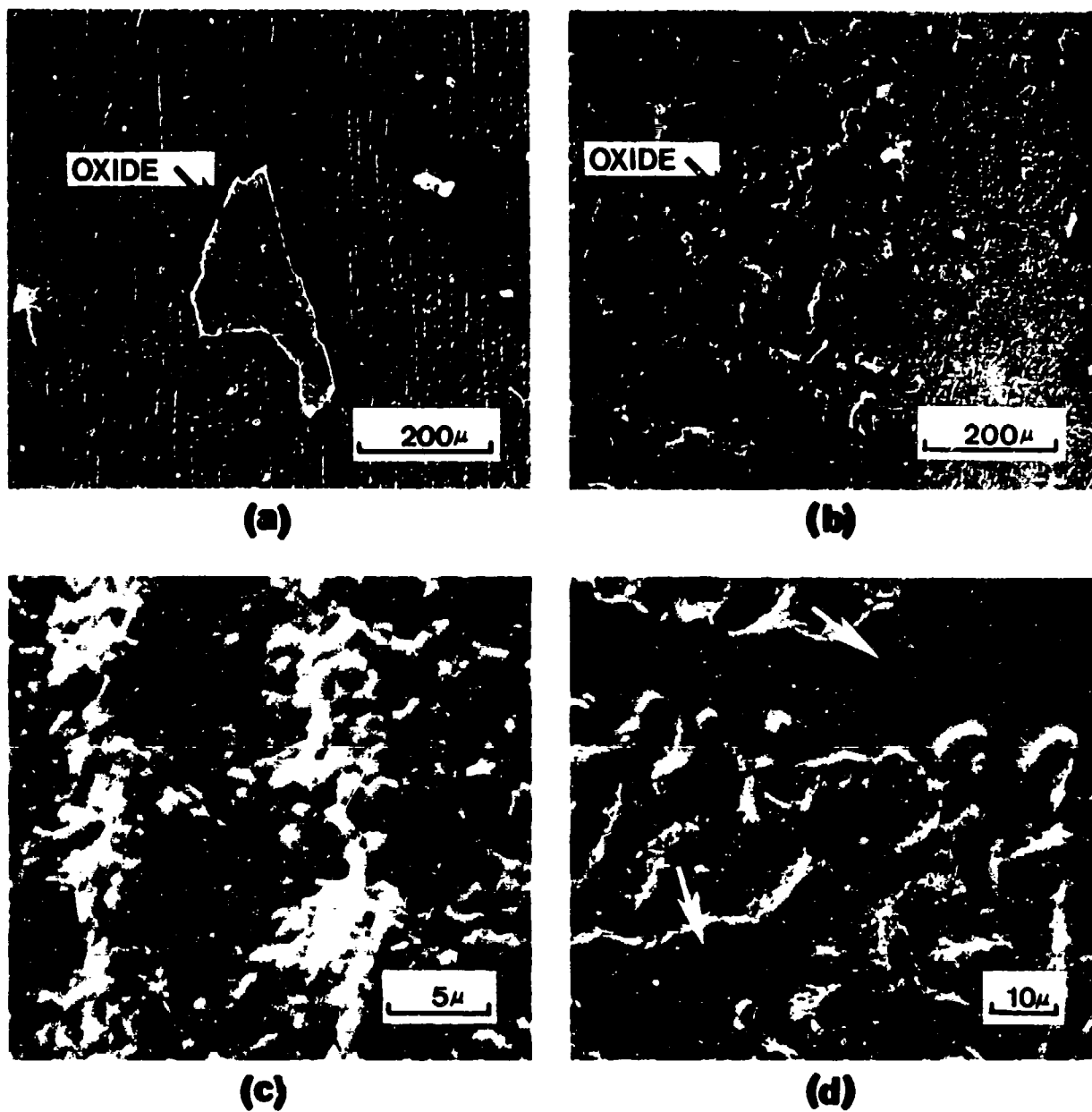


Figure 29 Comparison of Oxide and Substrate Morphologies After Oxidation of NiCrAl (HWA) at 1200°C in a CO₂-CO Mixture (CO₂/CO = 3) and In Air. After oxidation in the CO₂-CO mixture (24 hrs) the oxide, (a), was less wrinkled than after oxidation in air (16 hrs), (b). Furthermore, the specimen surface after oxidation in CO₂-CO contained imprints of oxide grains, (c), rather than numerous smooth areas (arrows) observed after oxidation in air, (d).

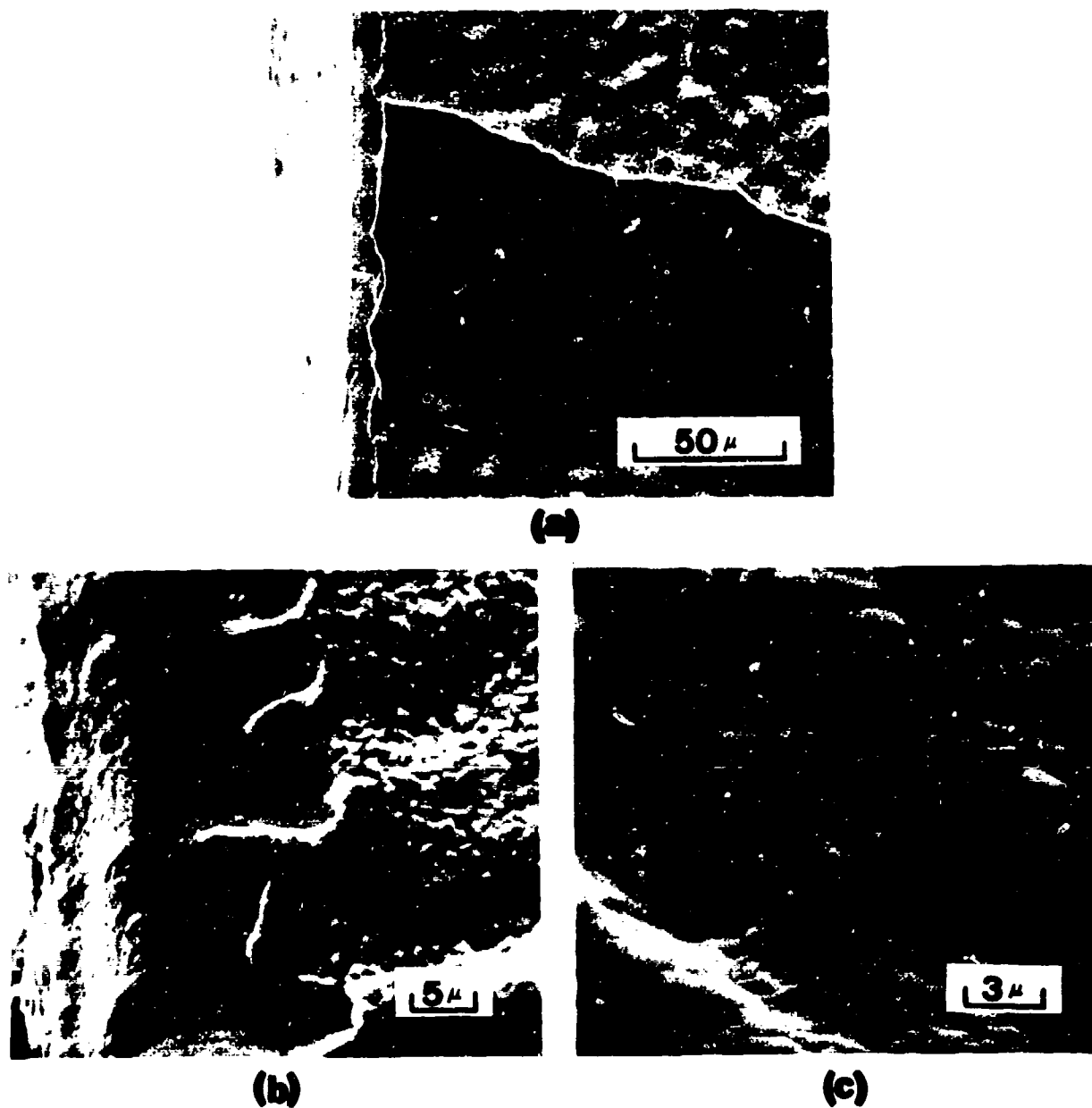
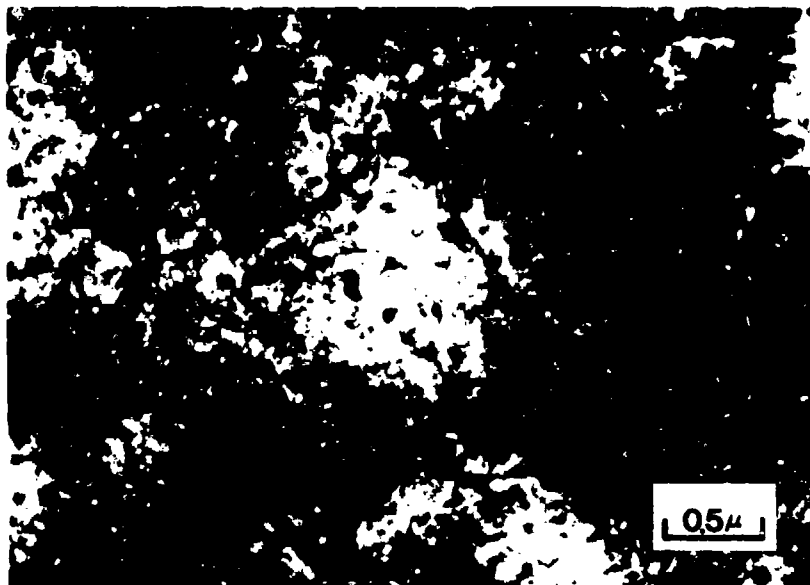


Figure 30 Oxide and Substrate Morphologies on NiCrAl (HWA) After Oxidation for 2 hrs in a CO₂-CO Mixture (CO₂/CO = 3) and Then 20 hrs in Air at 1200°C. The oxide surface did not contain wrinkles but had an undulating texture, (a). Smooth areas were only observed at the edges of the specimen (a) and (b). The surface of the Al₂O₃ at the Al₂O₃-substrate interface exhibited well defined oxide grains, oxide crystallites were not evident, (c).



(a)



(b)

Figure 31 Morphological Features of Oxides Developed on NiCrAlY and CoCrAlY Alloys. (a) After 5 minutes of oxidation at 1100°C in air of NiCrAlY (VD), bright field transmission electron micrographs indicated that a relatively uniform oxide film had developed. (b) After longer periods of oxidation a network of yttrium oxide was evident on the Al_2O_3 and also in the alloy substrate [CoCrAlY (HWA) 24 hrs in CO_2 -CO mixture ($\text{CO}_2/\text{CO} = 3$) at 1200°C].

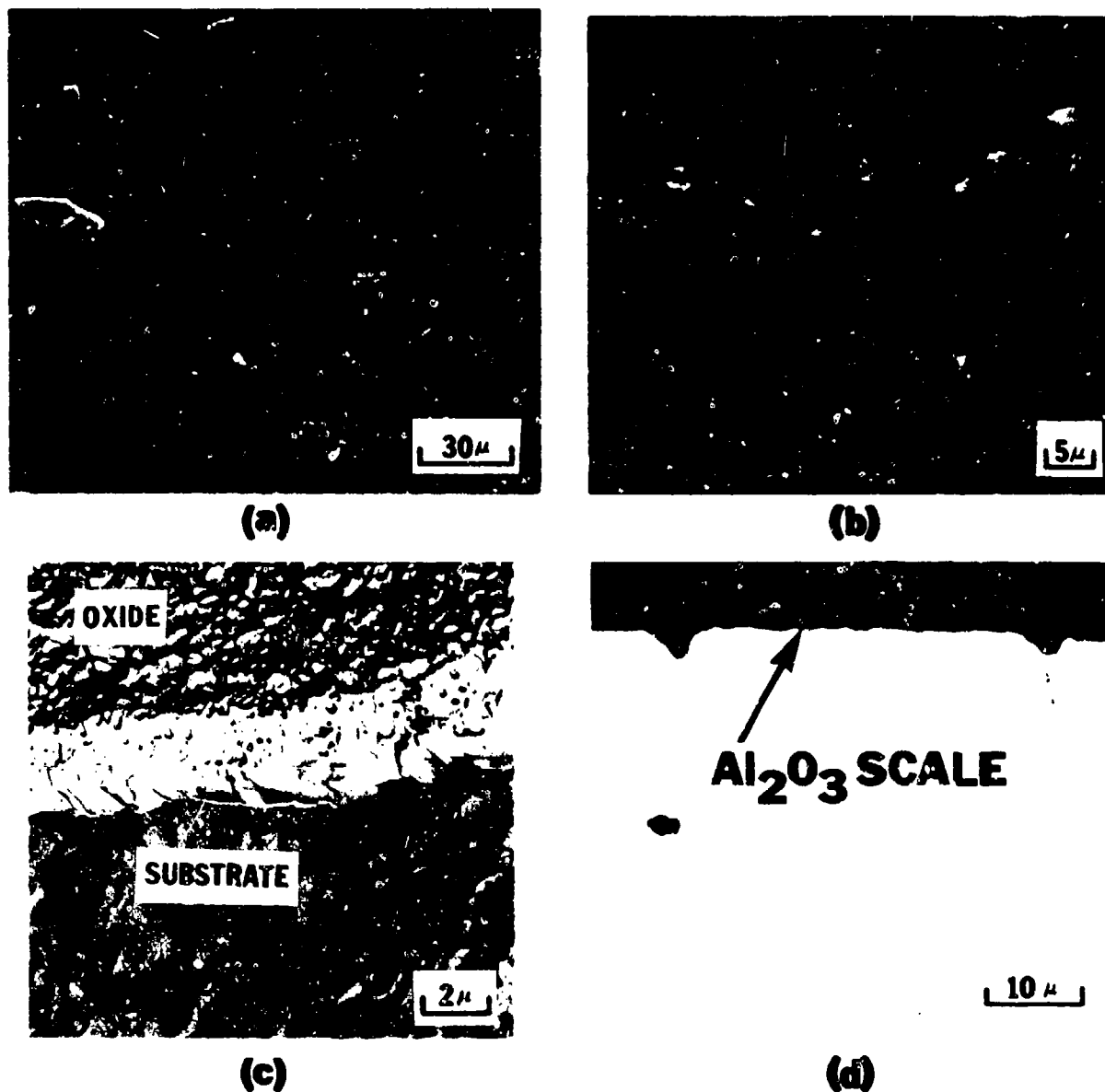


Figure 32 Morphological Features of Oxides and Substrates After Oxidation of NiCrAlY and CoCrAlY Alloys. (a) Surface of NiCrAlY (VD) specimen after 100 hrs of oxidation in air at 1100°C. (b) Photograph of the surface of the specimen described in (a) at an area where the oxide had spalled. (c) Replica electron micrograph showing features of oxide and substrate of CoCrAlY (AC) after 100 hrs of oxidation at 1100°C in air. (d) Photograph showing section through specimen described in (c).

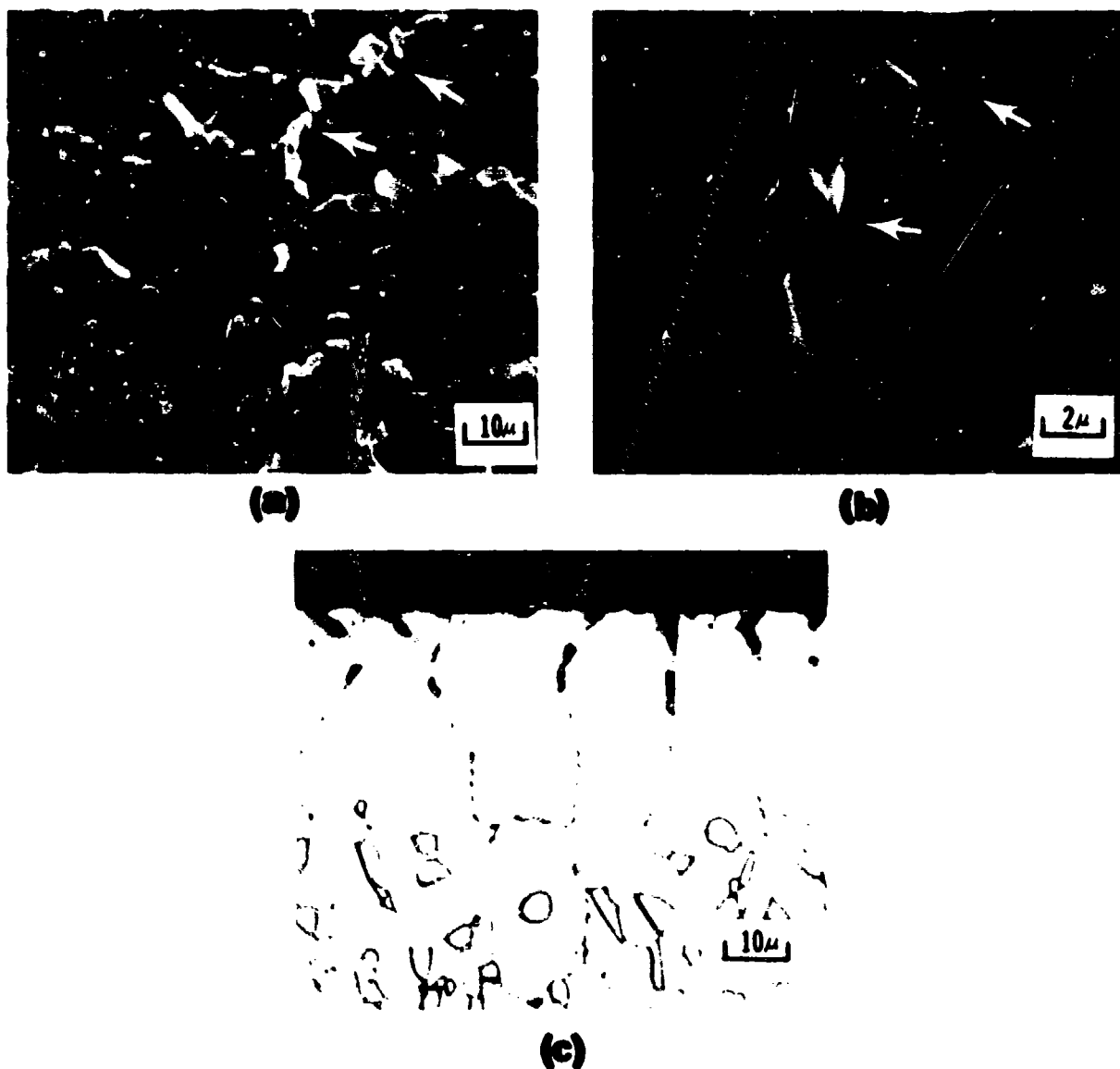


Figure 33 Photographs Showing the Network of Oxide Protrusions Which Were Formed On NiCrAlY and CoCrAlY Alloys. (a) and (b) Oxide scale morphology at alloy-oxide interface after extraction of the scale from a CoCrAlY (HWA) specimen which had been oxidized at 1100°C for 100 hrs in 1 atm of dry air. The oxide pegs are aligned (arrows). (c) Etched specimen of CoCrAlY (VD) after oxidation in air at 1100°C showing correspondence of internal pegs to grain boundaries in substrate.

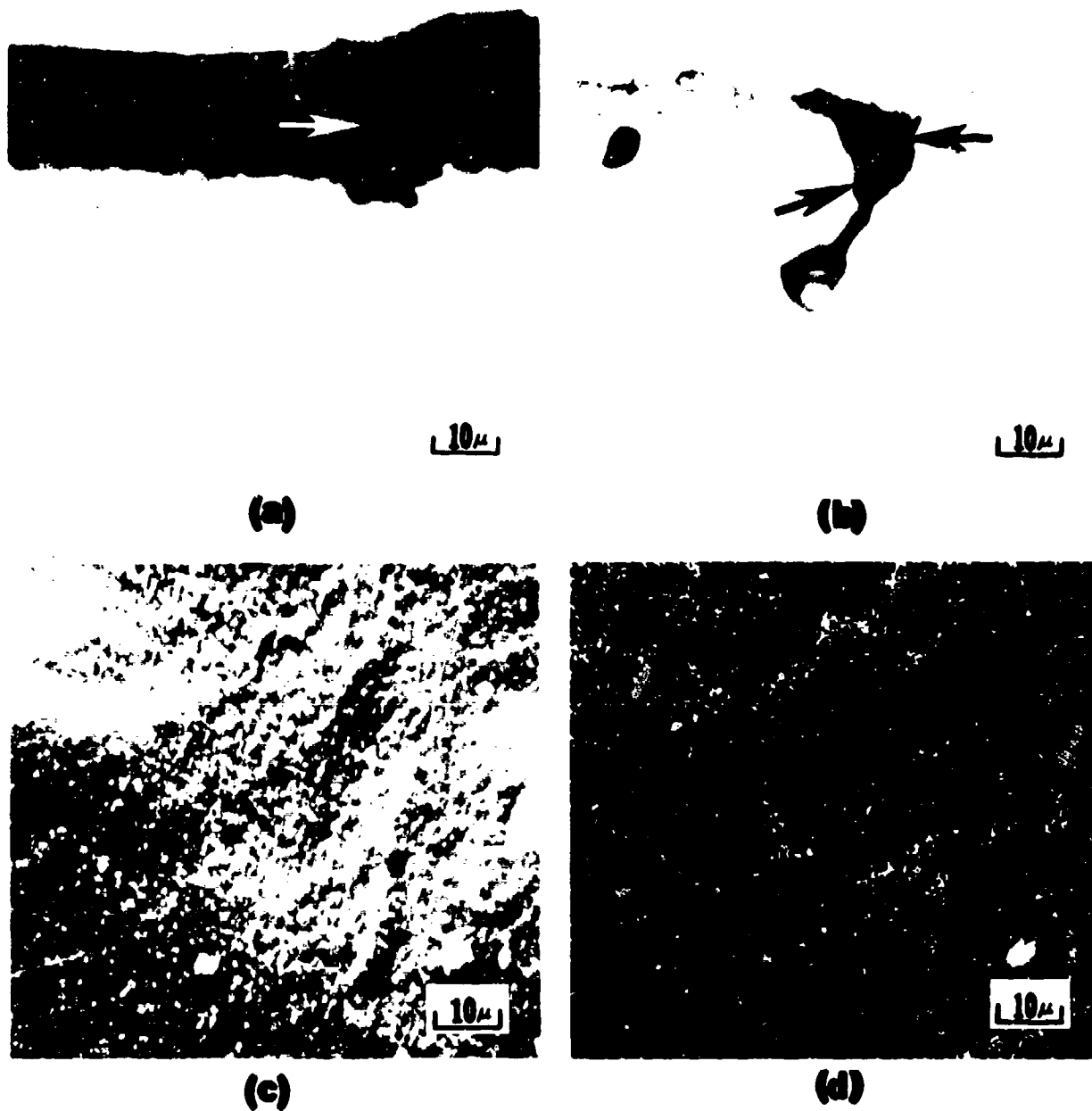
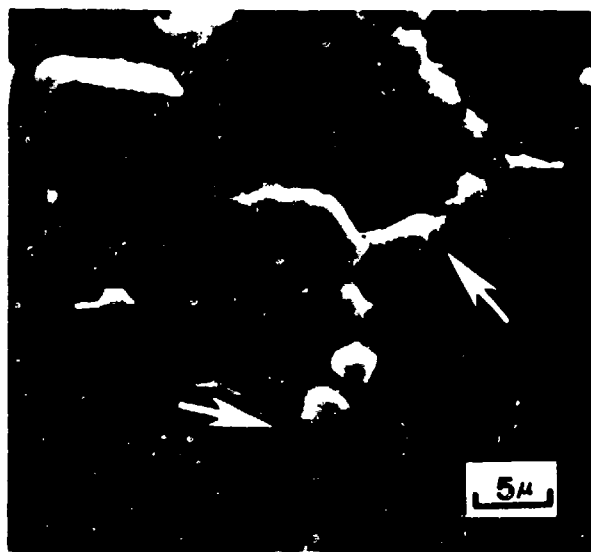
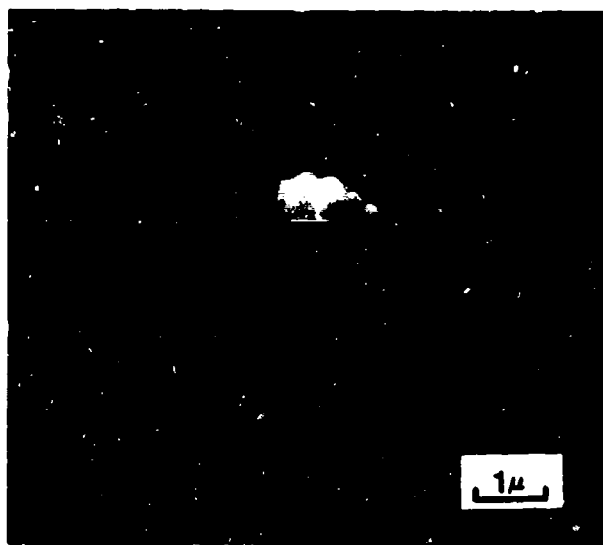


Figure 34 Photographs Showing Features of Yttrium Oxide After Oxidation of NiCrAlY and CoCrAlY Alloys. (a) and (b) Transverse sections through CoCrAlY (HWA) after oxidation at 1200°C for 1000 hrs in 1 atm of air. In (a) an enveloped yttrium oxide stringer (arrow) is visible. In (b) the arrows indicate areas of envelopment of a yttrium oxide stringer by Al_2O_3 . (c) and (d) Secondary electron image and corresponding yttrium x-ray image photographs, respectively, of the oxidized surface (oxide-gas interface) of NiCrAlY (VD) after 1000 hrs at 1200°C in 1 atm of air.



(a)



(b)



(c)

Figure 35 Photographs of Extracted Al_2O_3 Flakes From CoCrAlY (HWA) Showing Al_2O_3 -Substrate Interfaces. (a) At low magnifications the coarse network of yttrium oxide protrusions is evident (arrows). (b) and (c) At high magnifications much finer oxide particles are evident. (a) and (b) flakes formed after 16 hrs at 1200°C in air. (c) flake formed after 100 hrs at 1000°C in air.

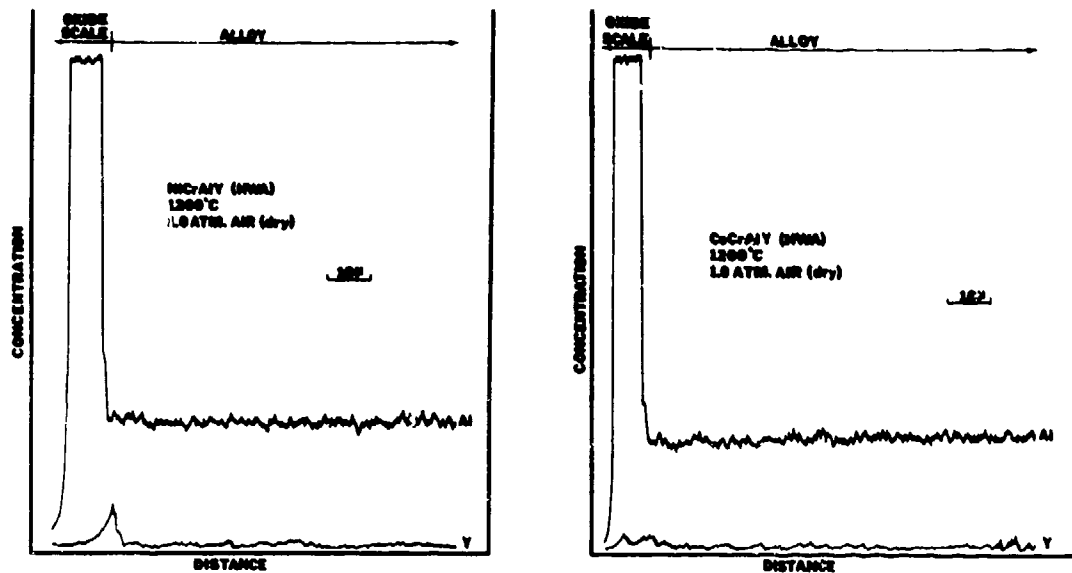


Figure 36 Intensity Profiles Showing the Distribution of Aluminum and Yttrium Across NiCrAlY (HWA) and CoCrAlY (HWA) Alloy Specimens After 100 hrs of Oxidation at 1200°C in 1 atm of Dry Air.

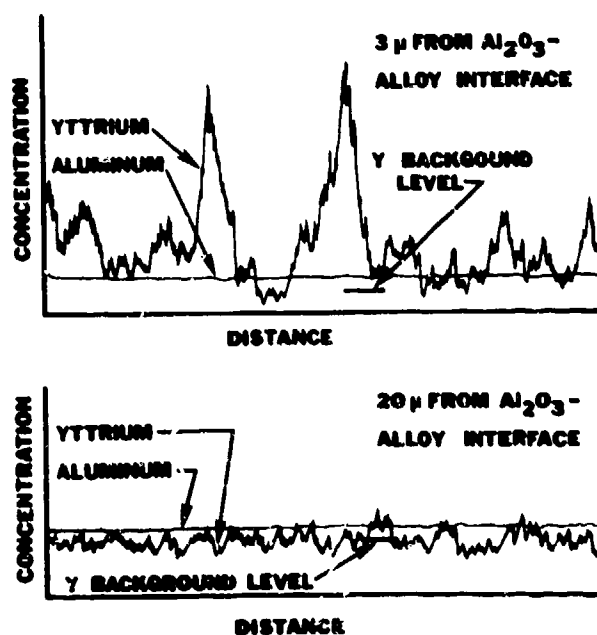


Figure 37 Intensity Profiles Showing the Distribution of Aluminum and Yttrium Parallel to the Al_2O_3 -Alloy Interface at Distances of 3 and 20 Microns Into The NiCrAlY Alloy Described in Figure 36.

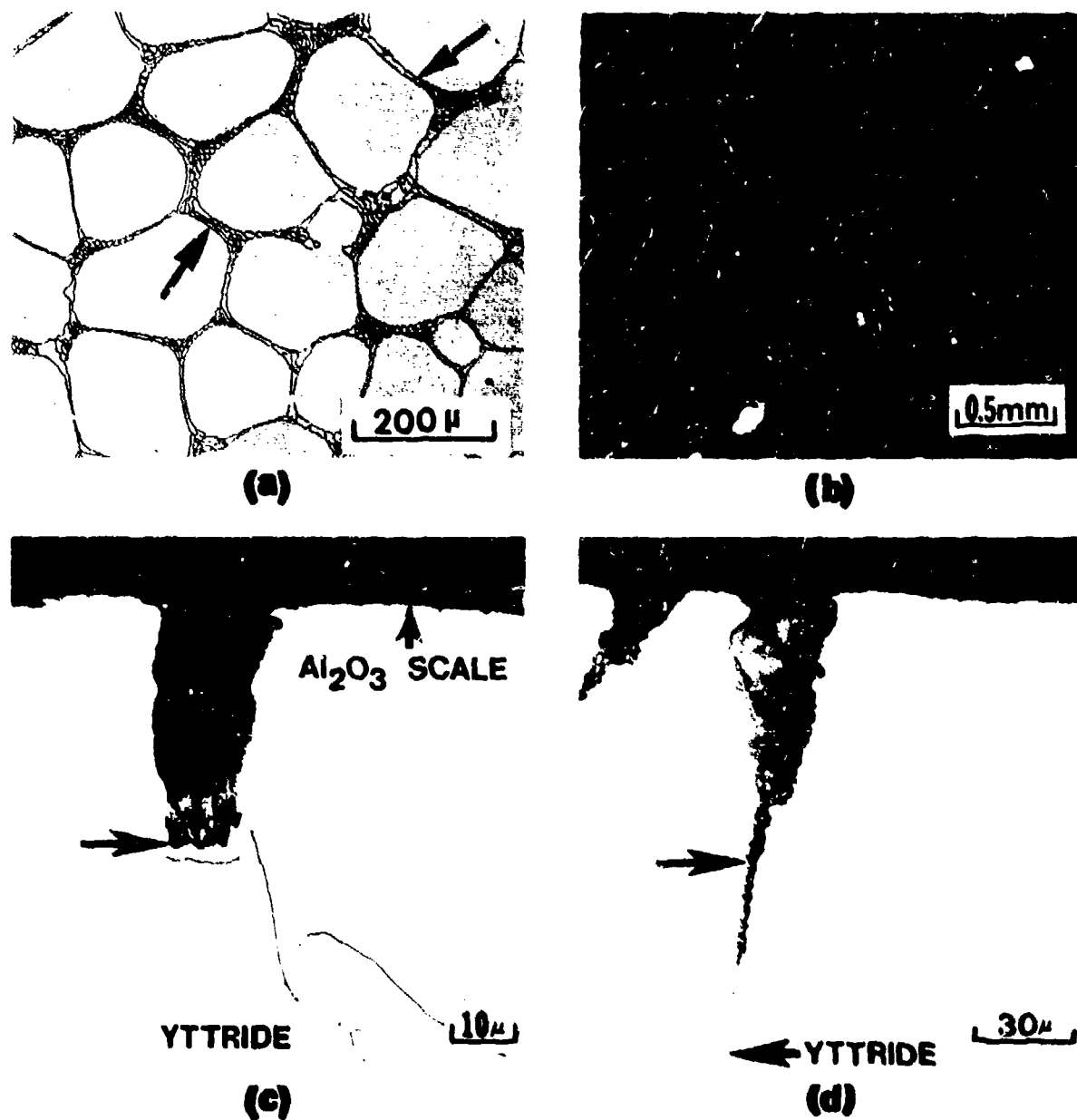
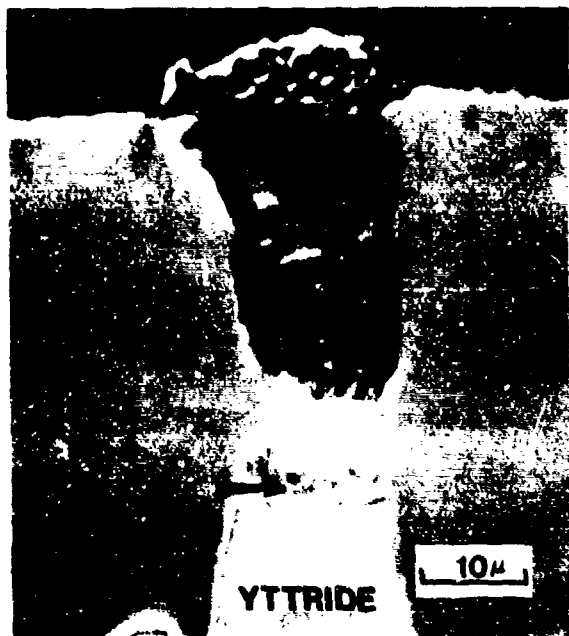
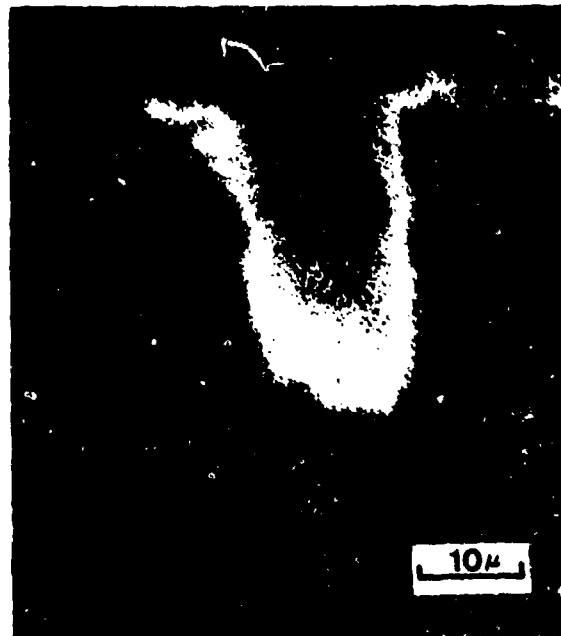


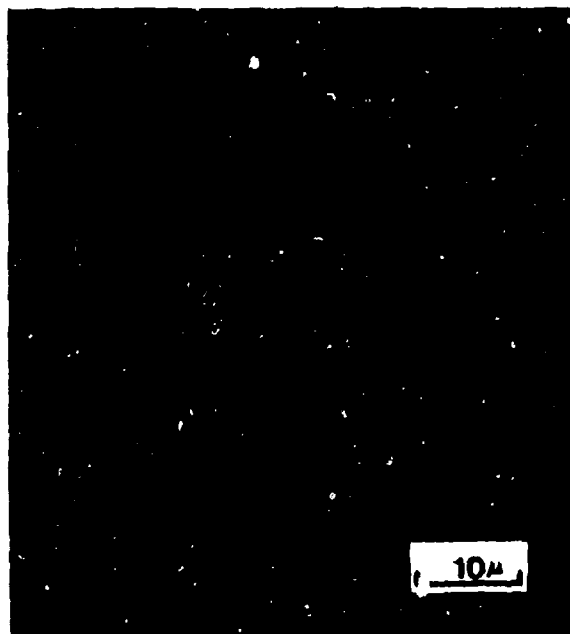
Figure 38 Features Developed on a Ni-15Cr-6Al-3Y Alloy (Plane-Front Solidified) After Oxidation at 1200°C in 1 atm of Air. (a) Microstructure of alloy prior to oxidation, (b) Surface morphology of specimen after 30 min of oxidation, (c) and (d) Transverse sections through specimens after 1 and 16 hrs of oxidation, respectively, showing features of preferential yttride oxidation.



(a)



(b)



(c)



(d)

Figure 39 Electron Back Scatter Photomicrograph and X-ray Image Photographs Showing Features of Preferential Yttride Oxidation. The results were obtained with the specimen described in Figure 38c. (a) Electron back scatter photomicrograph, the arrows indicate the diffusion zone in which yttrium oxide particles (white arrow) have been formed. (b), (c) and (d) X-ray image photographs for the distributions of aluminum, yttrium, and chromium, respectively.

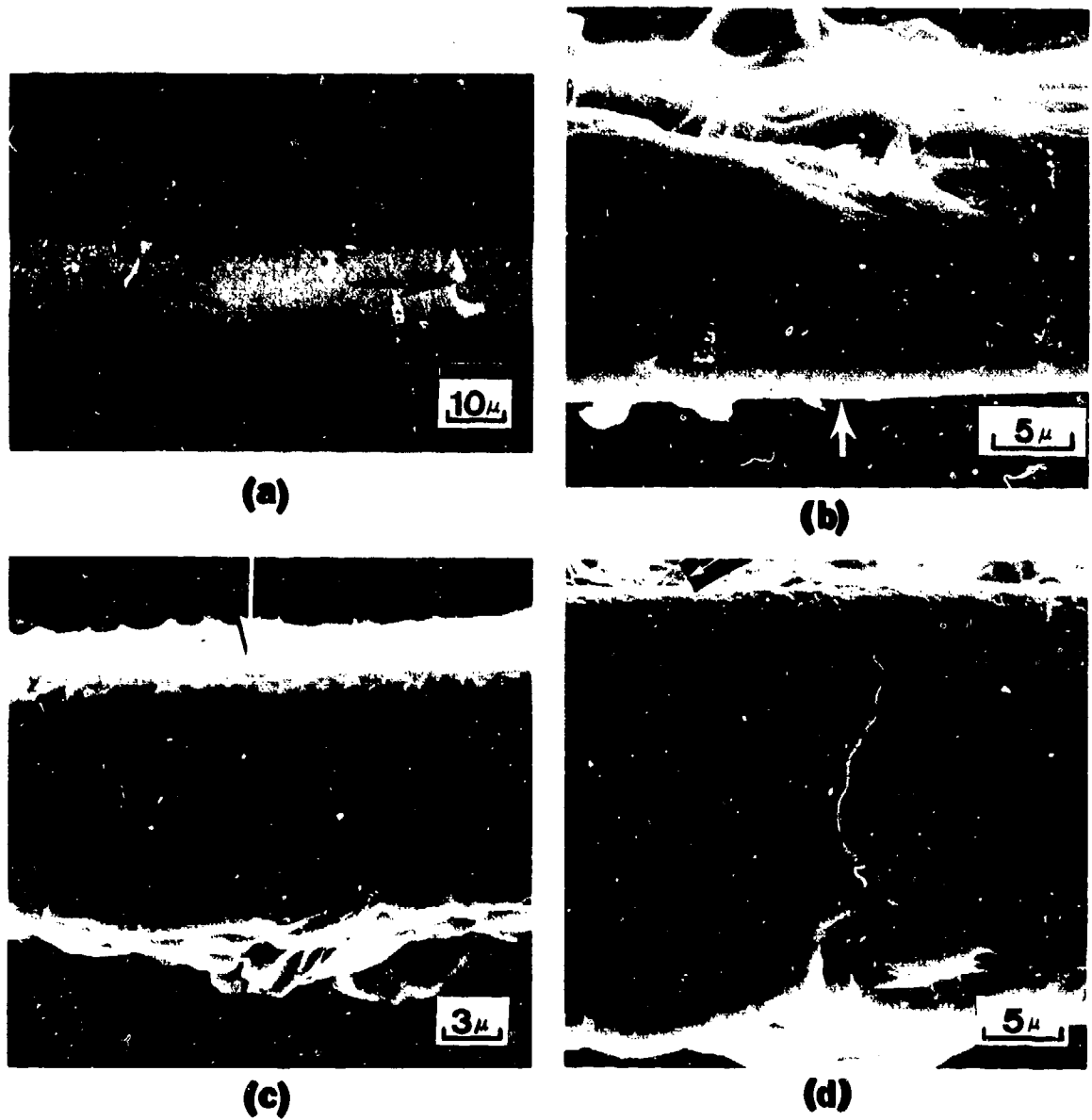


Figure 40 Photographs Showing Features of Transverse Sections Through Al_2O_3 Formed on CoCrAlY (HWA) After Oxidation at 1200°C in Air. (a) Unetched Al_2O_3 formed after 1000 hours, (b) and (c) Al_2O_3 described in (a) after etching (10 min in hot phosphoric acid), (d) etched Al_2O_3 after 3,716 hrs. Black arrows indicate yttrium rich oxides that have been incorporated into the Al_2O_3 scales. White arrows point to oxide-gas interface.

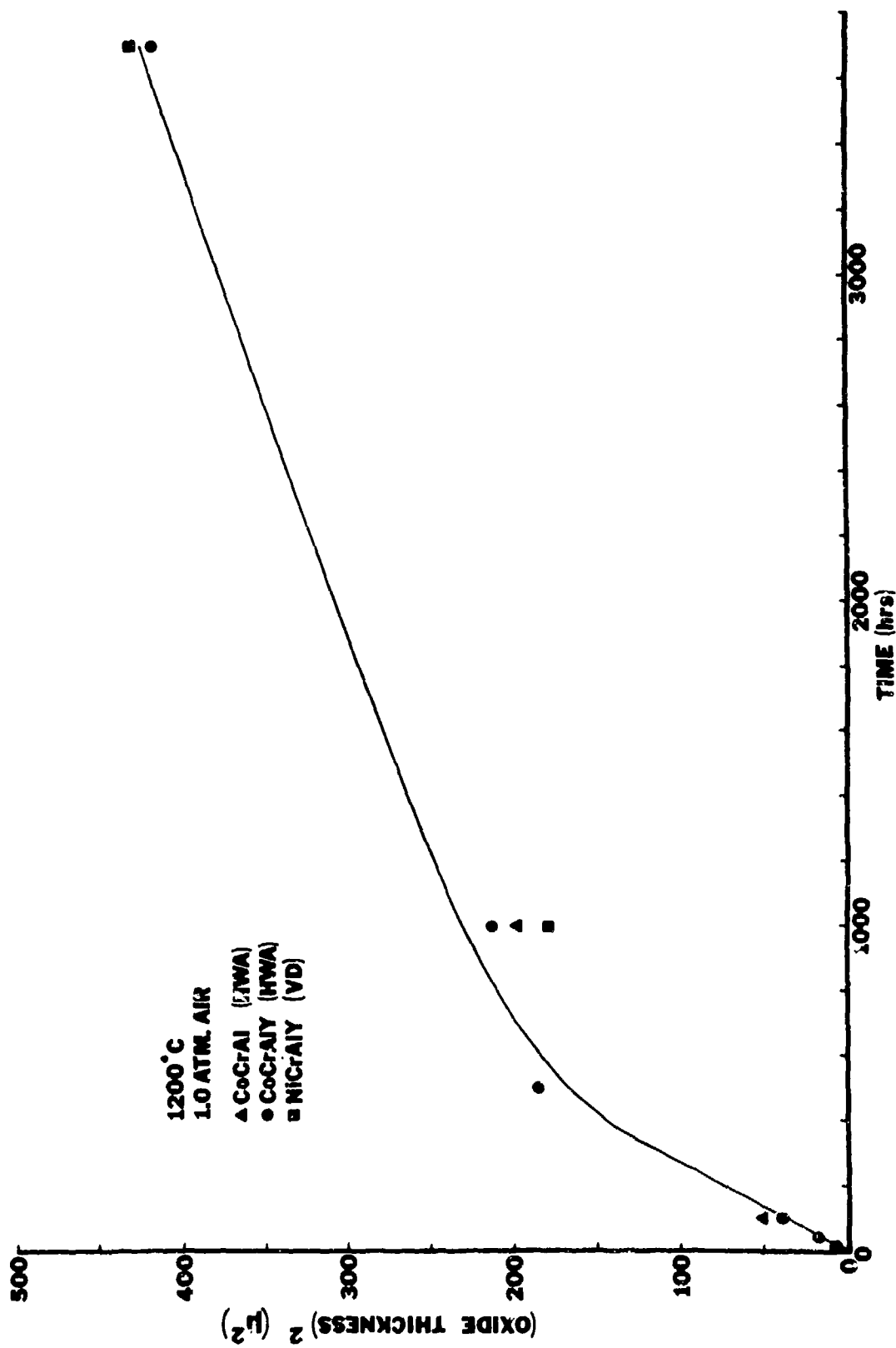


Figure 41. Data Obtained From Thickness Measurements of the Al_2O_3 Scales Formed on CoCrAl, CoCrAlY and NiCrAlY Alloys After Isothermal Oxidation at 1200°C in Air.

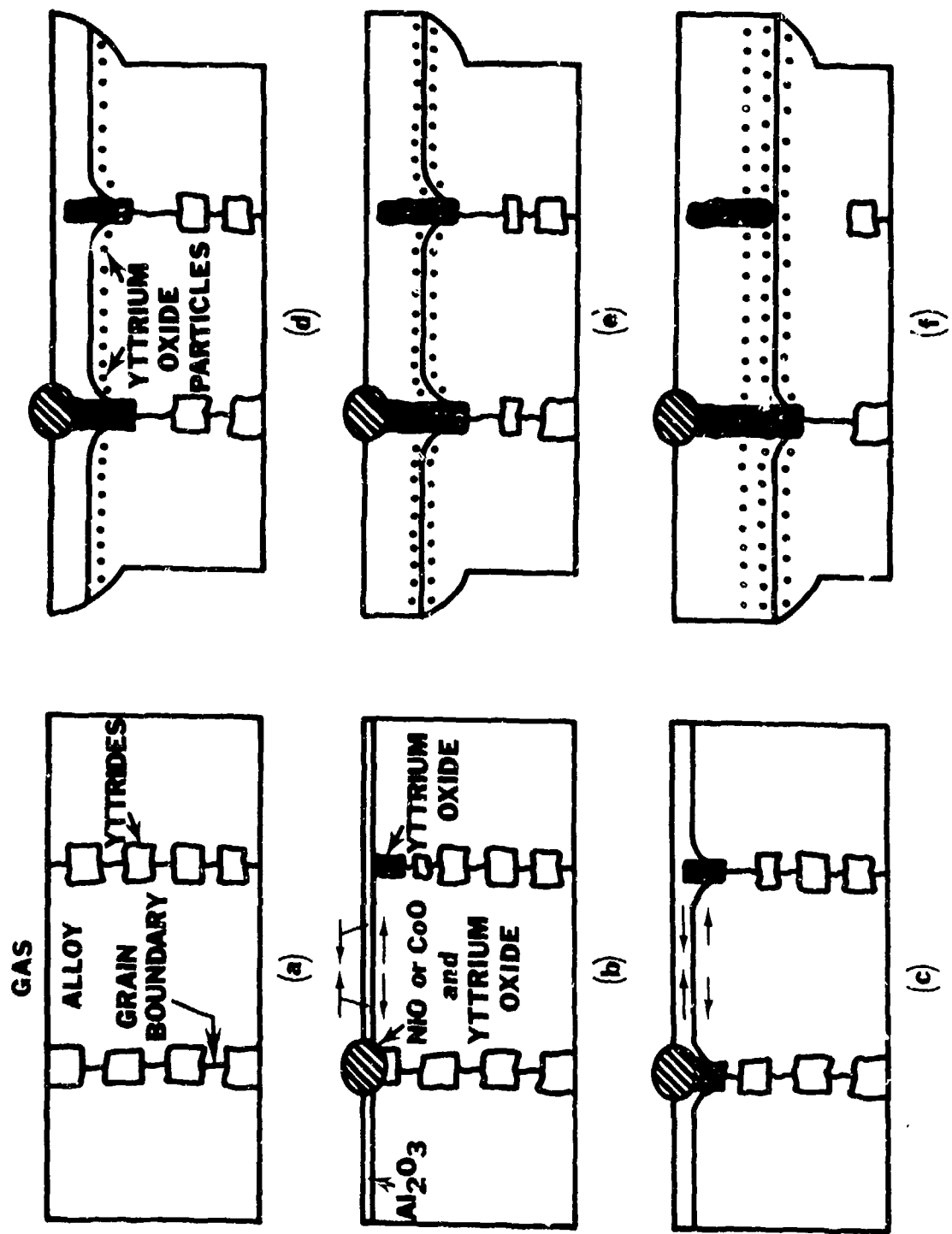


Figure 42 Schematic Diagrams Illustrating the Oxidation Mechanism of NiCrAlY and CoCrAlY Alloys.

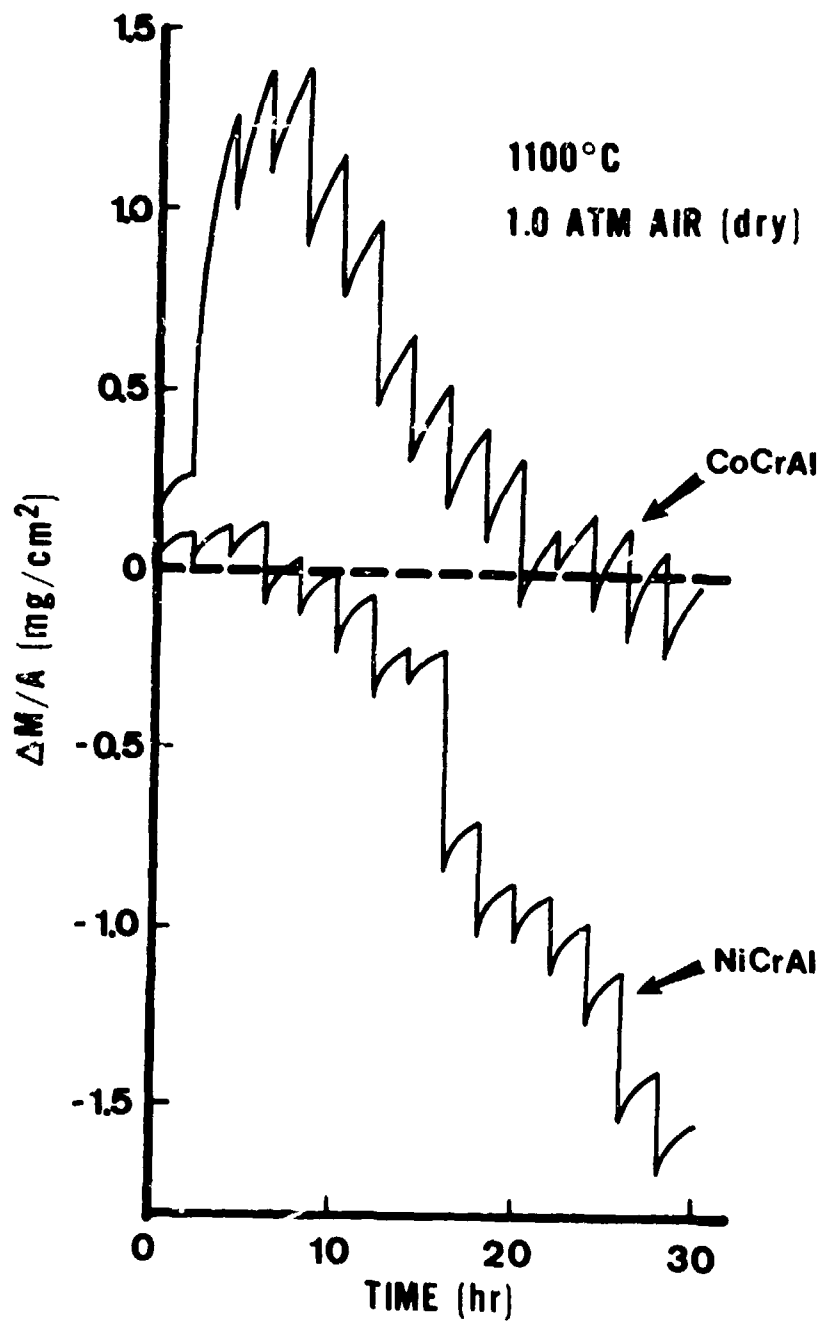


Figure 43 Continuous Weight-Change Versus Time Data Obtained for the Oxidation of the NiCrAl (HWA) and CoCrAl (HWA) Specimens at 1100°C in 1 atm of Dry Air. The shape of these curves indicates that the oxide scales formed on these specimens are cracking and spalling during each thermal cycle.

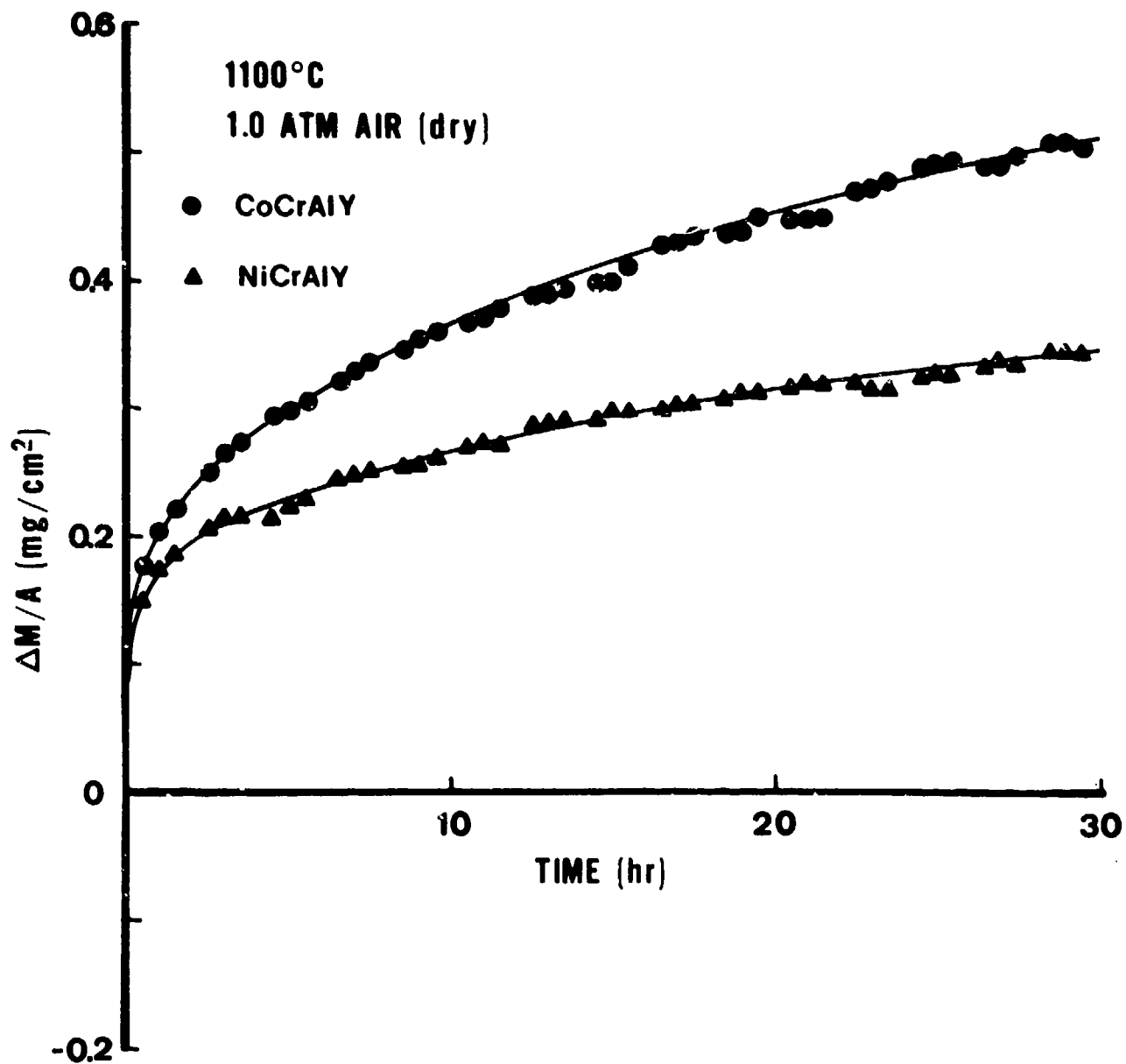
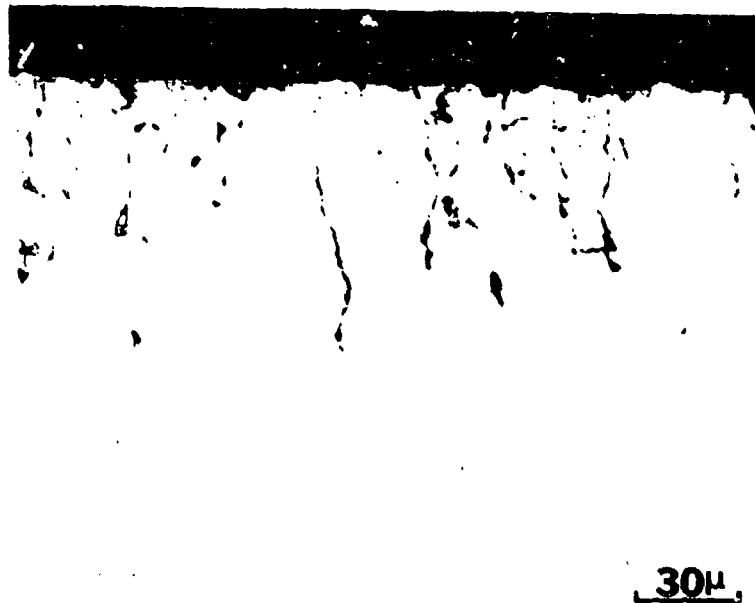


Figure 44 Continuous Weight-Change Versus Time Data Obtained for the Cyclic Oxidation of NiCrAlY (HWA) and CoCrAlY (HWA) Specimens at 1100°C in 1 atm of Dry Air. The shapes of the curves are very similar to those obtained for the same alloys under isothermal conditions. This indicates that negligible cracking of the oxide scales occurred during cycling.



(a)



(b)

Figure 45 Photographs Showing Microstructures of Transverse Sections Through CoCrAlY Specimens After Cyclic Oxidation Testing at 1100°C in Air. (a) As-cast alloy after 500 hrs, and (b) vapor-deposited alloy after 1000 hrs.

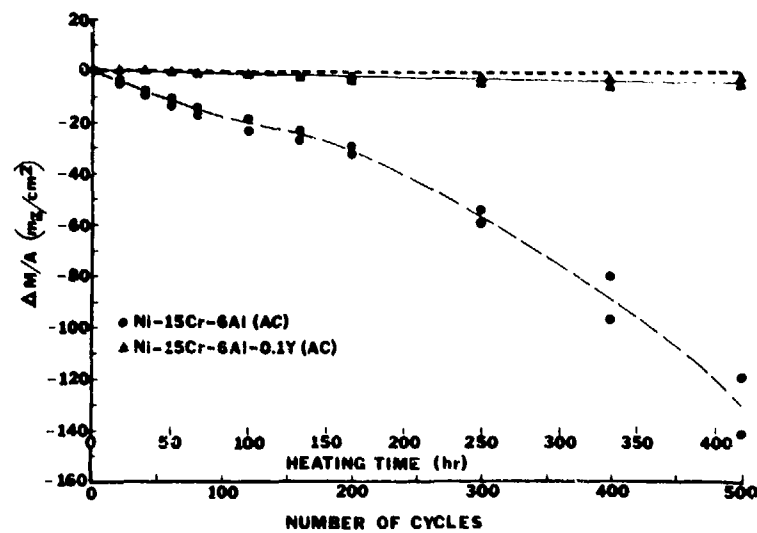
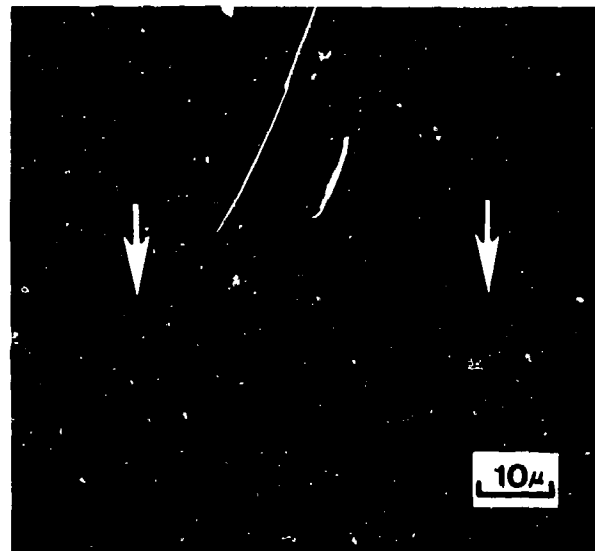
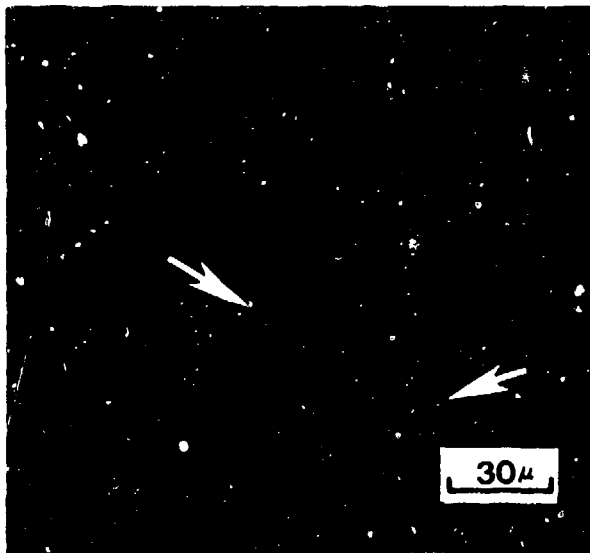


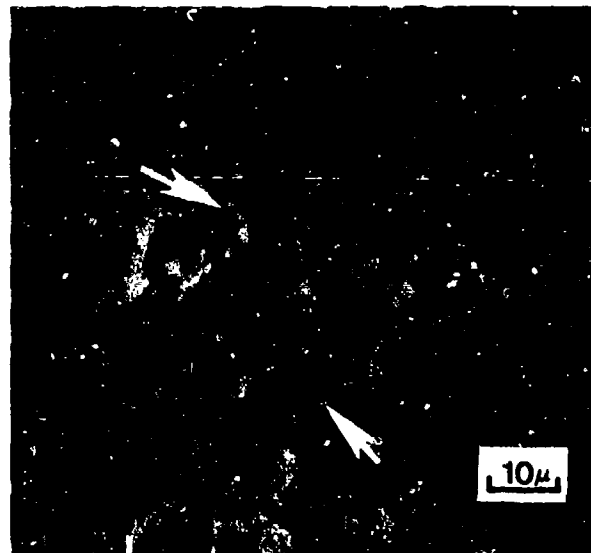
Figure 46 Weight-Change Versus Time Data Obtained for the Cyclic Oxidation of As-Cast NiCrAl and NiCrAlY Alloys in Air at 1150°C.



(a)



(b)



(c)

Figure 47 Photographs Showing the Networks of Yttrium Oxide Developed at the Al_2O_3 -Substrate Interfaces of As-Cast, Hot-Worked and Annealed and Vapor-Deposited Alloys. (a) Flake extracted from NiCrAlY (AC) after 2 hrs of oxidation in 1 atm of dry air at 1100°C . (b) Flake extracted from CoCrAlY (HWA) after 48 hrs of oxidation at 1100°C in 1 atm of dry air. (c) Flake extracted from CoCrAlY (VD) after 48 hrs of oxidation in 1 atm of dry air at 1100°C . The arrows indicate the coarse network of oxide protrusions.



Figure 48 Photograph Showing Large Flakes (Arrows) of Al_2O_3 Which Spalled From CoCrAl (VD) Specimen Upon Cooling to Room Temperature After 2 hrs of Oxidation at 1100°C in Air.

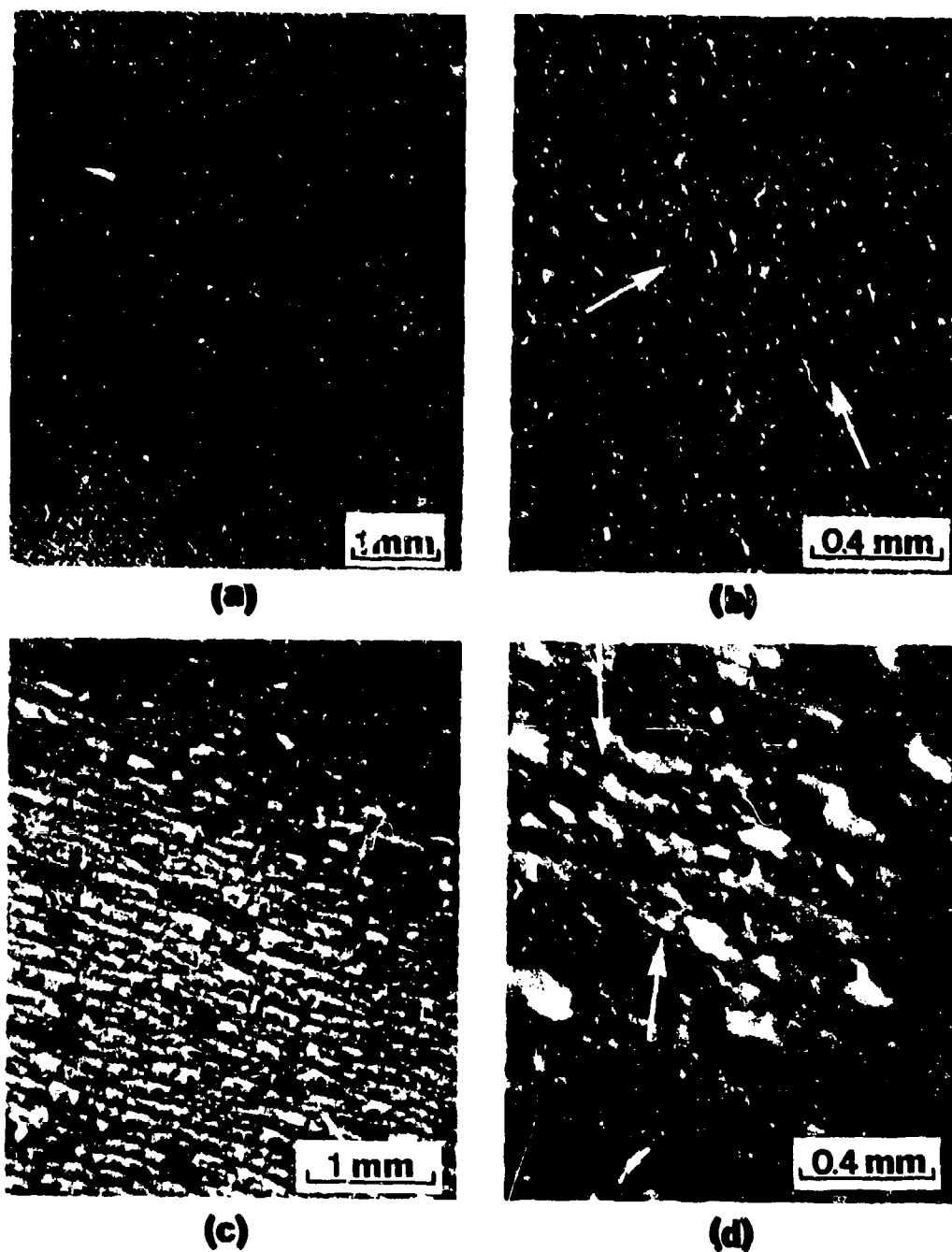
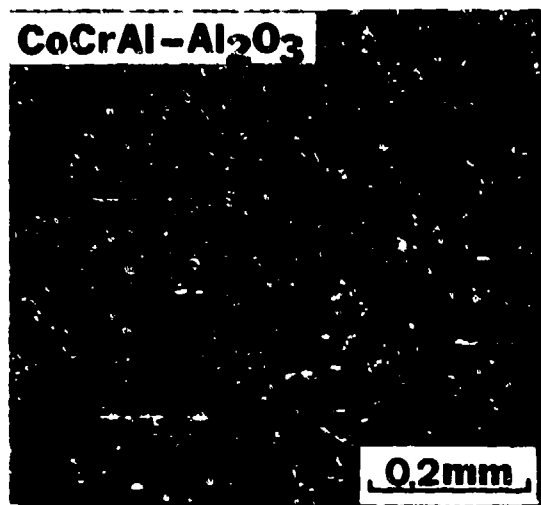
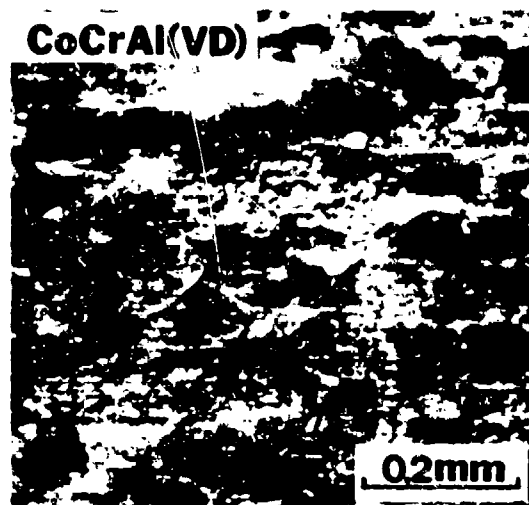


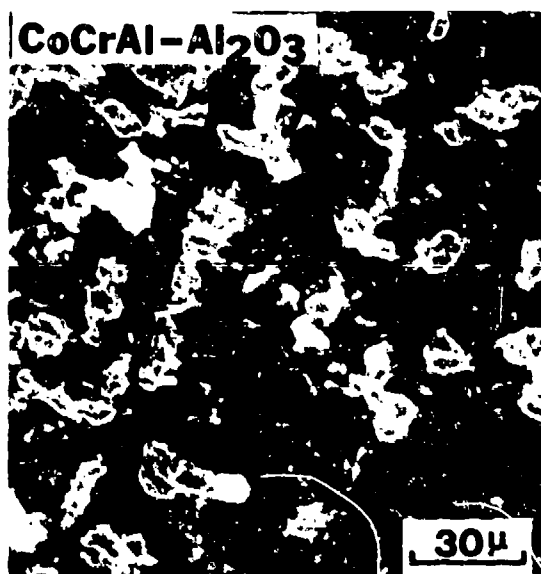
Figure 49 Photographs Showing Morphological Features of Spalling of Al_2O_3 as a Result of Bending an Oxidized CoCrAlY (VD) Specimen. The specimen was oxidized for 2 hrs at 1100°C in air and no spalling occurred on cooling. Upon bending, the Al_2O_3 on the surface that was in tension, (a) and (b), cracked but small patches of Al_2O_3 were still adherent (arrows in b). More spalling of the Al_2O_3 occurred from the surface in compression (c) and (d) but the flakes were small and small islands of adherent Al_2O_3 (arrows in d) were evident.



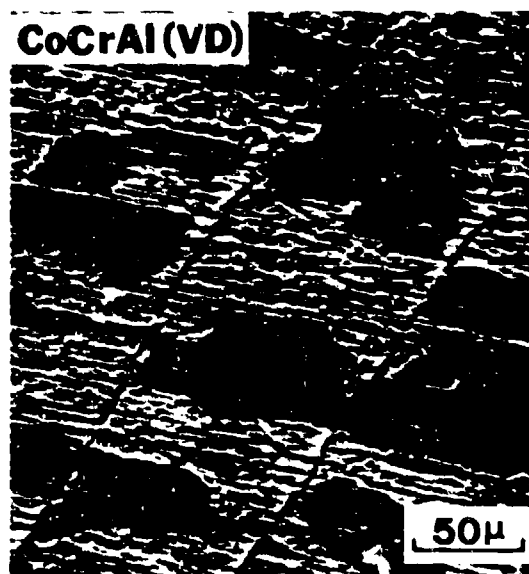
(a)



(b)



(c)



(d)

Figure 50 Photographs Showing the Surfaces of CoCrAl- Al_2O_3 and CoCrAl (VD) After 20 hrs of Oxidation at 1100°C in a CO_2 -CO Gas Mixture With $\text{CO}_2/\text{CO} = 3$. More spalling of the Al_2O_3 has occurred from the specimen which did not contain the dispersion of Al_2O_3 particles.



(a)



(b)

Figure 51 Transverse Section Through CoCrAlY (HWA) After Oxidation at 1200°C for 1000 hrs in 1 atm of Air. (a) A large denuded zone from the surface of the specimen to the remaining β (CoAl) and yttride (arrows) phases is evident. (b) Etched specimen shows the correspondence of internal oxide pegs (arrows) to grain boundaries.

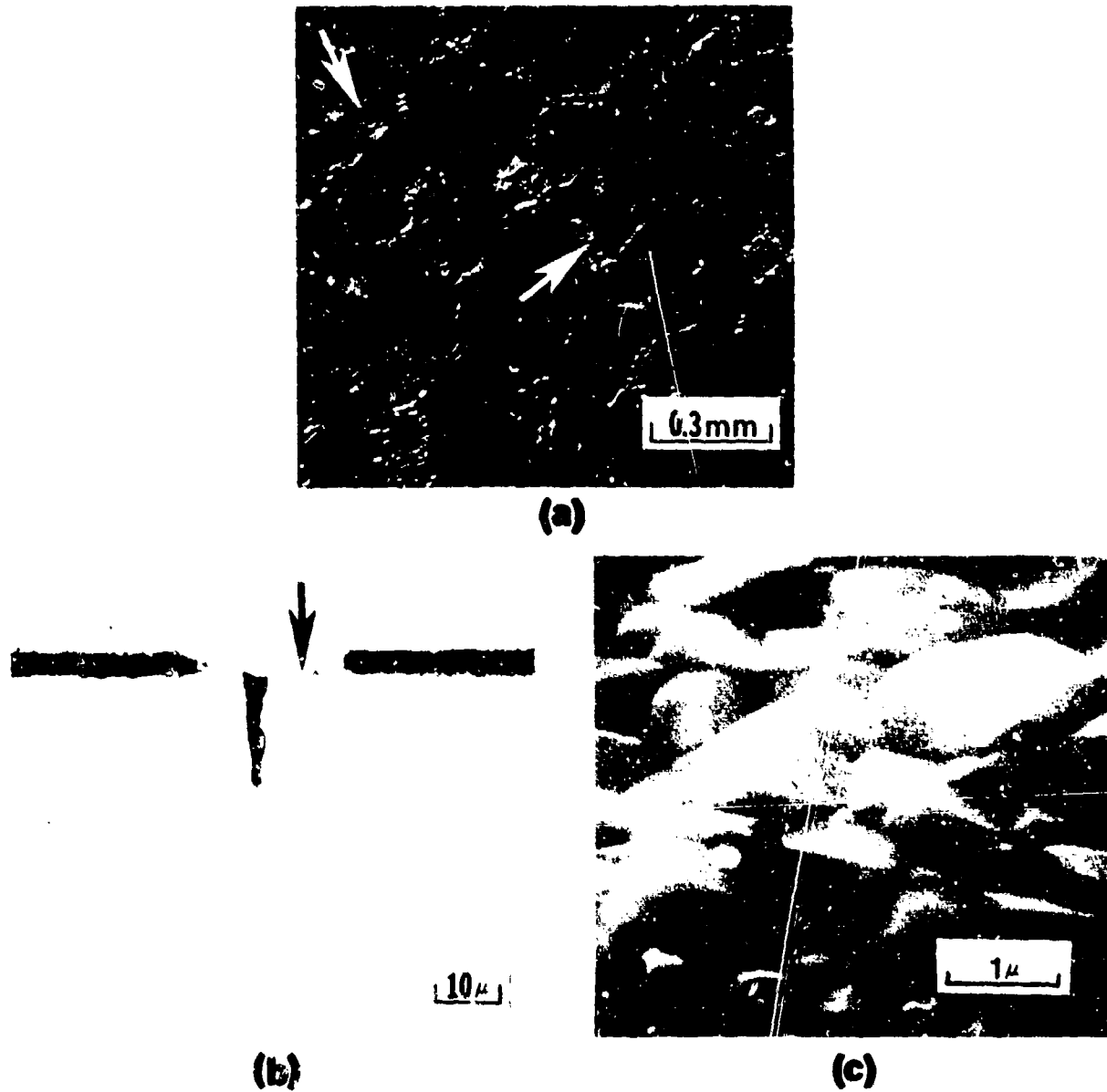


Figure 52 Oxidation Features Developed on NiCrAlY (VD) Specimen Which Had Been Oxidized 1000 hrs at 1200°C, Repolished and Then Oxidized 24 hrs at 1200°C in Air. (a) and (b) Surface morphology and transverse section, respectively, the arrows indicate areas where the oxide had spalled. (c) Photograph showing surface of oxide (oxide-substrate interface). Yttrium oxide particles are evident.

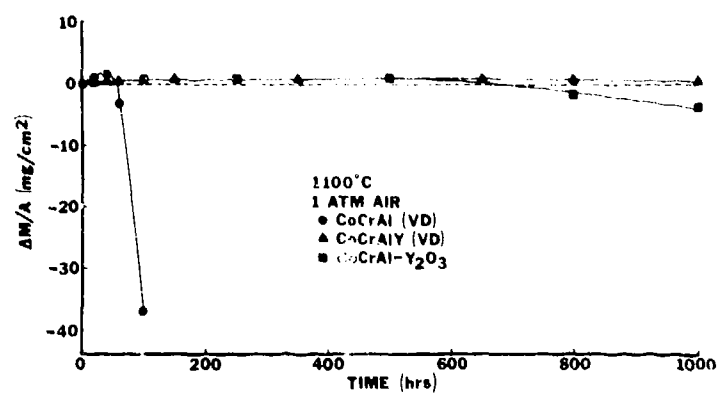
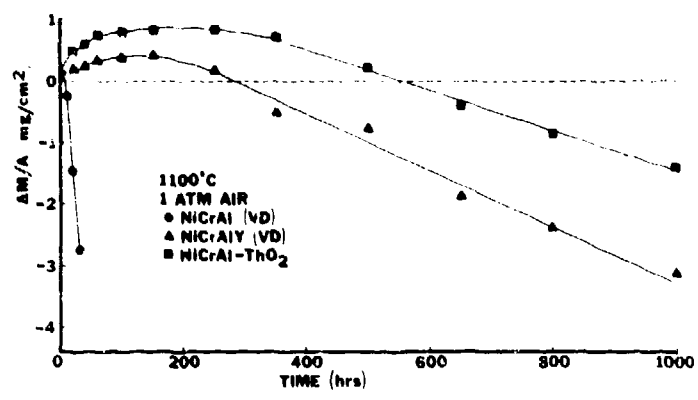
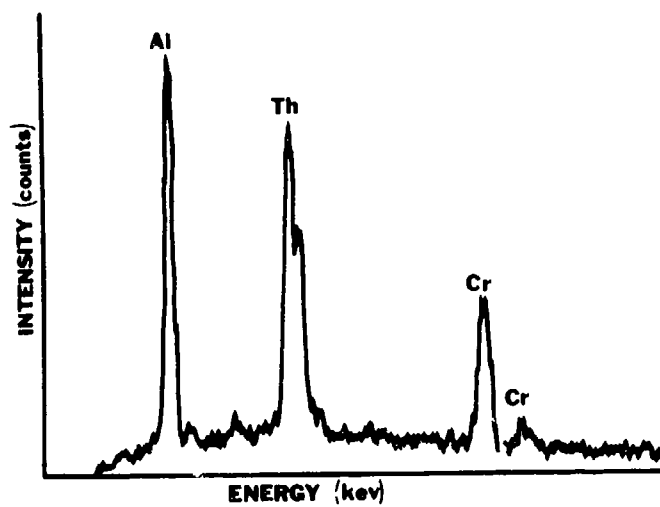
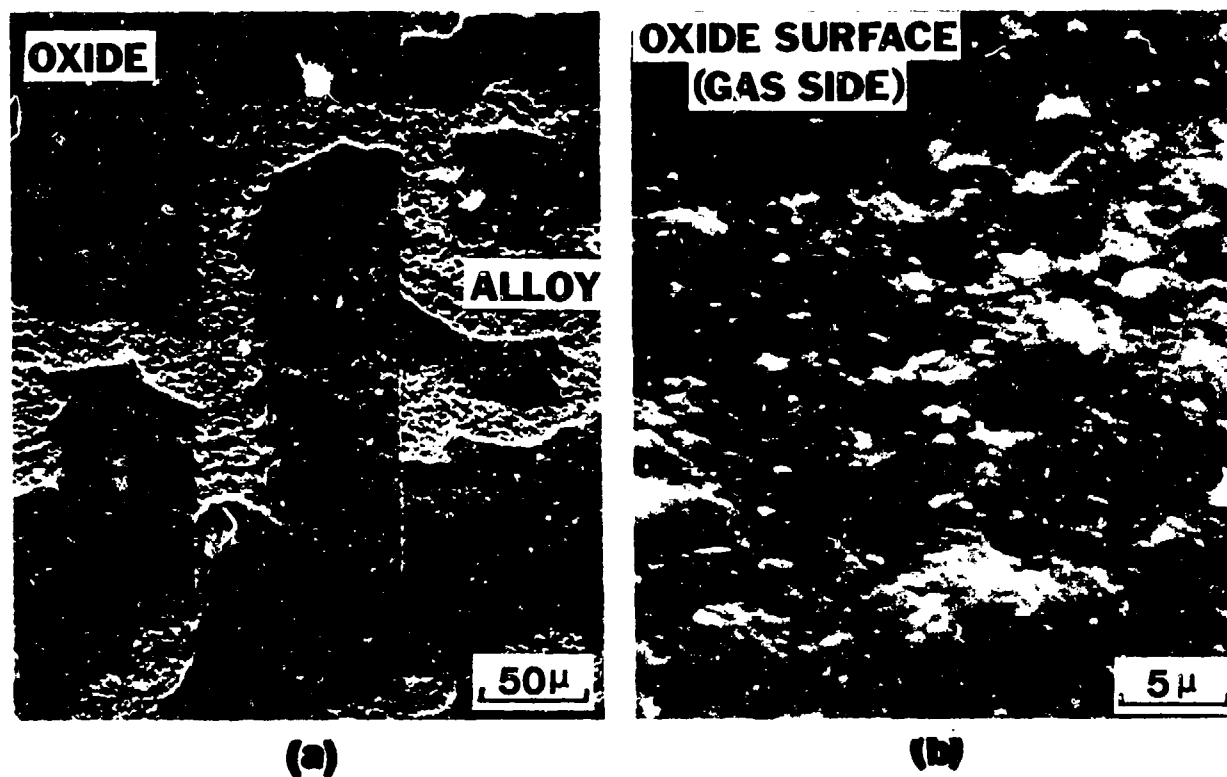


Figure 53 Weight-Change Versus Time Data Obtained for the Cyclic Oxidation (1 hr Cycles) of NiCrAl and CoCrAl Alloys and These Alloys Containing Oxide Particles or Yttrium. These data indicate that yttrium and oxide particles are equally effective in improving the adhesion of Al₂O₃.



Figure 54 Photomicrographs Showing Microstructures of Specimens After 1000 hrs of Cyclic Oxidation (1 hr Cycles) at 1100°C in Air. (a) NiCrAlY (VD), (b) CoCrAlY (VD), (c) NiCrAl-ThO₂, (d) CoCrAlY-Y₂O₃.



(c)

Figure 55 Scanning Micrographs and An X-ray Energy Spectroscopy Profile Which Show the Surface of NiCrAl-ThO₂ After 100 hrs of Oxidation at 1100°C in Air. The oxide surface at the gas interface had a nodular texture and contained thorium.



(a)



(b)

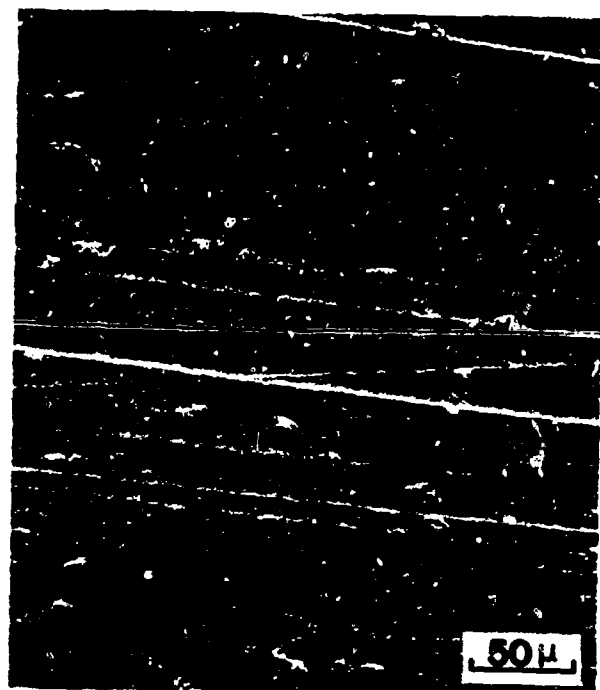


(c)

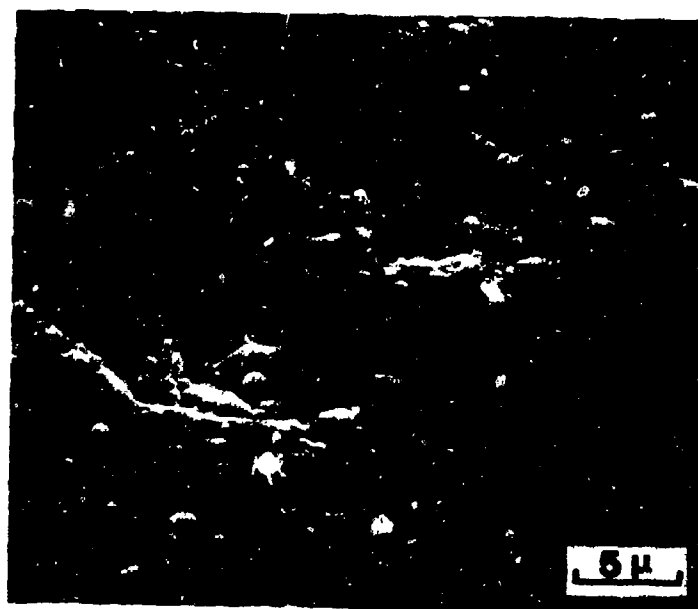


(d)

Figure 56 Scannir Micrographs Showing Features of the Al_2O_3 Scale at the Substrate Interface from NiCrAl-ThO₂ and the Matching Substrate Surface After 100 hrs of Oxidation at 1100°C in Air. The oxide surface contains grains with depressions into which protrusions of the alloy had extended.



(a)



(b)

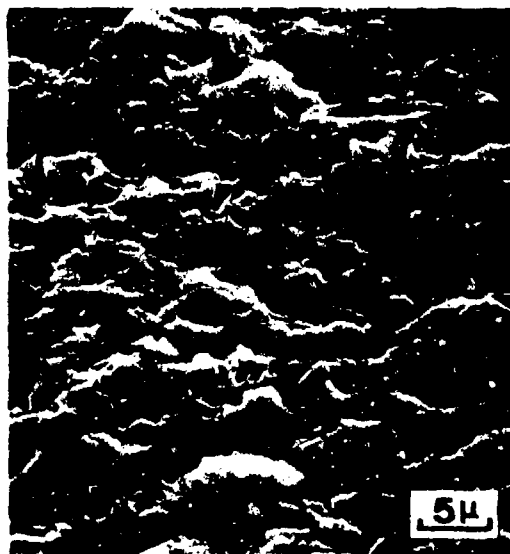
Figure 57 Scanning Micrographs Which Show the Surface of Oxidized $\text{CoCrAl-Y}_2\text{O}_3$ After 100 hrs of Oxidation at 1100°C in Air. (a) Surface of specimen containing polishing marks and localized areas where oxide has spalled. (b) Area where oxide has spalled and which also shows texture of the oxide surface.



(a)



(b)



(c)



(d)

Figure 58 Additional Scanning Micrographs of Specimen Described in Figure 57. At locations where the oxide has spalled, (a), the alloy is highly irregular because the oxide scale extended in the alloy, (b). (c) and (d) Surface of Al_2O_3 at the substrate interface, this surface contains numerous depressions where the alloy had extended into the oxide scale.

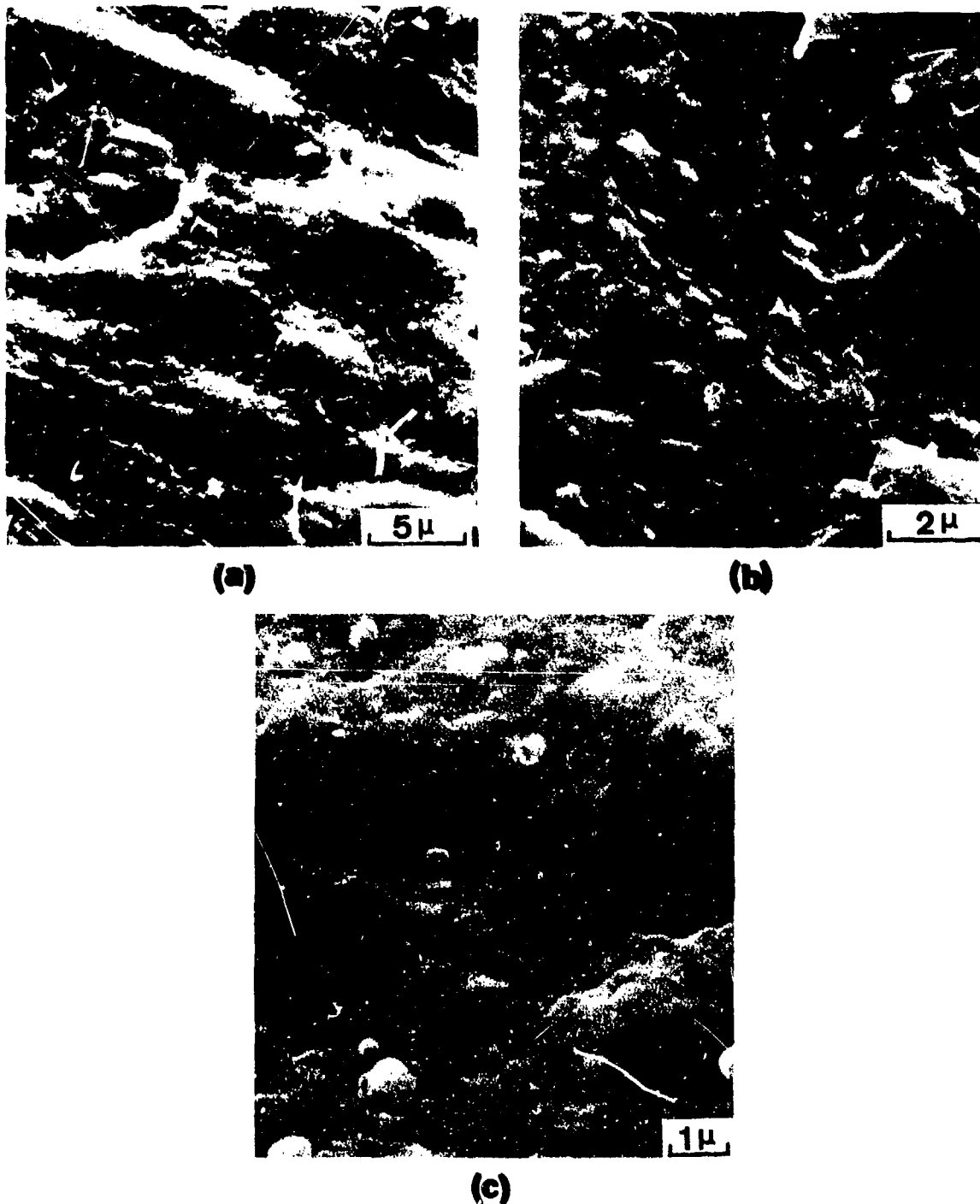
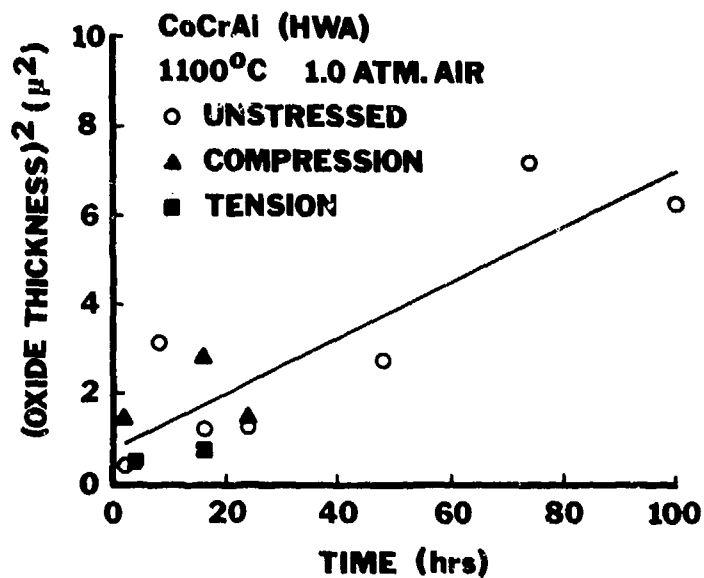
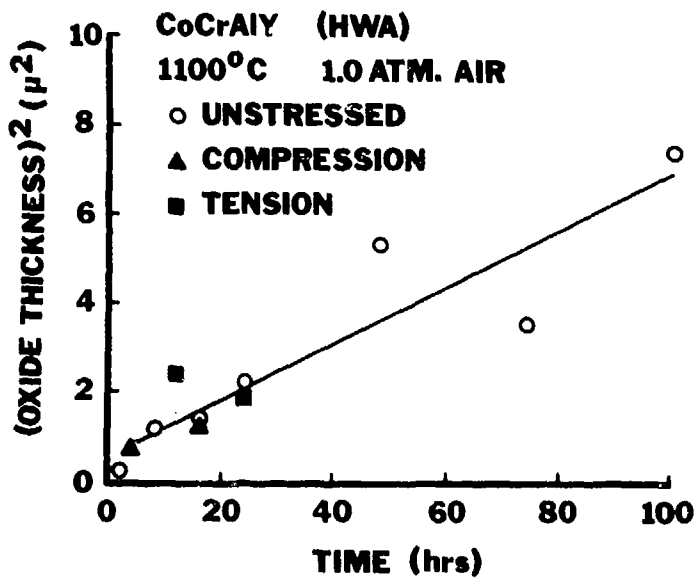


Figure 59 Scanning Micrographs Showing Morphological Features of $\text{CoCrAl-Al}_2\text{O}_3$ After 20 hrs of Oxidation at 1100°C in a $\text{CO}_2\text{-CO}$ Gas Mixture With $\text{CO}_2/\text{CO} = 3$. The oxide surface at the gas interface has a nodular texture, (a), and at locations where the Al_2O_3 had spalled, (b), the alloy surface contains imprints from oxide grains. The Al_2O_3 surface at the substrate interface, (c), contains a well defined grain structure with some of these grains having tooth-like shapes.



(a)



(b)

Figure 60 Comparison of Oxide (Al_2O_3) Thicknesses Formed on Unstressed and Stressed (Compression and Tension) CoCrAl and CoCrAlY Alloys. Compressive testing was performed at a constant strain rate of 0.042%/hr. The tensile testing was accomplished in a creep apparatus where 6-7% and 1-2% strains would have been developed after 24 hrs for CoCrAl and CoCrAlY, respectively.

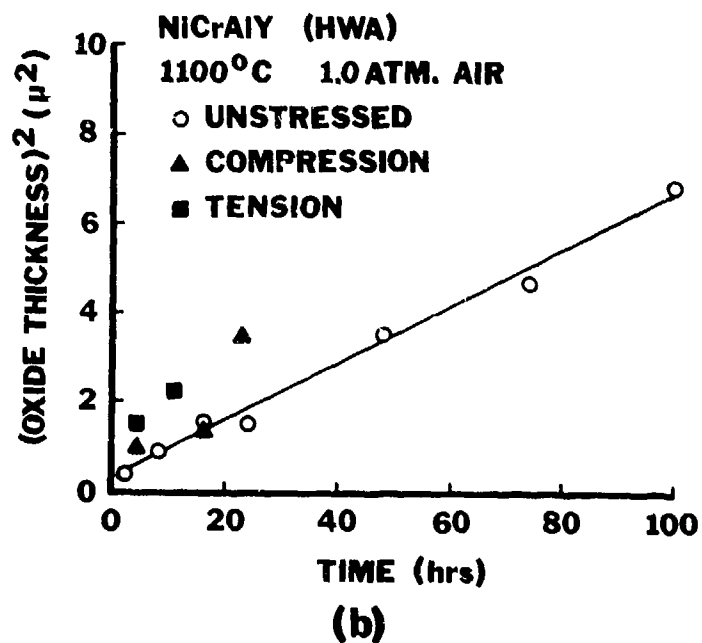
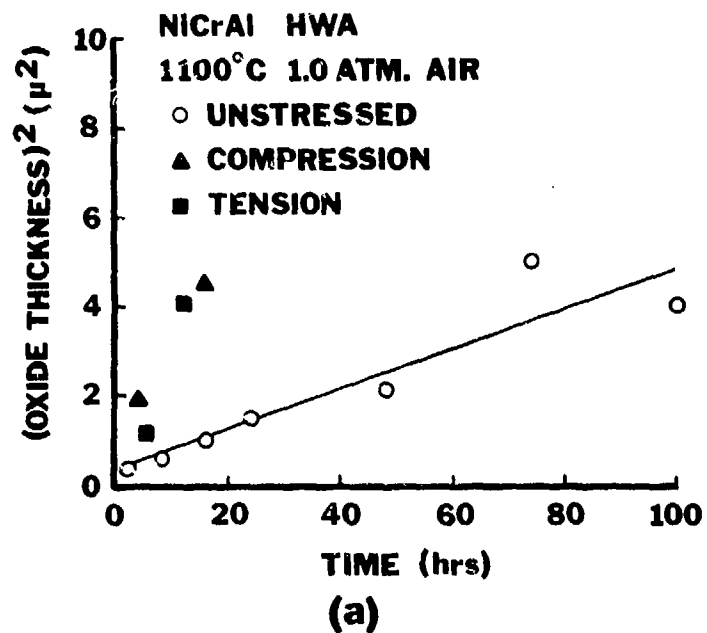
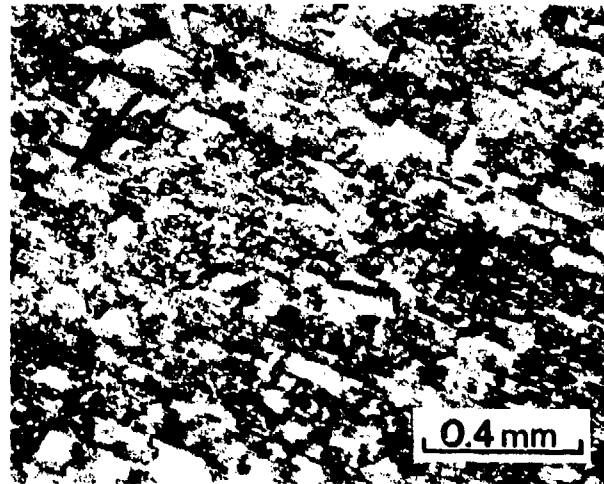


Figure 61 Comparison of Oxide (Al_2O_3) Thicknesses Formed on Unstressed and Stressed (Compression and Tension) NiCrAl and NiCrAlY Alloys. Compressive testing was performed at a constant strain rate of 0.042%/hr. The tensile testing was accomplished in a creep apparatus where 1-2% strain would have been developed after 24 hours.



(a)



(b)

Figure 62 Optical Photographs Showing Surface Features of CoCrAl (HWA) After 24 hrs of Oxidation at 1100°C in Air with an Applied Compressive Stress Producing 1% Strain (0.042%/hr). (a) Photograph showing partially adherent Al_2O_3 (arrows). (b) Photograph showing exposed alloy surface which contains smooth areas (arrows).

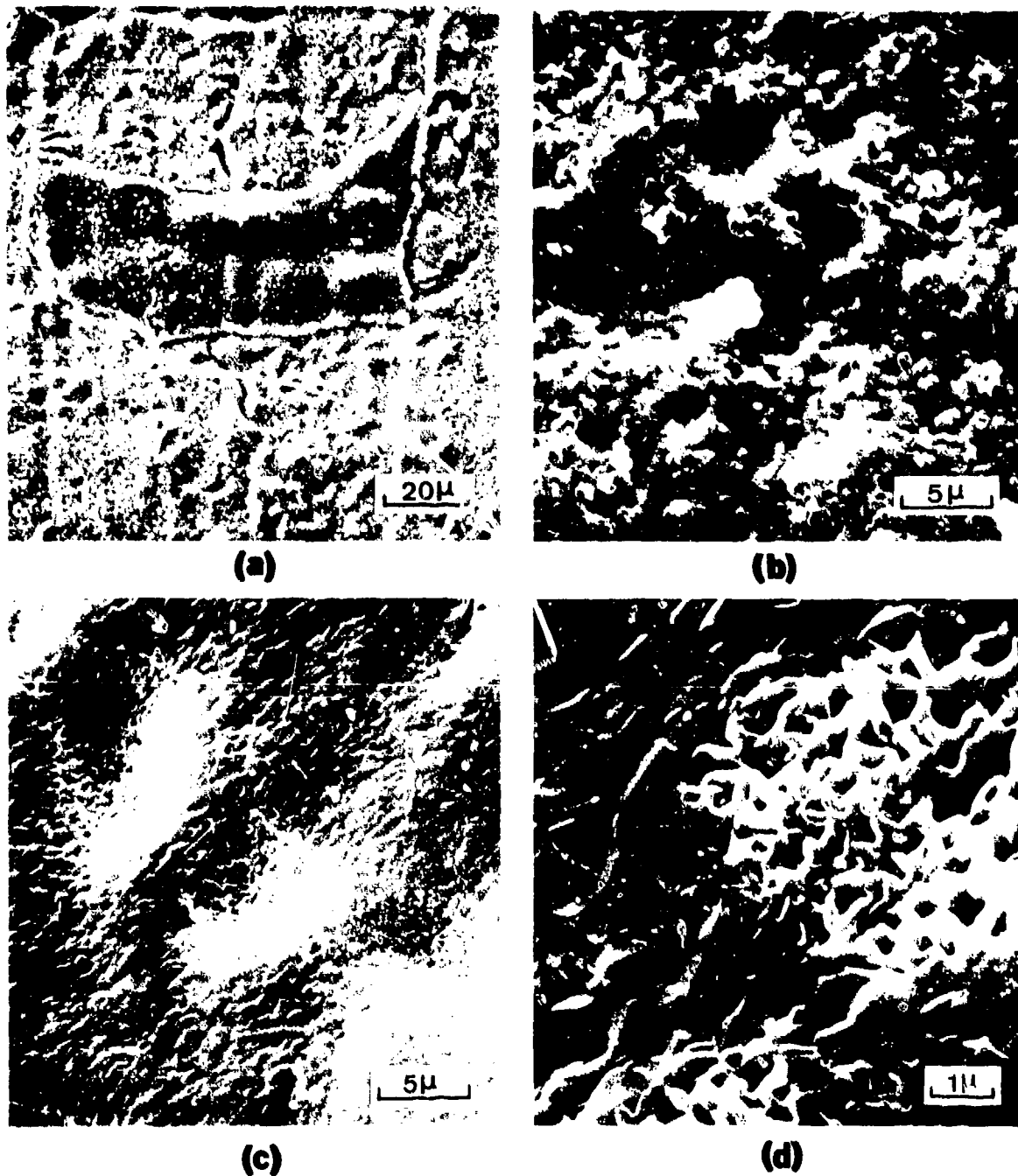


Figure 63 Scanning Micrographs Showing Some of the Typical, Morphological Structures of Oxide Scales and Substrates Formed on Alloys That Did Not Contain Yttrium After 16 hrs of Oxidation at 1100°C in Air with a Constant Strain Rate (Compressive) of 0.04%/hr. (a) and (b) Substrate features of CoCrAl (HWA) showing oxide imprints and smooth areas. (c) and (d) Features of Al₂O₃ surface at the oxide-substrate interface of NiCrAl (HWA) showing the areas having the lace-network pattern which results from void formation along this interface.

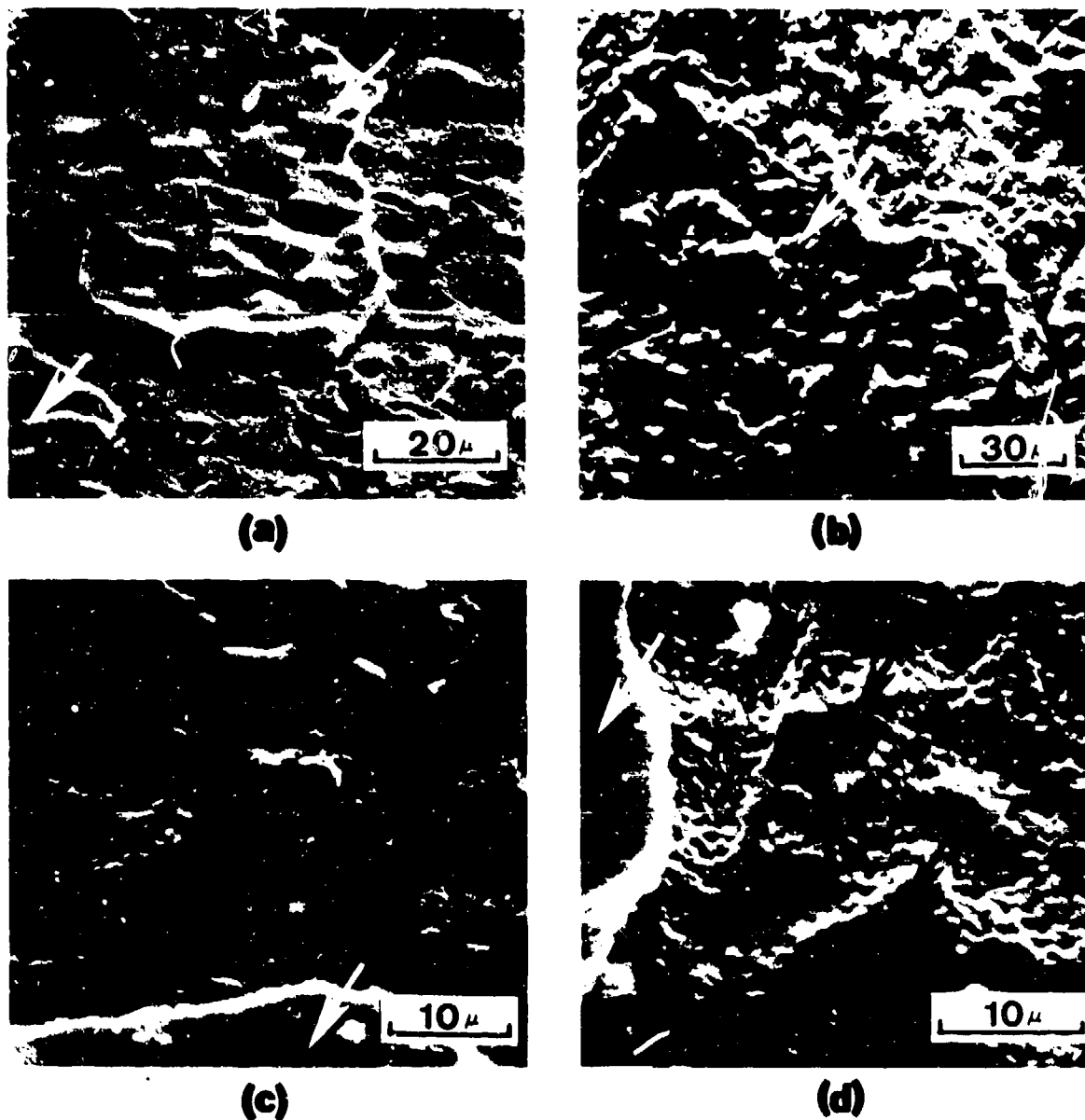


Figure 64 Scanning Micrographs to Compare Surface Features of Unstressed and Stressed CoCrAl (HWA) After Oxidation at 1100°C in Air. The unstressed specimen (a), (c) was oxidized for 48 hrs, whereas the stressed (0.045%/hr compression) alloy (b), (d) was oxidized for 24 hrs.

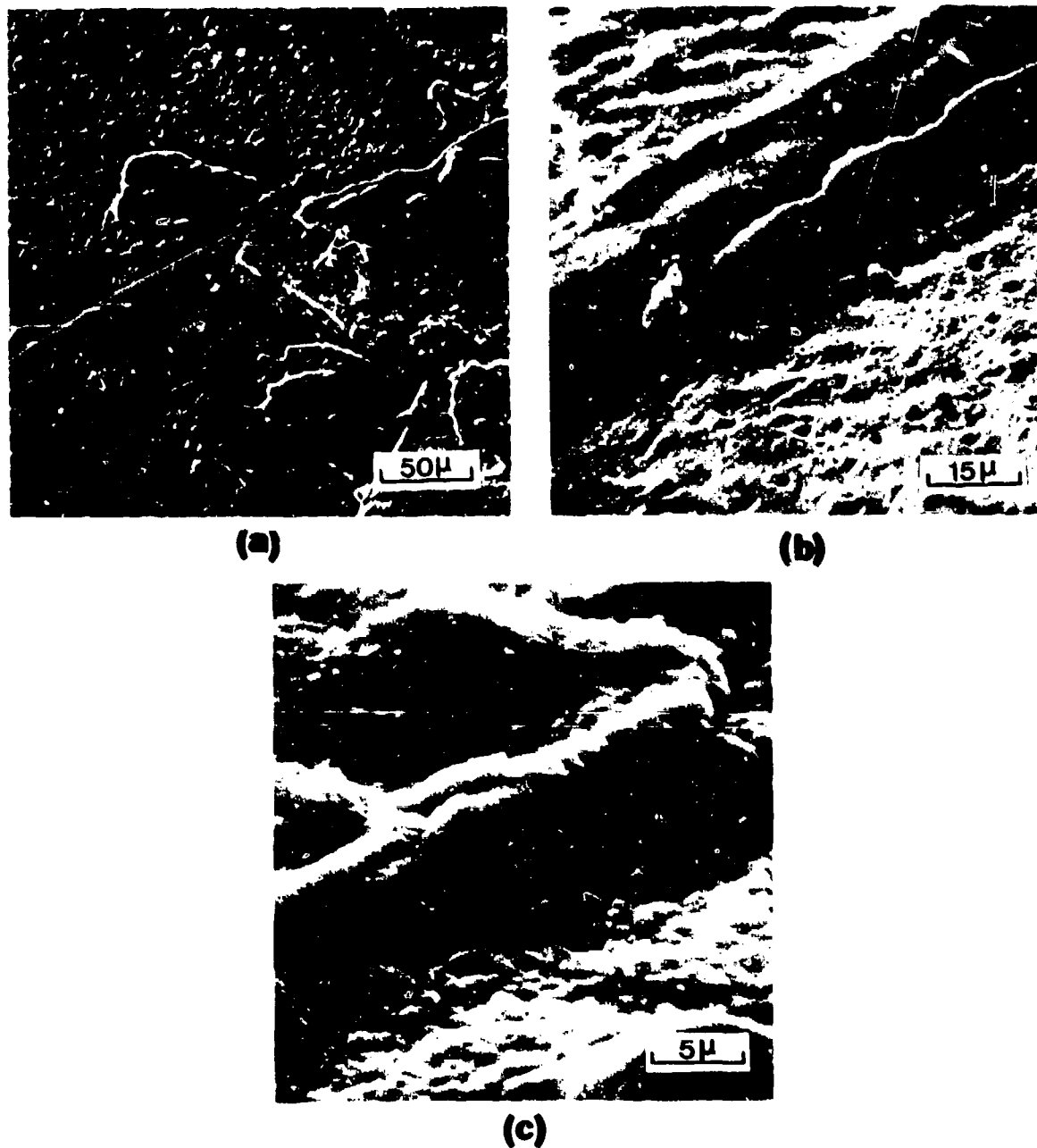
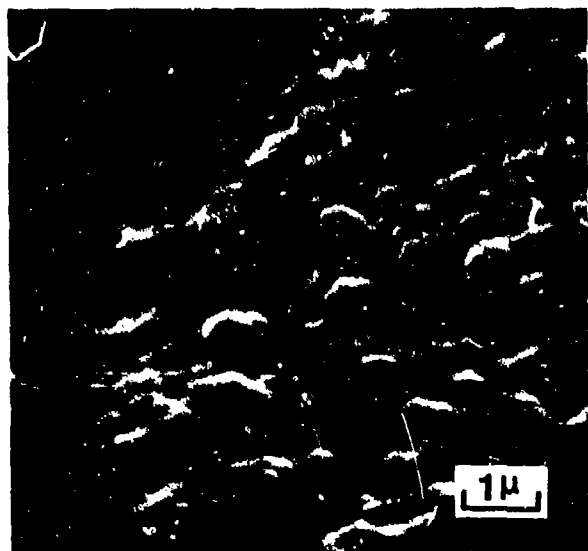
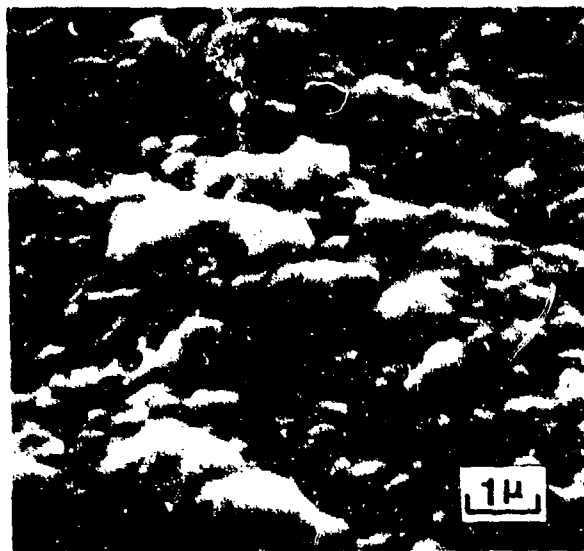


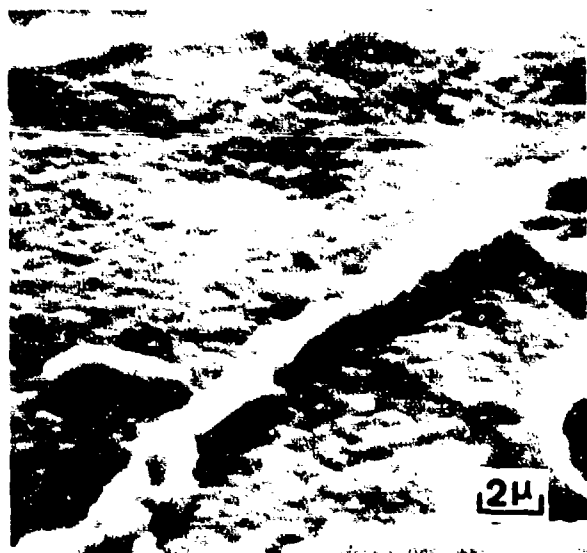
Figure 65 Scanning Micrographs Showing Typical, Morphological Structures of Oxide Scale and Substrate of NiCrAl (HWA) After 16 hrs of Oxidation at 1100°C in Air at a Constant Strain Rate (Compressive) of 0.42%/hr. (a) Low magnification photograph showing displacement of substrate grains and wrinkled features of oxide flakes. (b) Higher magnification photograph showing grain displacement and deformation of the oxide. Oxide grain imprints are evident in the substrate as well as smooth regions where the oxide and substrate were not in contact. (c) Wrinkled oxide flake over what appears to be extruded metal which may also have an oxide layer on its surface.



(a)



(b)

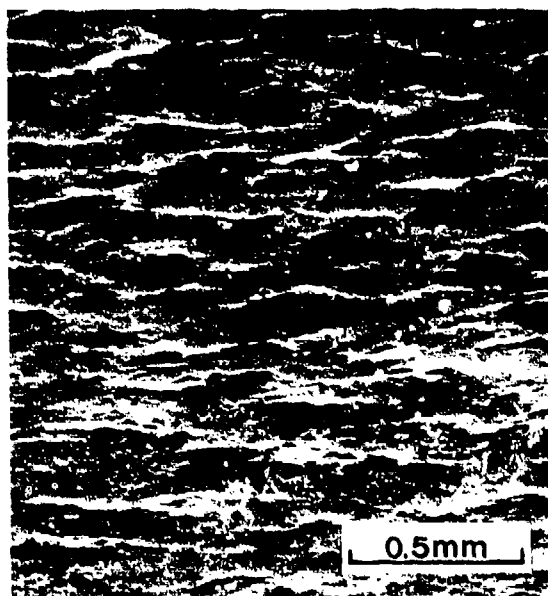


(c)



(d)

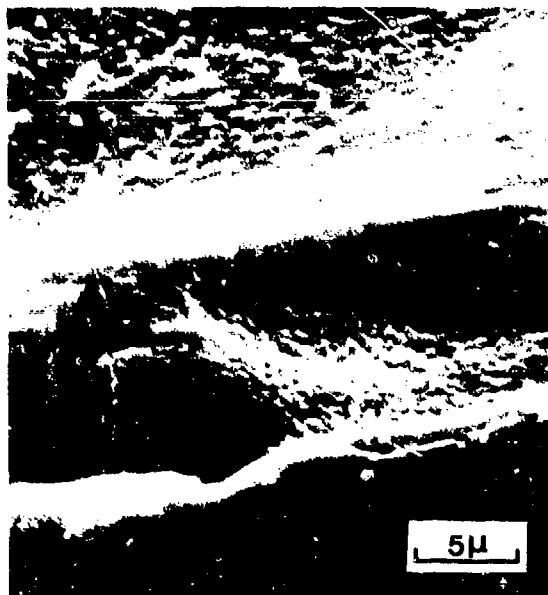
Figure 66 Scanning Micrographs Showing Morphological Structures of Oxide Scales Formed on NiCrAlY (HWA) Specimens After Oxidation at 1100°C in Air. (a) Oxide-gas surface of scale after 4 hrs of oxidation with an applied compressive stress. (b) Oxide-gas surface of scale after 8 hrs of oxidation with no externally applied stress. (c) Alloy-oxide surface of scale after 23 hrs of oxidation with an applied compressive stress. (d) Alloy-oxide surface of scale after 24 hrs of oxidation with no externally applied stress.



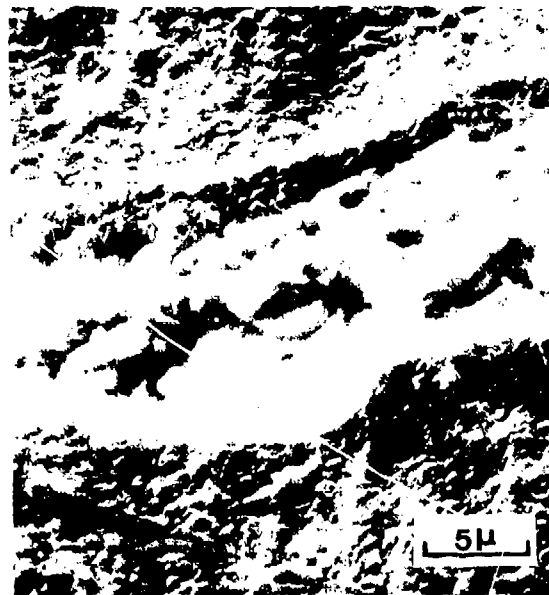
(a)



(b)



(c)



(d)

Figure 67 Scanning Micrographs Showing Typical, Morphological Structures of Oxide Scale and Substrate of CoCrAlY (HWA) After Oxidation at 1100°C for 16 hrs in Air at a Constant Strain Rate (Compressive) of 0.42%/hr. (a) and (b) Photographs which indicate a roughening of the specimen surface as a result of the development of ridges of alloy and oxide along with spalling of oxide. (c) A spalled oxide ridge which has become filled with new oxide within the separation region. (d) A typical area of spalled oxide which exhibits the faceted alloy structure indicating a lack of oxide contact with the alloy and spallation during cooling.

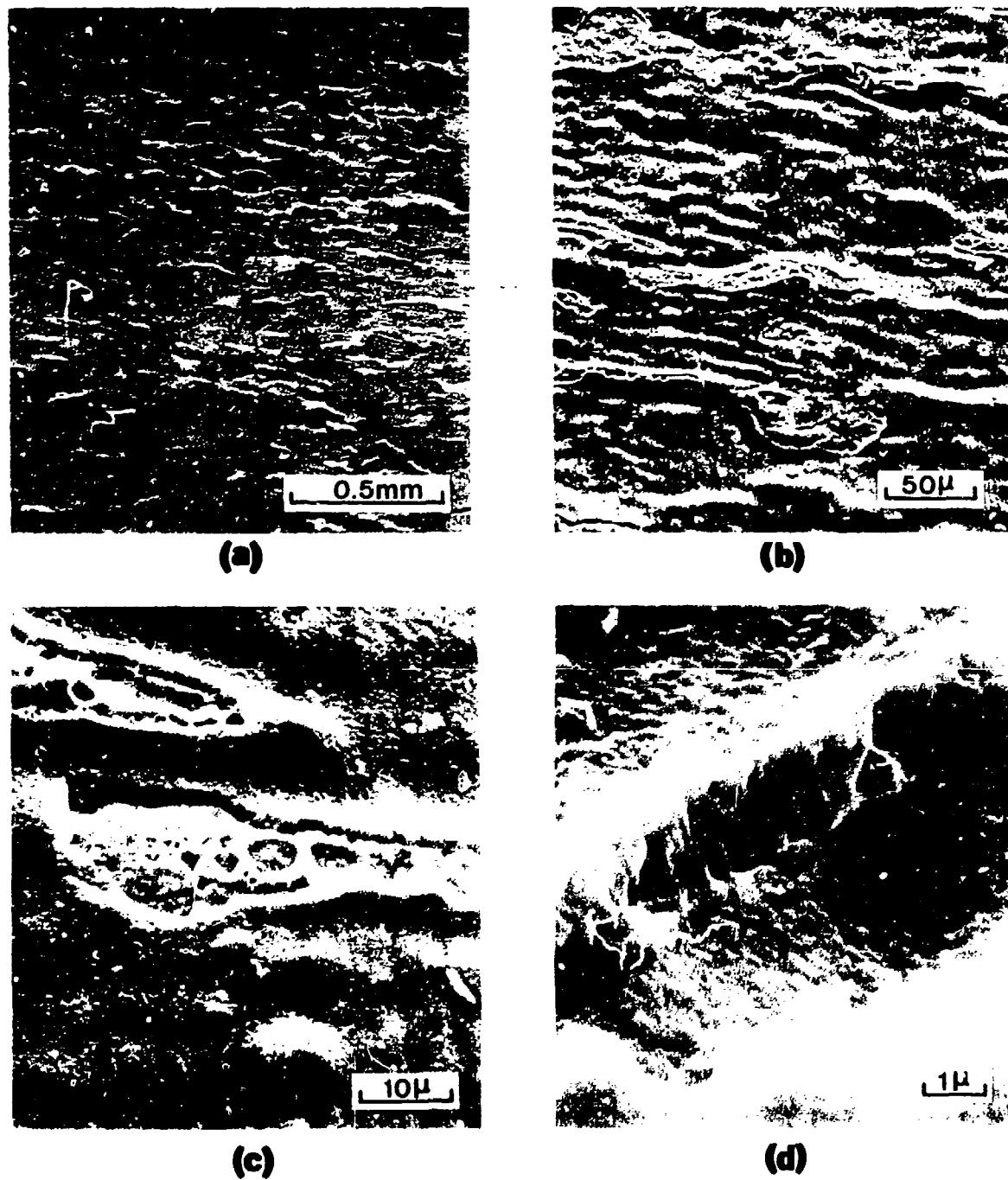
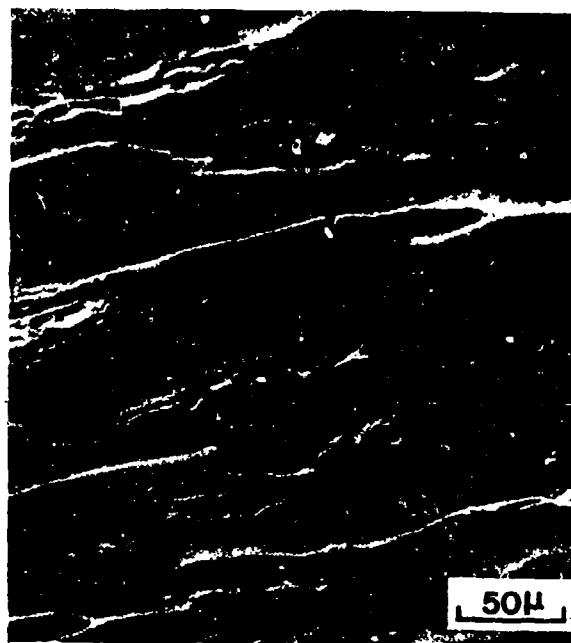


Figure 68 Scanning Micrographs Showing Typical, Morphological Structures of NiCrAlY (HWA) After 16 hrs of Oxidation at 1100°C in Air at a Constant Strain Rate (Compressive) of 0.42%/hr. (a), (b) and (c) Photographs exhibiting deformation of the specimen surface (both substrate and oxide), spalled oxide areas and small circular protrusions from the scale which correspond to oxidized yttrides. (d) Spalled area of a ridge which appears to be oxidized.



(a)



(b)

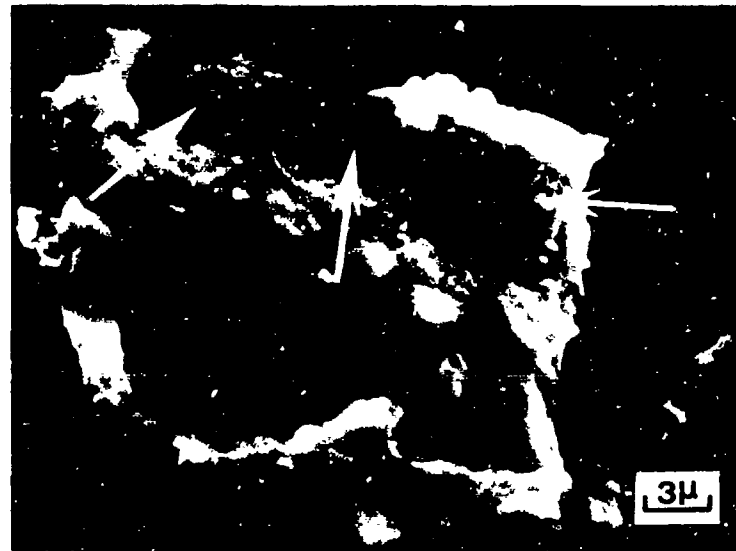


(c)



(d)

Figure 69 Scanning Micrographs Showing Typical, Morphological Structures of Oxide Scale and Substrate of CoCrAlY (HWA) After Oxidation at 1100°C in Air for 16 hrs at a Constant Strain Rate (Compressive) of 0.63%/hr. (a) Photograph exhibiting severe deformation of specimen surface and spallation of the external scale. (b), (c) and (d) Detailed features of a typical spalled area with arrows indicating some of the sites where contact between oxide and substrate is believed not to have been present at temperature.



(a)



(b)

Figure 70 Scanning Micrographs Showing the Morphological Structures of the Alloy-Oxide Surface for an Oxide Flake Spalled from the Specimen Shown in Figure 69. Porous appearing areas (arrows) are consistent with the proposal that some areas of oxide and substrate were not in contact at temperature.

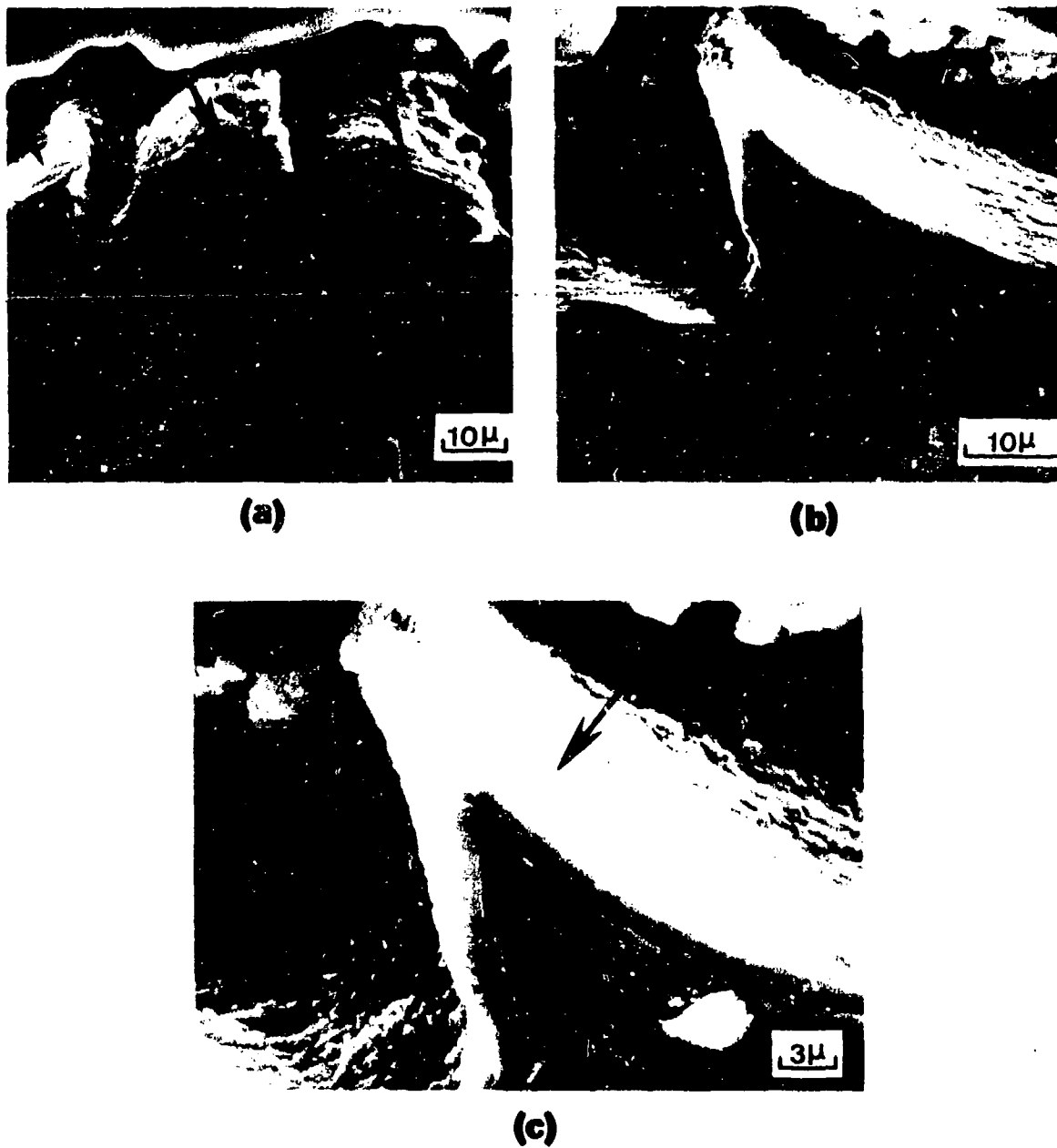
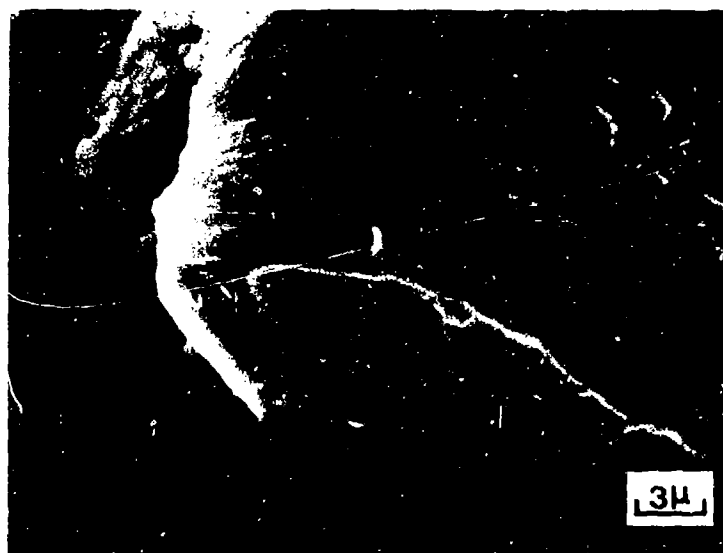


Figure 71 Scanning Micrographs of a Metallographically Polished Section of the Transverse Ridges on the Specimen Shown in Figure 69. Arrows have been used to indicate the oxide layer beneath which the substrate is evident. Severe deformation of the substrate as well as the oxide layer is apparent. Near the apex of some of the oxide ridges, (b) and (c), separation between the oxide and substrate is evident.

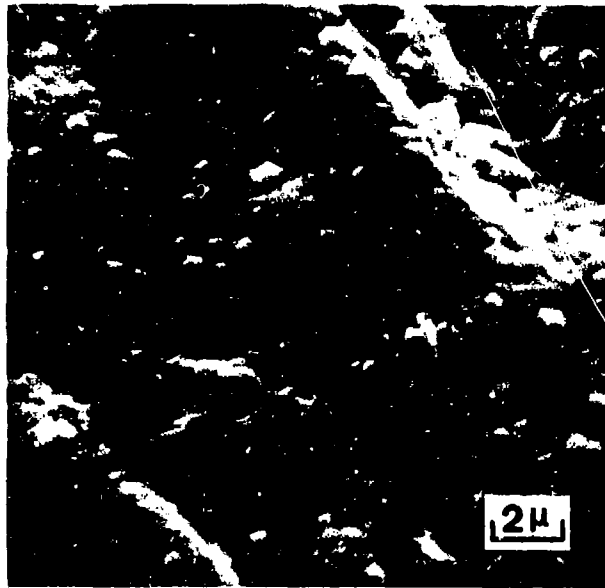


(a)

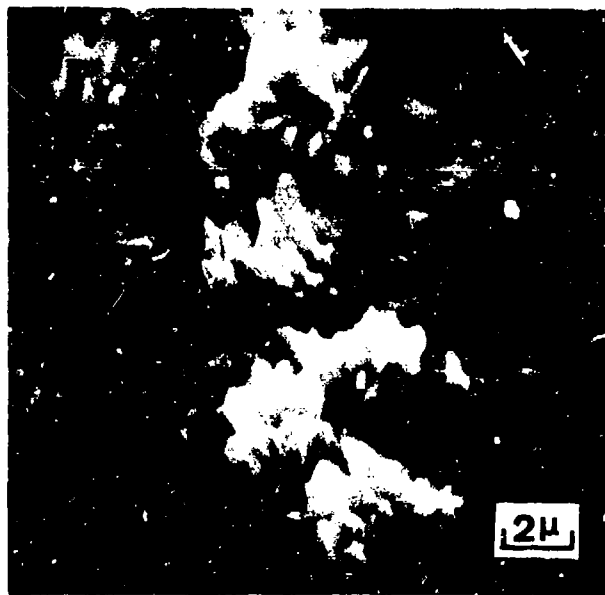


(b)

Figure 72 Scanning Micrographs of Another Deformed Area of the Specimen Shown in Figure 71. (a) A crack along external scale is evident. (b) Photograph of area shown in (a) taken at another angle to show that another layer of oxide appears to have been formed at the bottom of the crack adjacent to the alloy. Such a condition indicates the crack developed at temperature.

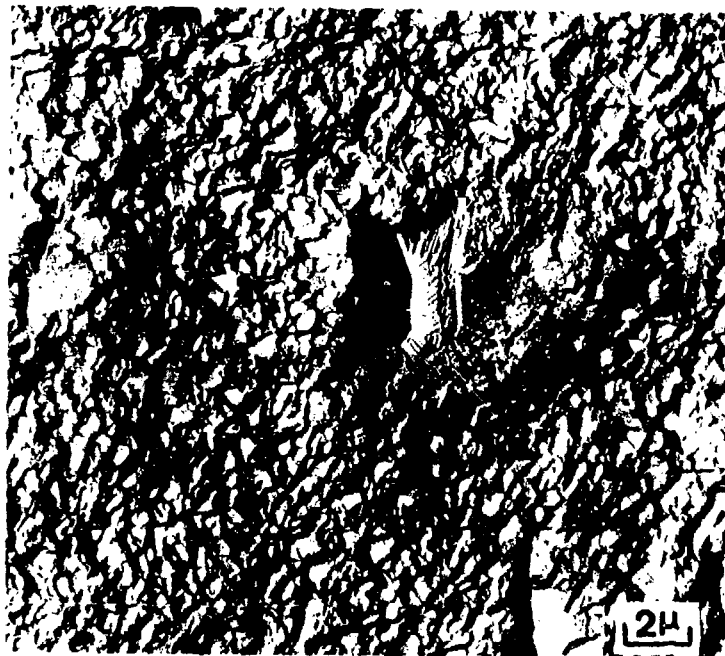


(a)



(b)

Figure 73 Scanning Micrographs Showing Morphological Structures of Oxide Scales Formed on a CoCrAl (HWA) Specimen After Oxidation at 1100°C in Air With an Applied Tensile Stress. (a) Oxide-gas surface of scale after 4 hrs of oxidation. (b) Oxide-gas surface of scale after 16 hrs of oxidation.



(a)



(b)

Figure 74 Replica Micrographs of Alloy Surfaces From Which the Oxide Scales Shown in Figure 73 Were Removed. (a) 4 hrs of oxidation, (b) 16 hrs of oxidation.

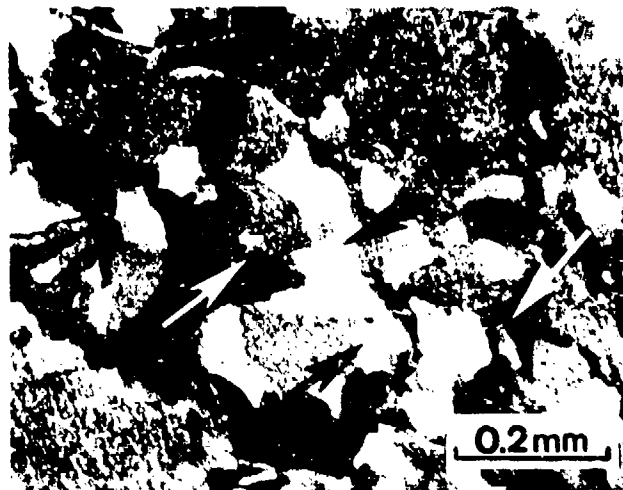


(a)

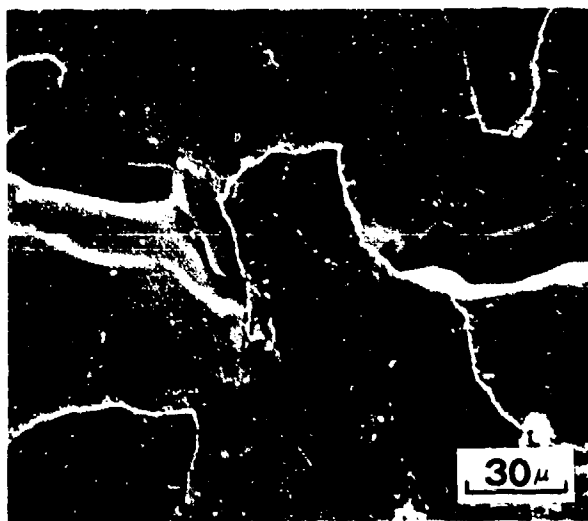


(b)

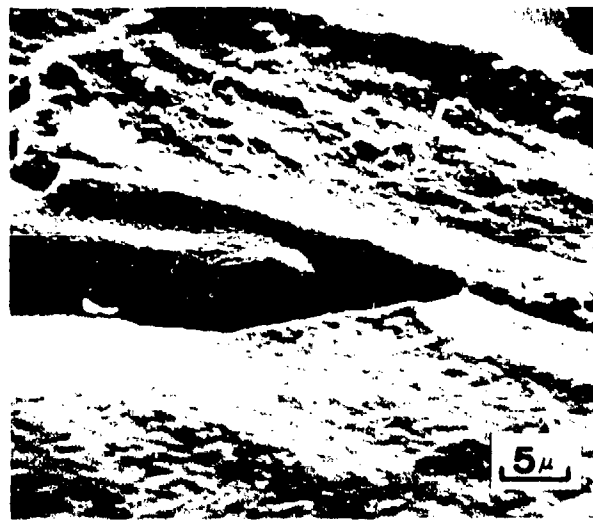
Figure 75 Scanning Micrographs Showing Morphological Structures of Oxide Scales Formed on CoCrAlY (HWA) Specimens After Oxidation at 1100°C in Air. (a) Alloy-oxide surface of scale after 16 hrs of oxidation with an applied compressive stress. (b) Alloy-oxide surface of scale after 24 hours of oxidation with an applied tensile stress.



(a)



(b)



(c)

Figure 76 Photographs Showing Surface Features of NiCrAl (HWA) Specimen After Oxidation for 21 hrs at 1100°C in Air with an Applied Tensile Stress Producing 17.4% Strain. (a) Optical photograph showing partially adherent Al_2O_3 (black arrows) and points of separation in the alloy (white arrows). (b) and (c) Scanning micrographs showing more detail of the features described in (a).

REFERENCES

1. Wagner, C., "Theoretical Analysis of the Diffusion Processes Determining the Oxidation Rate of Alloys", J. Electrochem. Soc., Vol. 99, pp. 369-380 (1952).
2. Wagner, C., "Oxidation of Alloys Involving Noble Metals", J. Electrochem. Soc., Vol. 103, pp. 571-580 (1956).
3. Wagner, C., "Formation of Composite Scales Consisting of Oxides of Different Metals", J. Electrochem. Soc., Vol. 103, pp. 627-633 (1956).
4. Wagner, C., "Reaktionstypen bei der Oxydation von Legierungen", Z. Elektrochem., Vol. 63, p. 772 (1959).
5. Rapp, R. A., "The Transition from Internal to External Oxidation and the Formation of Interruption Bands in Silver-Indium Alloys", Acta Met., Vol. 9, pp. 730-741 (1961).
6. Rapp, R. A., "Kinetics, Microstructures and Mechanism of Internal Oxidation - Its Effect and Prevention in High Temperature Alloy Oxidation", Corrosion, Vol. 21, pp. 382-401 (1965).
7. Chattopadhyay, B. and Wood, G. C., "The Transient Oxidation of Fe-Cr and Ni-Cr Alloys", J. Electrochem. Soc., Vol. 117, pp. 1163-1171 (1970).
8. Giggins, C. S. and Pettit, F. S., "Oxidation of Ni-Cr-Al Alloys Between 1000° and 1200°C", J. Electrochem. Soc., Vol. 118, pp. 1782-1790 (1971).
9. Kear, B. H., Lemaire, L. P., Fornwalt, D. E. and Pettit, F. S., "On the Transient Oxidation of a Ni-15Cr-6Al Alloy", Oxidation of Metals, Vol. 3, pp. 557-569 (1971).
10. Tylecote, R. F., "Factors Influencing the Adherence of Oxides on Metals", J. Iron Steel Inst., Vol. 196, pp. 135-141 (1960), "The Adherence of Oxide Films on Metals", J. Iron Steel Inst., Vol. 195, pp. 380-385 (1960).
11. Stringer, J., "The Effect of Alloying on Oxidation: Quantitative Treatments", Met. Rev., Vol. 11, pp. 113-128 (1966).
12. Hessenbruck, W., Metallen and Legierungen für Hohe Temperaturen, Part I, J. Springer, Berlin (1940).
13. Wukusick, C. S. and Collins, J. F., "An Iron-Chromium-Aluminum Alloy Containing Yttrium", Mater. Res. Stand., Vol. 4, pp. 637-646 (1964).
14. Talboom, F. P., Elam, R. C. and Wilson, L. W., "Evaluation of Advanced Superalloy Protection Systems", Final Report prepared by Pratt & Whitney Aircraft, Division of United Technologies Corporation for the National Aeronautics and Space Administration, Contract NAS3-12415, NASA CR-PWA-4055 (1970).

REFERENCES (Cont'd)

15. Felten, E. J., "High Temperature Oxidation of Fe-Cr Base Alloys with Particular Reference to Fe-Cr-Y Alloys", J. Electrochem Soc., Vol. 108, pp. 490-495 (1961).
16. Lustman, B., "The Intermittant Oxidation of Some Nickel-Chromium Base Alloys", Trans. TMS-AIME, Vol. 188, pp. 995-6 (1950).
17. Pfeiffer, H., "Influence of Trace Elements on Anti-Scaling Properties of Heat Resistant Alloys", Werkst. Korros., Vol. 8, pp. 574-579 (1957).
18. Francis, J. M. and Jutson, J. A., "High Temperature Oxidation of An Iron-Chromium-Yttrium Alloy in Carbon Dioxide", Corros. Sci., Vol. 8, pp. 445-449 (1968).
19. Tien, J. K. and Pettit, F. S., "Mechanisms of Oxide Adherence on Fe-25Cr-4Al (Y or Sc) Alloys", Met. Trans., Vol. 3, pp. 1587-1599 (1972).
20. Stringer, J., "Stress Generation and Relief in Growing Oxide Films", Corros. Sci., Vol. 10, pp. 513-543 (1970).
21. Hancock, P. and Hurst, R. C., "The Mechanical Properties and Breakdown of Surface Oxide Films at Elevated Temperatures", Advances in Corr. Sci. and Technology, Vol. 4, pp. 1-84 (1974).
22. Wright, I. G., Wilcox, B. A. and Jaffee, R. I., "Oxidation and Hot Corrosion of Ni-, Cr- and Co-Cr Base Alloys Containing Rare Earth Oxide Dispersions", prepared under Contract N62269-74-C-0291, Naval Air Development Center, Warminster, Pa., by Battelle, Columbus Laboratories, Columbus, Ohio, May 1975.
23. Benjamin, J. S., "Dispersion Strengthened Superalloys by Mechanical Alloying", Met. Trans., Vol. 1, pp. 2943-2951 (1970).
24. Pettit, F. S., "Oxidation Mechanisms for Nickel-Aluminum Alloys at Temperatures Between 900° and 1300°C", Trans. TMS-AIME, Vol. 239, pp. 1296-1305 (1967).
25. Pettit, F. S., Yinger, R. and Wagner, J. B., Jr., "The Mechanism of Oxidation of Iron in Carbon Monoxide-Carbon Dioxide Mixtures", Acta. Met., Vol. 8, pp. 617-623 (1960).
26. Seltzer, M. S., Wright, I. G. and Wilcox, B. A., "Development of High-Emittance Scales on Thoriated Nickel-Chromium-Aluminum-Base Alloys", for the National Aeronautics and Space Administration, Cleveland, Ohio (Contract No. NAS3-15845), October 1973.
27. Oishi, Y. and Kingery, W. D., "Self-Diffusion of Oxygen in Single Crystal and Polycrystalline Aluminum Oxide", J. Chem. Phys., Vol. 37, pp. 480-486 (1962).

REFERENCES (Cont'd)

28. Paladino, A. E. and Kingery, W. D., "Aluminum Ion Diffusion in Aluminum Oxide", J. Chem. Phys., Vol. 37, pp. 957-960 (1962).
29. Mistler, R. E. and Coble, R. L., "Rate-Determining Species in Diffusion-Controlled Processes in Al_2O_3 ", J. Amer. Ceramic Soc., Vol. 54, pp. 60-61 (1971).
30. Mistler, R. E. and Coble, R. L., "Grain-Boundary Diffusion and Boundary Widths in Metals and Ceramics", J. Appl. Phys., Vol. 45, pp. 1507-1509 (1974).
31. Gobel, J. A. and Rosen, S., "Phase Equilibria in the Nickel-Aluminum-Yttrium System at 1000°C", J. Less Common Metals, Vol. 16, pp. 285-287 (1968).
32. McDonald, J. E. and Eberhart, J. G., "Adhesion in Aluminum Oxide-Metal Systems", Trans. TMS-AIME, Vol. 233, pp. 512-517 (1965).